T cell-mediated cytotoxicity against patient-derived cervical cancer organoids

Inaugural-Dissertation
to obtain the academic degree
Doctor rerum naturalium (Dr. rer. nat.)

submitted to the Department of Biology, Chemistry, Pharmacy
of Freie Universität Berlin

by
Junxue Dong

2024

This thesis is based on research conducted from 2019 to 2023 at the Max Planck Institute for Infection Biology (MPIIB), Berlin, Germany, and the Institute for Clinical Molecular Biology, Christian-Albrechts-Universität zu Kiel and University Hospital Schleswig-Holstein, Germany, under the supervision of Prof. Dr. Thomas F. Meyer.

1st Reviewer: Prof. Dr. Thomas F. Meyer
2nd Reviewer: Prof. Dr. Haike Antelmann

Date of defence: 25.06.2024

Acknowledgments

I highly appreciate Prof. Thomas F. Meyer for his guidance in academia, constant willingness to help with scientific advice and a big credit of support to set up network and collaboration. It is really appreciated all the effort he made to establish a new lab in Kiel in an city, unfamiliar for us, to allow for continuing with our projects even during the pandemic. He is not only my scientific mentor but also a lighthouse of life. Whenever there are difficulties, there comes his encouragement to move forward and never give up. Meanwhile, I acknowledge Prof. Haike Antelmann who kindly offered me great support to register my doctoral project and start my academic journey.

I would like to express my great appreciation to Prof. Dieter Kabelitz and Christian Peters who provided me not only materials for γδ T experiments but also fruitful scientific discussions during my doctoral study. Their coffee chat and party invitations warmed up my heart and lightened my life in Kiel.

I acknowledge my earlier direct supervisor Rajendra Kumar Gurumurthy and Cindrilla Chumduri for sharing with me their scientific knowledge and showing me how to ask essential questions and where to find the answers. I feel also grateful to Saskia F. Erttmann, Stefanie Koster, David Holthaus, and Michal Zarobkiewicz who taught me numerous lab techniques, analytic methods and writing skills, which were essential for closing this project and resulted in one amazing publication.

For the results from RNAseq and peptidome sequencing of organoid samples provided in the thesis, I would like to thank Hilmar Berger, Alvaro Quevedo-Olmos, Marcel Wacker, and Prof. Juliane Walz. I thank Prof. Mandy Mangler and Prof. Daniela Wesch for obtaining patient tissues and leukocyte concentrates.

For establishing the organoid-T cell co-culture model, I am really grateful for Nina Hedemann's strong technic support, kind sharing and fruitful discussion. I would thank Wiebe Schaefer, and Anna Willms from SYNENTEC GmbH for the provision of the Cellavista 4 automated cell imager, the SYBOT X-1000, the CYTOMAT 2 C-LiN system, and technical assistance throughout the live cell experiments.

Special thanks to the whole Meyer laboratory: Huopeng, Shihan, Zeyang, Xiaochen, Marzieh, Lukas, and Yadvir for their daily support, help with my lab work, but also for the meetings, conversations, which made every day more enjoyable.

I am really grateful for all the support, but also unforgettable moments that I received from a lot of friends and mentors in both Germany and China: Manqiang, Weijie, Yen, Mingbo, Prof. Tianmin Xu, Prof. Wei Liu. Moreover, I would like to thank my mom and dad who convinced me to move to Berlin and start my doctoral studies and always encouraged me to be confident and relaxed to find work and life balance. I am grateful to the China Scholarship Council for providing me the scholarship. Finally, I would like to thank my boyfriend Wei for his support, and selfless tolerance. He is always there to be my backup and we faced many difficulties together.

Declaration of authorship

I hereby declare that I alone am responsible for the content of my doctoral dissertation and that I have only used the sources or references cited in the dissertation.

Outline

1 ABSTRACT

Cervical cancer is one of the most common cancers affecting women, and the mortality-to-incidence ratio (MIR) of cervical cancer varies between developed and developing regions, North America had the lowest MIR (0.36), followed by MIR in Europe (0.40), while Africa had the highest MIR (0.68) (Shen et al.,2023). Infection with human high-risk papillomaviruses (HR-HPV) is the most important driver of cervical cancer, but after persistent HR-HPV infection, infected cervix cells still need many years to transform into cancer. Since 90% of failures in current treatments are related to drug resistance, the development of more effective therapies is urgently required. However, many new therapies have to be terminated because of the unsatisfactory drug efficacy at clinical phases, which reflects the current flaws of preclinical drug models. In this context, establishing precise *in vitro* models to screen out the therapeutic targets and to assess the new drug efficacy against cervical cancer is vital.

In this study, based on patient-derived cervical organoids, multi-omic analysis including RNA sequencing and HLA-restricted peptidome sequencing was used to investigate dysregulated genes, biology processes, and HLA-presented epitopes in HPV-transformed and cancerous cervical organoids. Totally 6,515 HLA class I and 719 HLA class II restricted peptides were yielded, thereafter the immunogenicity of the epitopes was predicted with public machine-learning-based tools. Interestingly, a large number of upregulated genes and highly immunogenic epitopes in HPV+ and cancer samples were associated with DNA repair. Thus, the role DNA repair-related molecules appear to play in cervical cancer therapies and prognosis was further explored. I first constructed a DNA repair-related gene score (DRGscore) with the public cervical cancer dataset of the Cancer Genome Atlas Program (TCGA-CESE). In the following, I observed a negative correlation between DRGscore and the prognosis of cervical cancer patients. The tumor microenvironment of patients with lower DRGscore contained more immune effectors and less immune suppressors, which suggested the negative correlation between DRGscore and sensitivity to immunotherapy. This finding could provide clues for patient medication guidance: high DRGscore patients might benefit from DNA repair inhibitors to reduce chemoradiotherapy resistance and gain a better prognosis. In contrast, low DRGscore patients rather might be sensitive to different immunotherapy including immune checkpoint inhibitors, and adoptive T cell therapy.

Due to HPV infection and viral genome integration, HPV+ and cervical cancer cells are generally under stress conditions, which induces the intracellular accumulation of phosphoantigens (pAgs) that can be recognized by Vγ9Vδ2 T cells in an HLA-independent manner. The DNA repair activities in host cells are exploited by HPV for replication, which may provide some potential ligands recognized by Vγ9Vδ2 T cell receptors. To figure out our

hypotheses, I investigated the Vγ9Vδ2 T cell cytotoxic effect against HPV-transformed and cervical cancer cells based on our cervical organoid model. Importantly, the cytotoxic effect was significantly enhanced against HPV+ and cancer organoids compared to healthy organoids in the presence or the absence of bromohydrin pyrophosphate (BrHPP), a synthetic phosphoantigen which activates Vγ9Vδ2 T. Moreover, the BrHPP dependent cytotoxic effect was found strikingly to be reduced to the level in non-activated Vγ9Vδ2 T group with the blockade of butyrophilin-subfamily members (BTN3A, BTN2A1). Besides, CD107a over-expression was also associated with BrHPP stimulation. Both pieces of evidence indicated the BTN-subfamily members were mainly responsible for the cytotoxic effect with BrHPP activation and the self-active Vγ9Vδ2 T cells induced indiscriminate killing against HPV+, cancer cells but also healthy cells via degranulation including granzyme B (GzmB), platelet-rich fibrin (Prf), interferon gamma (IFNγ) secretion. While the mechanism of the specific cytotoxicity against HPV+ and cancer organoids in the BrHPP absence condition still remained vague. I concluded based on the bioinformatic analysis of multi-omic data that the differential recognition of non-healthy cells by Vγ9Vδ2 T cells depends on multiple-ligand interactions, which should be further explored in the future.

Overall, within my thesis project, stable patient-derived cervical organoid lines were established, which acted as a promising *in vitro* model for screening cervical cancer-associated epitopes and for exploring T cell-induced cytotoxic effects. Thus, the organoid-T cell coculture model that I established could prove useful for testing additional modulators (e.g. small molecules, antibodies, tumor sensitizers, etc.). Consequently, my investigations on the Vγ9Vδ2 T-mediated killing effect against HPV-transformed cervical cancer cells have shed light on the potential future utilization of Vγ9Vδ2 T in clinical settings.

ZUSAMMENFASSUNG

Gebärmutterhalskrebs ist eine der häufigsten Krebsarten bei Frauen, und das Verhältnis von Mortalität zu Inzidenz (MIR) von Gebärmutterhalskrebs variiert zwischen entwickelten und sich entwickelnden Regionen: Nordamerika hatte das niedrigste MIR (0,36), gefolgt vom MIR in Europa (0,40), während Afrika das höchste MIR (0,68) hatte. Die Infektion mit humanen Hochrisiko-Papillomviren (HR-HPV) ist der wichtigste Auslöser für Gebärmutterhalskrebs, doch trotz Beginn einer chronischen HR-HPV-Infektion benötigen infizierte Gebärmutterhalszellen noch viele Jahre, um sich als Krebszellen zu manifestieren. Da 90% der ausbleibenden Behandlungserfolge auf Arzneimittelresistenz zurückzuführen sind, ist die Entwicklung neuer wirksamer Therapien dringend geboten. Zahlreiche neue Therapieansätze müssen jedoch wegen unbefriedigender Wirksamkeit von Medikamenten in der klinischen Prüfung eingestellt werden, was die aktuelle Problematik der präklinischen Medikamentenentwicklung widerspiegelt. Daher wird nun der Entwicklung präziser In-vitro-Modelle zum Screening und der Bewertung der therapeutischen Wirksamkeit neuer Medikamente gegen Gebärmutterhalskrebs vermehrt größere Bedeutung zugeschrieben.

In der vorliegenden Studie wurden Organoide des Gebärmutterhalses von Krebspatientinnen gewonnen und unterschiedlichen Analysen unterzogen. Dabei wurden mittels RNA-Sequenzierung und HLA-restringierter Peptidom-Sequenzierung dysregulierte Gene, biologische Prozesse und HLA-präsentierte Epitope in HPV-transformierten und kanzerösen Organoiden des Gebärmutterhalses untersucht. Insgesamt wurden 6.515 HLA-Klasse-I- und 719 HLA-Klasse-II-restringierte Peptide ermittelt, deren Immunogenität anschließend mit Hilfe öffentlicher, auf maschinellem Lernen basierender Methoden vorhergesagt wurde. Interessanterweise standen eine Reihe hochregulierter Gene und immunogener Epitopen in HPV+ und Krebsproben in Bezug zu DNA-Reparatur-Prozessen. Im Folgenden wurde daher die Rolle der mit der DNA-Reparatur verbundenen Moleküle bei der Therapie und Prognose von Gebärmutterhalskrebs genauer untersucht. So konnte ich auf der Basis öffentlicher Datensätze des Cancer Genome Atlas Program (TCGA-CESE) von Gebärmutterhalskrebs einen DNA-Reparatur-bezogenen Genscore (DRGscore) erstellen und dabei eine negative Korrelation zwischen dem DRGscore und der Prognose von Gebärmutterhalskrebs feststellen. In der Tumormikroumgebung von Patienten mit einem niedrigeren DRGscore wurden mehr Immuneffektoren und weniger Immunsuppressoren festgestellt, was auf eine negative Korrelation zwischen DRGscore und Empfindlichkeit gegenüber einer Immuntherapie hindeutete. Dieses Ergebnis könnte Anhaltspunkte für die medikamentöse Behandlung der Patienten liefern: Patienten mit hohem DRGscore könnten von DNA-Reparaturinhibitoren profitieren, um die Resistenz gegen Chemoradiotherapie zu verringern und eine bessere

Prognose zu erhalten. Patienten mit niedrigem DRGscore hingegen könnten empfindlich auf verschiedene Immuntherapien wie Immun-Checkpoint-Inhibitoren und adoptive T-Zell-Therapie reagieren.

Aufgrund der HPV-Infektion und der genomischen Integration des viralen Genoms befinden sich HPV+- und Gebärmutterhalskrebszellen grundsätzlich in einem Stresszustand, was zu einer Anhäufung intrazellulärer Phosphoantigene (pAgs) führt, die von Vγ9Vδ2-T-Zellen auf HLA-unabhängige Weise erkannt werden können. Unter den DNA-Reparaturfaktoren der Wirtszellen werden einige von HPV für die Replikation genutzt, was die Bildung potenzieller Liganden für die Erkennung durch Vγ9Vδ2-T-Zell-Rezeptoren begünstigen könnte. Um diese Hypothesen zu überprüfen, untersuchte ich die zytotoxische Wirkung von Vγ9Vδ2-T-Zellen gegen HPV-transformierte Zellen und Gebärmutterhalskrebszellen anhand meines Gebärmutterhals-Organoidmodells. In Gegenwart von Bromhydrinpyrophosphat (BrHPP), einem synthetischen Phosphoantigen für Vγ9Vδ2 T-Zellen, war die zytotoxische Wirkung gegen HPV+ und Krebsorganoide im Vergleich zu gesunden Organoiden erhöht. Jedoch wurde die BrHPP-abhängige zytotoxische Wirkung durch eine Inhibition von Mitgliedern der Butyrophilin-Unterfamilie (BTN3A, BTN2A1) auf das Niveau der nicht aktivierten Vγ9Vδ2 T-Gruppe deutlich reduziert. Andererseits korrelierte die Überexpression von CD107a mit der BrHPP-Stimulation. Beides deutet darauf hin, dass für die zytotoxische Wirkung der BrHPP-Aktivierung insbesondere die Mitglieder der BTN-Unterfamilie verantwortlich sind und die selbstaktiven Vγ9Vδ2-T-Zellen über Degranulation, einschließlich Granzyme B (GzmB), plättchenreiches Fibrin (Prf) und Sekretion von Interferon gamma (IFNγ), eine unspezifische Abtötung von HPV+, Krebszellen, wie auch gesunder Zellen bewirken. Demgegenüber war der Mechanismus der spezifischen Abtötung von HPV+ und Krebsorganoiden in Abwesenheit von BrHPP weniger offensichtlich. Meine bioinformatische Analyse von Multi-Omicdaten lässt mich jedoch vermuten, dass die unterschiedliche Erkennung gesunder und nicht-gesunder Zellen durch Vγ9Vδ2-T-Zellen auf einer multiplen Interaktion mit Liganden beruht, was jedoch in zukünftigen Studien belegt werden müsste.

Insgesamt konnte ich im Rahmen meines Dissertationsprojekts stabile Organoidlinien von Gebärmutterhalskrebs-Patienten etablieren, die als vielversprechendes In-vitro-Modell für das Screening von Gebärmutterhalskrebs-assoziierten Epitopen und die Analyse der zytotoxischen Aktivität von T-Zellen dienen. Darüber hinaus könnte sich das von mir etablierte Organoid-T-Zell-Kokulturmodell als nützlich erweisen, um zusätzliche Modulatoren zu definieren, wie etwa kleine inhibitorische Moleküle, Antikörper und Tumorsensibilisatoren. So gelang mir der Nachweis einer zytotoxischen Funktion von Vγ9Vδ2 T-Zellen auf HPV-transformierte Gebärmutterhalskrebszellen wie auch eine partielle Aufklärung zugrundeliegender

Mechanismen, womit ich einen Weg für zukünftige klinisch-therapeutische Anwendungen aufzeige.

2 INTRODUCTION

2.1 The uterine cervix anatomy and physiology

The cervix is a conical fibromuscular organ located at the lower end of the uterus, an essential part of the female reproductive tract. Usually, the diameter of the cervix is about 2.5 cm, and the length is about 3 cm. The cervix consists of two parts: the endocervix, also called the endocervical canal, is the tube-like connection between the uterus and the vagina; the ectocervix is the lower part of the cervix that extends into the vaginal canal. The internal opening (internal os) is located internally and opens into the uterus, while the external opening (external os) is the opening located at the end of the ectocervix (Figure 1) (Standring et al.,2005). There is a transformation zone between the endocervix and the ectocervix, where cervical metaplasia usually occurs (Chumduri et al.,2021). The histology of the endocervix and ectocervix differs significantly, and various theories have been proposed for the origin of different cervical epithelial cells. Besides stroma, cell types of ectocervix are significantly more complex than those of the endocervix. The ectocervical epithelium is a stratified squamous epithelium consisting of basal, parabasal, intermediate, and superficial squamous epithelium, and the endocervical epithelium is a monolayer columnar epithelium (Figure 1) (Standring et al.,2005). The development of the transformation zone (TZ) concept is based on the mutual transformation of these two types of epithelia, which is essential to understand the high incidence of cervical carcinogenesis in the TZ (Fritsch et al.,2021).

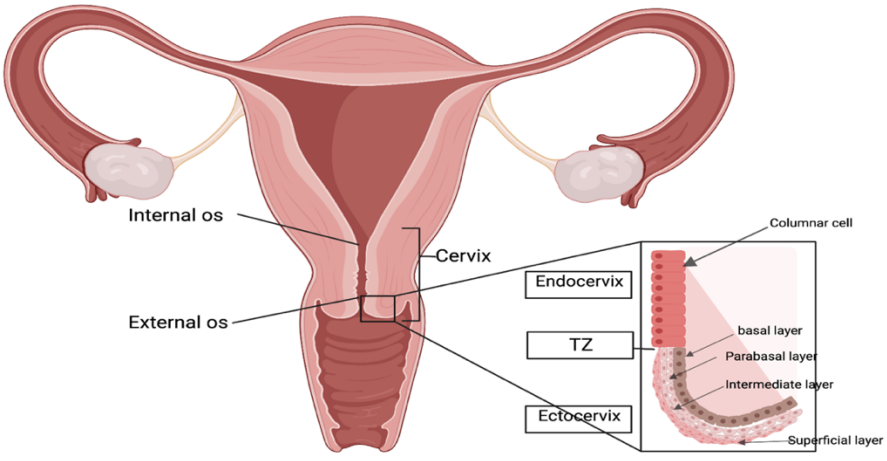

Figure 1. Anatomy and histology of the human cervix. The cervix is located in the pelvis and connects the uterus to the vagina. It consists of endocervix and ectocervix. The endocervix and uterus are separated by the internal os whereas endocervix and ectocervix are separated by the external os. The ectocervix is the lower part of the cervix that extends into the vaginal canal. The endocervix is lined

with columnar epithelium; the ectocervix is a stratified epithelium containing a basal layer, parabasal layers, intermediate and superficial layers. The transformation zone (TZ) is the area where columnar epithelium meets stratified squamous epithelium. (Created with BioRender.com. at MPIIB)

2.2 Cervical cancer onset and treatment landscape

2.2.1 Epidemiology, histology, and FIGO stage of cervical cancer

The International Federation of Gynecology and Obstetrics (FIGO) CANCER REPORT 2021 shows that cervical cancer is the fourth most common cancer in women worldwide (Bhatla et al.,2021). In recent decades, with the development and widespread use of the HPV vaccine, cases of cervical cancer have declined in many countries. However, Knaul et al. stated that “cervical cancer is not a disease of the past, it is a disease of the poor”, which is confirmed by the differences in morbidity and mortality rates between developing and developed countries (Knaul et al.,2019). Approximately 85% of new cases and 90% of deaths occur in low- and middle-income countries that lack effective intervention programs (Bhatla et al.,2021).

There are ten critical histologic subtypes of cervical cancer, among which squamous cell carcinoma and adenocarcinoma are the most common types, both of them are highly associated with persistent infection with high-risk oncogenic HPV (HR-HPV) (Campos-Parra et al.,2022). About 30 HPV types can be transmitted through sexual contact and HR-HPVs including genotypes 16,18, 59, 58, 52, 45, 35, 33, 31 are mainly involved in cervical cancer (Okunade,2020;Serrano et al.,2015). HPV16 and HPV18 induce about 70% of cervical cancers (Ramakrishnan et al.,2015). Most cervical cancers originate from the TZ between the endocervix and ectocervix, where HR-HPV infection most commonly occurs. HR-HPVs usually infect the basal cells of the cervix first, and early HPV infection causes low-grade cervical intraepithelial neoplasia (CIN 1-2) that resolves spontaneously within 1-2 years, however, the risk of developing CIN3 and cervical cancer increases within 10-15 years if left untreated (Venkatas and Singh,2020). There are four clinical stages of cervical cancer, depending on where the cancer has spread: the carcinoma strictly limited to the cervix is defined as the stage I; the stage II is a carcinoma that extends beyond the cervix and does not reach the wall of the pelvis; when the lower third of the vagina and/or the pelvic wall is involved, the stage III is defined; the stage IV is the most severe stage that the lesion has invaded the actual pelvis or clinically involves the bladder and/or rectal mucosa (Sobin et al.,2011) (Bhatla et al.,2021).

2.2.2 HPV carcinogenesis and DNA damage repair

Human papillomaviruses (HPVs) are a group of prevalent, sexually transmitted, dsDNA viruses that contains six early and two late genes (E1, E2, E4, E5, E6, E7, L1, and L2) (Hong and Laimins,2013). The subtypes of HPV are identified by L1 gene diversity. Among the most cervical cancer-relevant HPV genotypes, HPV16 is the highest-risk genotype, followed by HPV18 based on its oncogenic potential (Bordigoni et al.,2021;Fan et al.,2020;Layman et al.,2020). To establish a productive infection, HPV infection normally originates from basal cells and integrates its viral DNA into the host genome, which results in genome instability through different molecular pathways and induces double- or single-stranded breaks that recruit DNA repair activities leading to chromosomal rearrangement and prompting cell transformation (Gusho and Laimins,2021). Oncogenic proteins E6 deregulates the cell cycle via p53 and E7 mediates Rb degradation thus removing some of the ‘brakes’ on replication (Prati et al.,2018). The host cell replication and DNA repair are exploited by HPV for its own survival and replication. DNA repair processes were vigorous during cervical malignant transformation, thus DNA damage repair genes may act as potential targets for new therapeutic agents (Helleday et al.,2008;Prati et al.,2018).

In HPV-positive cells, the molecular interplay between viral oncoproteins and the host cell's DNA repair machinery is intricately orchestrated to facilitate viral replication and persistence. (Ciccia and Elledge,2010). The stabilization and increased expression of topoisomerase II beta (TOP2β) are pivotal in this process, as they contribute significantly to the generation of DNA breaks that subsequently engage repair pathways (Kaminski et al.,2021; Gusho and Laimins,2021). These DNA lesions are predominantly repaired through homologous recombination, with rapid recruitment of repair factors such as RAD51 and BRCA1 to the viral episomes in differentiated cells (Mehta and Laimins,2018). Furthermore, the HPV E7 protein is instrumental in the constitutive activation of the ataxia-telangiectasia mutated (ATM) pathway, which predominantly utilizes the non-homologous end-joining (NHEJ) pathway for DNA repair, alongside homologous recombination (Spriggs and Laimins,2017). In addition to ATM, the total and phosphorylated levels of ataxia telangiectasia and RAD3-related protein (ATR) and its downstream target, CHK1, are increased as well (Helt et al.,2005). The activation of ATM and ATR is further exacerbated by the concerted action of E6, E7, and E1 viral proteins, leading to the phosphorylation and assembly of a multitude of repair and signaling effectors, including γH2AX, TOP2β, TopBP1, and pBRCA1 (Sakakibara et al.,2013). This intricate network of interactions ensures the maintenance and amplification of viral episomes, with TopBP1 forming complexes with E2 and being upregulated by E7 in

conjunction with the immune signaling protein STAT5 (Donaldson et al.,2012; Hong et al.,2015).

Unlike cervical cancer, in many other types of cancer, DNA repair deficiency was definitely observed, which contributes to somatic alterations accumulation in DNA and induces the cancer transformation (Volkova et al.,2020). Somatic alterations, encompassing point mutations, insertions and deletions, chromosomal translocations, and segment losses drive oncogenesis by modifying tumor-suppressor genes. Recent insights have revealed that these genetic modifications not only contribute to the intrinsic characteristics of the tumor cells but also exert profound effects on the surrounding tumor microenvironment, thereby modulating the interplay between cancer cells and the immune system (Samstein and Riaz,2018). Notably, mutations in BRCA1 and DNA repair inactive signalings have been identified to upregulate the expression of immune checkpoint molecules, such as PD-1, CTLA-4, and LAG-3, on the surface of tumor cells, which is posited to enhance the susceptibility of cancer cells to immune checkpoint blockade therapies (Zhu et al.,2021). DNA repair-deficient tumors also recruited more infiltrating T cells and responded better to cytotoxic T cells due to hyperexpression of FAS on tumor cells leading to better prognosis (Xu et al.,2023). Besides immunotherapy, DNA repair inactive contributes to the sensitivity to chemotherapy and radiotherapy (Zhu et al.,2016). Chemotherapy resistance occurs in the short term when the tumor DNA breaks can be rapidly repaired, and it will promote tumor recurrence and metastasis (Mansoori et al.,2017). PARP inhibitor, a well-known DNA repair inhibitor, has shown a definite therapeutic effect against tumor with or without chemotherapy (Helleday et al.,2008). Overall, DNA repair disorder play a vital role in malignant transformation and contribute to HPV carcinogenesis. The DNA repair activities also interfere the anti-tumor effect of chemoradiotherapy, immunotherapy, and small molecule inhibitors.

2.2.3 Prevention and common treatment of cervical cancer

The HPV prophylactic vaccines are designed to protect people from infection of the most dangerous HPV genotypes, including HPV16, HPV18, and other seven genotypes. There are three types of HPV prophylactic vaccines have been launched: 9-valent HPV vaccine (Gardasil 9, against HPV 6, 11, 16, 18, 31, 33, 45, 52, and 58), quadrivalent HPV vaccine (Gardasil, against HPV 6, 11, 16, 18), and bivalent HPV vaccine (Cervarix, against HPV 16 and 18) (Chatterjee,2014;Kavanagh et al.,2017). It is discovered that the vaccines can protect people from not only cervical cancer, but also head and neck cancer and benign genital warts. Clearly, boys also benefit from government HPV vaccine programs (Tsang et al.,2020). Clinical trials have shown that 9 valent HPV vaccine and quadrivalent HPV vaccine are nearly 100% effective in preventing reproductive infections and pre-cancers caused by the HPV types

they target, and the protection can last for at least 6 and 11 years respectively (Huh et al.,2017;Kjaer et al.,2018). The development of cervical cancer is a long-term and complex process, thus it is essential to participate in regular cytology and HPV testing to detect prevalent cervical precancerous lesions (Bhatla et al.,2021). Additionally, smoking cessation and avoidance of high-risk sex reduce the risk of cervical cancer (Shepherd,2000).

FIGO Cancer Report 2021 updated the treatment guideline for cervical lesions (Bhatla et al.,2021) : conization and hysterectomy are regularly performed in patients with stage IA1- IA2; beyond stage IB1 to IIA2, radical hysterectomy is performed followed by concurrent chemoradiotherapy (CCRT) if there are high risk factors such as positive margin, positive lymph nodes, or microscopic parametrial involvement; beyond stage IIB, treatment depends on the para-aortic lymph node status, if the para-aortic lymph node is not involved by the original cancer, patients are treated with a combination of pelvic radiotherapy and concurrent chemoradiotherapy (CCRT), and if para-aortic lymph node metastasis is detected, para-aortic lymph node radiotherapy must be performed in addition to the combination treatment.

2.2.4 Immune checkpoint inhibitors

Tumor microenvironment (TME) consists of variable cell types and cytokines. Immune and non-immune cells including endothelial cells, cancer-associated fibroblasts are the main composition (Hanahan and Robert,2011). The immune effectors such as CD8+T cells, natural killer (NK) cells, and dendritic cells, inhibit tumor development and metastasis, while suppressive effectors such as regulatory T cells (Tregs), myeloid-derived suppressor cells (MDSCs), and tumor-associated macrophages (TAMs) protect tumor cells from clearance and inhibit the immune surveillance of immune effectors through immune checkpoints (Labani-Motlagh et al.,2020; Veglia et al.,2021). In past decades, a number of immunoreceptors suppressing immune response have been identified as “immune checkpoints” (Bernard et al.,2007). PD-1, CTLA-4, LAG3, TIM3, TIGIT and BTLA are the ones best known (Shi et al.,2021). To release the functions of immune effectors against tumors, the inhibitors of the immune checkpoints have been created to prevent the receptor-ligand engagement. The most commonly used inhibitors are the ones against PD-1/PD-L1 and CTLA-4 (He and Xu,2020).

Cytotoxic T-lymphocyte-associated protein 4 (CTLA-4), a CD28 subfamily member, serves as a critical inhibitory receptor on T-cells, which is upregulated upon activation (Buchbinder and Desai,2016). This receptor, alongside CD28, engages with CD80 and CD86 molecules present on antigen-presenting cells (APC), eliciting either costimulatory or co-inhibitory signals respectively. Notably, CTLA-4 exerts its inhibitory function by employing trans-endocytosis, a mechanism through which it internalizes CD80 and CD86 molecules, inclusive of their

cytoplasmic domains, from the APC surface (Phan et al.,2003;Qureshi et al.,2011). This process effectively precludes the interaction between CD28 and its ligands, thereby attenuating the costimulatory signals necessary for full T-cell activation. Ipilimumab, the anti-CTLA-4 monoclonal antibody, was the first checkpoint inhibitor to be approved and introduced into routine clinical practice (Wojtukiewicz et al.,2021). Ipilimumab was first approved for melanoma patients, which significantly extended the overall survival period (Jain and Clark,2015). As CTLA-4 is widely distributed on T cells, many severe side effects were caused by CTLA-4 inhibitors, including hepatitis, colitis and thyroiditis. And the therapeutic efficacy takes months to show (Tan et al.,2020). In addition to the usage of CTLA-4 in advanced melanoma patients, there are many ongoing clinical trials testing combination treatment of anti-PD-1/PD-L1 and anti-CTLA-4 in cervical cancer (Wolf and Xu,2023). It will be exciting to see the outcome.

Programmed cell death protein 1 (PD-1), also recognized as CD279, is another T cell surface checkpoint receptor predominantly involved in modulating cell death and immune homeostasis. The upregulation of PD-1 on tumor-specific circulating or tumor-infiltrating lymphocytes is associated with an attenuated functionality of these immune cell (Nishimura et al.,1999). This diminished functionality is attributed to the interaction between PD-1 and its cognate ligands, PD-L1 (CD274) and PD-L2 (CD273). These ligands are aberrantly expressed on the surface of antigen-presenting cells and tumor cells, engaging PD-1 and thereby initiating inhibitory signals that dampen T cell-mediated immune responses. They can also be upregulated by interferon (IFN)-γ and promote immune resistance and tumor evasion (Garcia-Diaz et al.,2017). PD-1 signaling interferes with early TCR/CD28 signaling and reduces the production of cytokines such as IL-2, IFN-γ, and tumor necrosis factor (TNF)-α. Bcl-xL gene expression and the expression of transcription factors involved in effector functions are also affected by PD-1/PD-L1 activity (Latchman et al.,2001;Nurieva et al.,2006;Tumeh et al.,2014). Blockade of PD-1 or PD-L1 has been identified as an effective way to enhance the anti-tumor response in a wide range of cancers (Brown et al.,2003;Jia et al.,2021).

2.2.5 Adoptive cell therapy

Adoptive cell therapies, including tumor-infiltrating lymphocyte therapy, engineered T-cell receptor (TCR) therapy, chimeric antigen receptor (CAR) T-cell therapy and natural killer (NK) cell therapy, are providing new options for cervical cancer patients (Kousar et al.,2022). Cellular therapies are designed to recognize heterogenetic epitopes on the surface of cancer cells.

The therapeutic potential of tumor-infiltrating lymphocytes (TIL) is underscored by their ex vivo expansion and subsequent reinfusion into patients as a form of adoptive immunotherapy, a technique that has shown promise in enhancing anti-tumor immune responses (Lee et al.,2017). TILs represent a heterogeneous ensemble of immune cells, including CD4+ and CD8+ T cells, γδ T cells, B cells, natural killer cells, and regulatory T cells (Tregs), which are naturally derived from the tumor microenvironment (TME) (Zemanek et al.,2023). These T cell subsets exert their positive and negative roles depending on their characteristics and ratios (phenotypic changes), which provide useful information for tumor progression and treatment prognosis (Kumar et al.,2021). The presence of CD8+ and CD4+ T cells within TILs is positively correlated with improved patient outcomes, with CD8+ cytotoxic T cells playing a pivotal role in the direct elimination of cancer cells through an HLA class I-dependent mechanism, while CD4+ T cells primarily function as helper cells to support CD8+ T cell activity (Riazi Rad et al.,2015). Conversely, Treg cells suppress the immune system from attacking tumor cells. Within cervical cancer studies, it was shown that the number of infiltrating CD8+ cytotoxic T cells is enhanced after treatments involving chemotherapy and immunotherapy (van Luijk et al.,2022). However, compared with healthy tissue, infiltrating CD8+ cytotoxic T cells become dysfunctional due to immune tolerance mechanisms employed by cervical cancer cells (Farhood et al.,2019). In addition, T helper 9 (Th9) cells are newly found subset with the capacity to enhance apoptosis and suppress proliferation of cervical cancer through its signatory cytokines IL-9 and IL-21 (Chauhan et al.,2019;Farhood et al.,2019).

Compared to TILs, TCR-T and CAR-T are the other two types of T cell therapies with genetically engineered receptors on the surface that can bind to specific tumor-associated antigens (TAAs). With TCRs (T cell receptors) and CARs (chimeric antigen receptors), the modified T cells can eliminate cancer cells by recognizing TAAs. The current mainstream of TCR-T and CAR-T preparation involves several steps: collection of the patient's peripheral blood mononuclear cells (PBMC), selection of the T cell population, followed by activation, and the transduction of target CAR or TCR chain gene; finally, the *in vitro* modified T cells are infused back into the patient. In the past three decades, CARs have been continuously optimized. The structure of CARs has evolved from the simple designation of the single CD3 intracellular domain to the addition of co-stimulators for enhanced proliferation and activation (Dotti et al.,2014). The risk of graft-versus-host disease (GVHD) against transplanted CAR-T cells has been reduced by knocking out the HLA and TCR genes of T cells (Tokarew et al.,2019). Compared to TCR-T, CAR-T cells are HLA-independent and directly bind surface-expressing antigens, which are taken as promising off-the-shelf adoptive T cell products (Kast et al.,2022). To date, CAR-CD19 and CAR-BCMA remain the dominant targets for liquid

tumors, while HER2, MSLN, GD2 and EGFR are the leading targets for solid tumors, including cervical cancer (Upadhaya et al.,2021).

T cell receptors (TCRs) are specific receptors that recognize the TAA peptides restricted to different human leukocyte antigen (HLA) allotypes. Therefore, the cytotoxicity of TCR-T mainly depends on the precise matching of TCR chains and peptide-HLA complex, leading to personalized autologous cell therapy (Baulu et al.,2023). Moreover, TCR-T cells recognize epitopes derived from not only membrane-bound TAA but also cytoplasmic TAA. Consequently, the potential of TCR-Ts dramatically outweighs that of CAR-Ts in the treatment of solid tumors (Jiang et al.,2019). Clinical and preclinical studies have shown that TCR-T recognizing HR-HPV E6 and E7 derived epitopes specifically kill cervical cancer cells without cross-reactivity to human self-peptides. This suggests that identification of HPV epitopes is essential for TCR-T manufacturing (Draper et al.,2015;Jin et al.,2018).

2.3 Tumor-associated antigens (TAAs) and tumor-specific antigens (TSAs) in cervical cancer

Tumor antigens could be generally summarized as two classes: tumor-associated antigens (TAAs) and tumor-specific antigens (TSAs). TSAs have no expression in normal tissues, while TAAs can be found in both tumors and normal tissues but are significantly over-expressed in malignant cells compared to non-malignant cells.

TAAs constitute a diverse array of molecules, including differentiation antigens (such as melanocyte differentiation antigens), overexpressed cellular antigens (such as HER2), viral antigens (such as human papillomavirus proteins), and cancer testis (CT) antigens (such as MAGE and NY-ESO-1) (Criscitiello,2012). Mutation-derived TSAs, also referred to as neoantigens, emerge from nonsynonymous genetic alterations such as single nucleotide variants (SNVs), insertions and deletions (indels), gene fusions, frameshift mutations, and structural variants (SVs) (Xie et al.,2023). The quality of the neoantigen depends on the position of the mutated peptide. If the mutation occurs in the anchor, the affinity to HLA will be influential, while the mutation outside the anchor affects the interaction with TCR (Baulu et al.,2023). In cervical cancer, the top 10 mutated genes were TTN (31%), PIK3CA (29%), KMT2C (19%), MUC16 (17%), MUC4 (16%), KMT2D (15%), SYNE1 (13%), FLG (13%), EP300 (13%), and DMD (13%), however, the use of genetic mutation information to identify the neoantigen landscape in cervical cancer remains limited (Akinyemi I Ojesina 1,2017;Ojesina et al.,2014;Qin et al.,2017). In addition to single nucleotide polymorphism (SNP), missense and other genomic mutations, there are some regulators that correlate with mutations and neoepitopes load (Wirth and Kühnel,2017). OVOL1 is one of regulators and

has validated the association with a higher expression of TGFB1 (Fan et al.,2022). The overexpression of TGFB1 affects immunosuppression and HLA expression (Rodriguez et al.,2023). In the network, OVOL1 also represses c-Myc transcription, leading to poor prognosis in cervical cancer (Liu et al.,2016). Neoepitopes are a rich source for the design of therapeutic cancer vaccines and TCR sequences for adoptive TCR-T cell therapy (Mahdavi and Moreau,2016;Wei et al.,2019). The number of neoepitopes is highly related to the tumor mutational burden (TMB), broadly defined as the number of somatic mutations per megabase of interrogated genomic sequence (Sha et al.,2020). It was interesting to find a positive correlation between neoepitopes load and immune checkpoint expression, and the patients with high TMB are always more sensitive to immune checkpoint inhibitors (Marabelle et al.,2020).

In addition to neoepitopes, HPV-derived peptides are specific immunogenic peptides of HPV-associated cancer such as cervical cancer. The overexpression of E6 and E7 in HPV-infected host cells opens the possibility of finding E6/E7 derived epitopes that can be recognized by cytotoxic CD8+ T cells leading to the infected cell clearance (Vonsky et al.,2019;Xie et al.,2023). Due to the deletion of the open reading frames (ORFs) encoding E1, E2, E4, E5, L1, and L2 proteins, it is unlikely to find relevant immunogenic targets (Chabeda et al.,2018). In addition to HPV oncoprotein epitopes, DNA repair-relevant proteins overexpressed in HPV-transformed and cervical cancer were another group of potential tumor-associated antigens in cervical cancer. After synthesis of the TSAs and TAAs, a fraction of the resulting protein is processed by the proteasome and lysosomes into peptides. These peptides are transported to the endoplasmic reticulum via the TAP transporter, where they are loaded onto HLA-I molecules for presentation on the cell surface. The peptides with high affinity and tight TCR interaction can lead to the recognition of T cells with anti-tumor activity (Cordeiro et al.,2018;Trimble et al.,2015;Wong et al.,2016) (Figure 2). Epitope presenting process is complex, and any mistakes can result in the failure of foreign epitopes presenting, which is exploited by tumor cells to escape from immune surveillance. It was observed in clinical trials that central T cell tolerance may contribute to the suboptimal T cell responses against TAAs (Xie et al.,2023), thus it is vital to develop strategies that augment the immune response against TAAs, including not limited to combination usage cytokine support, toll-like receptor (TLR) agonists, costimulatory signals, chemoradiotherapy, immunoregulatory modulation, adjuvants and vector-driven immunity (Leko and Rosenberg,2020;Sahin et al.,2020).

To identify the TAA or TSA derived peptides/epitopes, multi-omic analysis is one of the main tools to evaluate the dysregulated genes and their expression. However, the genome and transcriptome data cannot provide enough information to identify the sequence of the HLA-

restricted peptides. To meet this unmet need, the peptidome sequencing acquisition via mass spectrometry offers complementary information and improves accuracy of immunopeptidomics prediction with IEDB (the Immune Epitope Database) database and computational prediction tools such as NetMHC, NetMHCpan, MHCflurry, SYFPEITHI (Jiang et al.,2019;Okada et al.,2022;Wirth and Kühnel,2017). Nevertheless, predicting the precise immunogenic epitopes still faces challenges, such as the parameters for determining an HLA-peptide complex and the T-cell response cannot be confidently predicted through computational algorithms of the binding affinity and immunogenicity. Thus, robust *in vitro* and *in vivo* experiments are vital for preclinical validation.

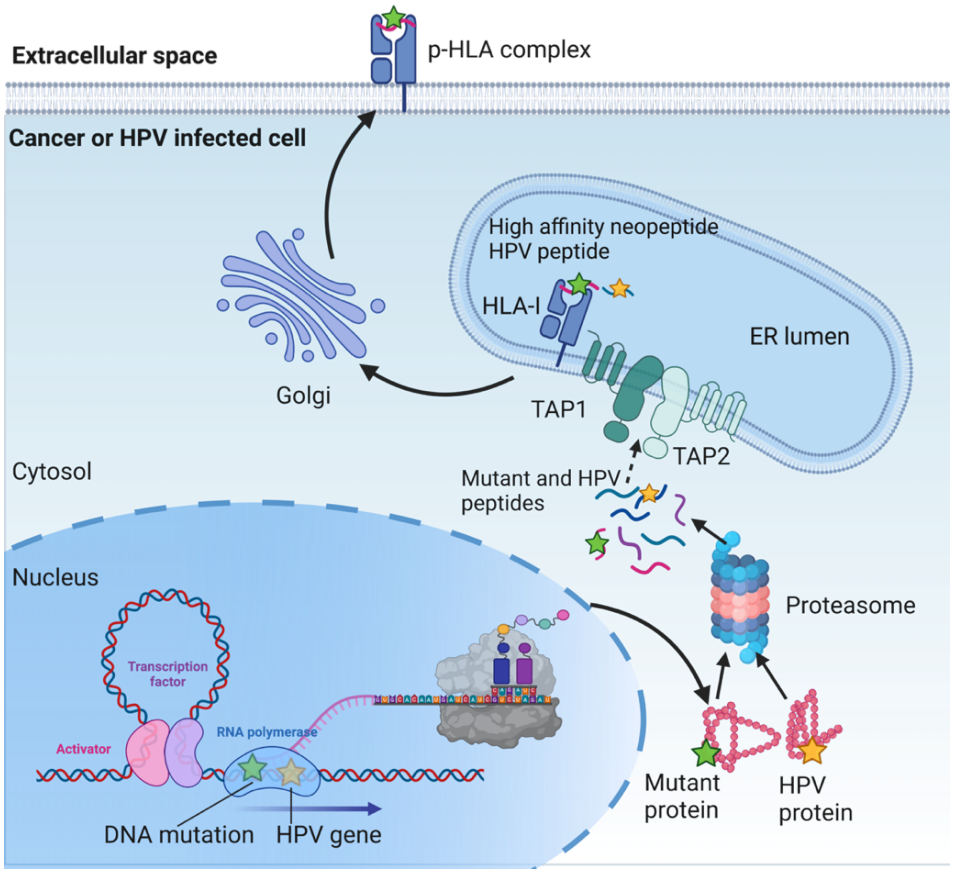

Figure 2. HLA-restricted peptides processing and presenting. In cervical cancer or HPV-transformed cells, the mutant and HPV integration sequences are first transcribed and translated. Thereafter, the resulting proteins are degraded via proteasome into neopeptides and HPV-peptides (HPV relevant peptides). The peptides are translocated into the endoplasmic reticulum (ER) through ATP-dependent activation of TAP transporters. In ER lumen, the mutant and HPV peptides are loaded on the HLA-I binding groove and followed by transport of the p-HLA complex via the Golgi apparatus to the cell surface. (Created with BioRender.com. at MPIIB)

2.4 Vγ9Vδ2 T cell and its anti-tumor/infection efficacy

2.4.1 Vγ9Vδ2 T cells

γδT cells represent a distinct subset of T lymphocytes that deviate from the traditional αβ T cells by expressing T-cell receptors (TCRs) comprising γ and δ chains (Cordova et al.,2012). Like other cytotoxic effectors, γδT cells not only directly participate in the elimination of tumor cells, but also indirectly shape the tumor immune response by influencing the behavior of other immune cells (Macleod and Havran,2011;Toulon et al.,2009). In the human immune system, γδT cells are categorized into three predominant subsets: Vδ1 T cells are mainly found in mucosal tissues including skin, small intestine and uterus, Vδ2 T cells account for 1%-10% of CD3+ T cells in peripheral blood, and a small subset of Vδ3 T cells are located in the liver (Hudecek et al.,2021;Li et al.,2020;Raverdeau et al.,2019;Vallvé-Juanico et al.,2019). The proportion of circulating Vγ9Vδ2 T cells in healthy adults ranges from 0.5% to 10%, a figure that can escalate dramatically to 60% in response to infection (Chan et al.,2022).

Vγ9Vδ2 T cells can be activated and function by TCR-dependent recognition of non-peptidic phosphorylated antigens, called phosphoantigens. Bacteria can produce natural phospho-antigens such as I-4-hydroxy-3-methyl-but-2-enyl pyrophosphate (HMBPP) through the non-mevalonate isoprenoid pathway (Hintz et al.,2001). Phosphoantigens can also be generated by eukaryotic cells through the mevalonate-isoprenoid pathway, such as isopentenyl pyrophosphate (IPP) (Gober et al.,2003). Although endogenous phosphoantigens are weaker activators compared to HMBPP, they are secreted through the mevalonate pathway and stimulate the anti-tumor activities of Vγ9Vδ2 T cells (Gao et al.,2023). These properties make Vγ9Vδ2 T cells play a key role in tumor immune, underlining their potential as a therapeutic modality in anti-cancer treatments (Bonneville and Scotet,2006). Many clinical trials involving adoptive Vγ9Vδ2 T cells have corroborated the safety and feasibility of such therapeutic approaches. Vγ9Vδ2 T cells can be effectively expanded with *in vitro* stimulation using clinical approved agonists, and 10-33% of patients respond to Vγ9Vδ2 T cells with *in vivo* agonist stimulation (Buccheri et al.,2014;Gomes et al.,2010).

HLA-independent activation of Vγ9Vδ2 T cells minimizes the risk of alloreactivity in allogeneic Vγ9Vδ2 T cell therapies (Xu et al.,2021). A patient with stage IV cholangiocarcinoma with recurrent mediastinal lymph node metastases achieved a significant clinical response after receiving consecutive infusions of allogeneic Vγ9Vδ2 T cells from a healthy donor (Alnaggar et al.,2019). Another clinical trial of allogeneic γδ T cells against advanced pancreatic cancer shows that irreversible electroporation (IRE) can enhance the efficacy of allogeneic γδ T cells and reduce immunosuppression (Lin et al.,2020). In addition to their anti-tumor function,

Vγ9Vδ2 T cells can also have immunosuppressive effects on the efficacy of the cytotoxic response. Upon activation, Vγ9Vδ2 T cells can display a Th1-, Th2-, Th17-, or Th1/reg-like profile and synthetize IFN-γ, IL-4, IL-17 or IL-10, and TGF-β, resulting in inhibition of T cell proliferation (Kühl et al.,2009;Lafont et al.,2014).

2.4.2 Molecules interacting with Vγ9Vδ2 T cell receptors

The generation of T-cell receptors (TCRs) in γδ T cells is a sophisticated process that occurs in the thymus, involving somatic rearrangements of the genes encoding the TCR δ chain variable (V), diversity (D), joining (J) segments, in addition to the V, J, and constant (C) gene segments of the TCR γ chain (Sherwood et al.,2011). This intricate genetic recombination potentially gives rise to an immense repertoire of γδ TCRs, with estimates suggesting up to 10^{17} distinct specificities (Sebestyen et al.,2020). Despite this theoretical diversity, human γδ T cell population can be categorized into two major subsets based on their TCR Vδ chain utilization: Vδ2+ subsets, commonly paired with the Vγ9 chain, while Vδ2- subsets exhibiting a broader range of Vγ chain usage (Janeway Jr et al.,2001). Tumor cells with accumulation of IPP phosphoantigen can be directly recognized by Vγ9Vδ2 T via Vγ9Vδ2 TCR (Adams et al.,2015). Butyrophilins (BTN) belong to the B7 family and their genes are situated at the telomeric region of the MHC complex on chromosome 6 and are integral to the modulation of immune responses. Four key molecules of the BTN family are BTN2A1, BTN3A1 (CD277), BTN3A2, and BTN3A3 (Herrmann et al.,2020). They perform a wide range of functions including immunomodulation and contribute to the Vγ9Vδ2 T cell activation (Karunakaran et al.,2020). One intensively studied molecule is BTN3A1; the binding of phosphoantigens (pAgs) to its cytoplasmic B30.2 domain initiates a cooperative mechanism between BTN2A1 and BTN3A1, leading to the formation of a plasma membrane-exporting complex. BTN3A2 can assist and increase the export of BTN3A1 to the plasma membrane (Uldrich et al.,2020). BTN2A1-associated Vγ9Vδ2 T cell cytotoxicity was found to be dependent on plasma membrane exposure. The exposure of BTN2A1 on the cell surface, quantified by the extracellular to intracellular ratio, is significantly modulated by the co-expression of BTN3A1 (Herrmann et al.,2020). Phosphoantigens derived from the mevalonate or non-mevalonate pathway bind to the intracellular B30.2 domains of BTN3A1 in tumor or pathogen-infected cells, followed by the conformational change of BTN3A1 and promote the interaction of BTN2A1 and BTN3A1 intracellular domains, which activate Vγ9Vδ2 T cell by Vγ9 chain binding to BTN2A1 (Karunakaran et al.,2020;Sandstrom et al.,2014). The expression of BTN3A1 and BTN2A1 on Vγ9Vδ2 T cells facilitates a form of self-activation in the presence of extracellular phosphoantigens (pAgs) without the intervention of APCs or target cells (Giannotta et al.,2023). This autonomous activation pathway bypasses the conventional need for APC intervention, highlighting a unique aspect of Vγ9Vδ2 T cell biology. Furthermore, the engagement of the T

cell receptor (TCR) on Vγ9Vδ2 T cells with molecules such as human MutS homolog 2 (hMSH2) initiates a cascade of events leading to the secretion of Th1 cytokines, including tumor necrosis factor-α (TNF-α) and interferon-γ (IFN-γ), as well as the release of pro-apoptotic granzyme B and perforin-containing cytolytic granules, which are essential for their cytotoxic function (Fichtner et al.,2020;Karunakaran et al.,2020;Willcox et al.,2019;Yang et al.,2019). In addition to BTN molecules, F1-ATPase on tumor cells can bind to the adenylated form of IPP, contributing to the activation of Vγ9Vδ2 T cells and their anti-tumor activity (Mookerjee-Basu et al.,2010). Besides the ligands that interact with the TCR, there are other ligands on Vγ9Vδ2 T that are responsible for tumor recognition and cytotoxicity (Figure3).

The NKG2D receptor belongs to nature killer receptor (NKR), which is expressed by γδ T cells. It can bind to stress-induced MHC class I chain-related antigens A and B (MICA/MICB) and ULBP families on tumor cells, which efficiently trigger the release of IFN-γ and TNF-α and promote the direct anti-tumor functions of γδ T cells (Kong et al.,2009). In particular, the ULBP families have been implicated in the recognition by Vγ9Vδ2 T cells of not only blood cancers, but also solid tumors such as ovarian and colon cancers. For example, ULBP1 and ULBP4 expression levels determine the susceptibility of lymphomas and solid tumors to γδ T cell-mediated cytolysis upon NKG2D binding (Lança et al.,2010). DNAM-1 (also called CD226) has been detected on the surface of several tumors, which is another NKR involved in regulating the cytotoxic activity of γδ T cells (Toutirais et al.,2009). Recognition between different receptors and ligands leads to activation, a robust immune surveillance process, and elicits a swift γδ T cell immune response. This γδ T cells activation exhibits cytotoxic properties, enabling them to directly target and destroy infected or malignant cells. Concurrently, they secrete a plethora of cytokines and chemokines to exert immunomodulatory properties and to interact with the network of immune cells, including αβ T cells, B cells, dendritic cells, macrophages, monocytes, natural killer cells, and neutrophils, to strongly influence the outcome of immune responses (Chan et al.,2022). (Figure3)

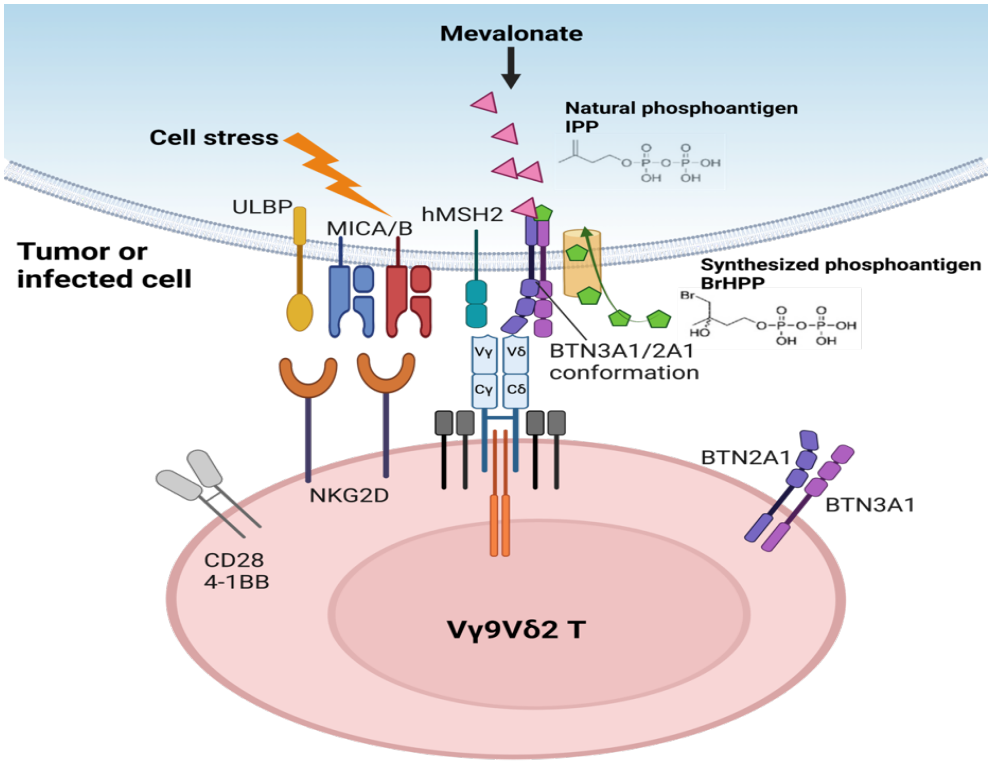

Figure 3. Ligands interaction and activation of Vγ9Vδ2 T cell. Cancer or infected cells under stressful conditions can lead to MICA/B and ULBP overexpression and phosphoantigens (such as IPP) accumulation. BrHPP, a synthesized phosphoantigen can be transported into epithelial cells via a transporter. Both IPP and BrHPP can bind to the BTN3A1 intracellular domain and induce the conformation changes of BTN3A1 and BTN2A1 complex that interact with TCR of Vγ9Vδ2 T, which activate Vγ9Vδ2 T. Because of the BTN3A1 and BTN2A1 expression on Vγ9Vδ2 T cells, BrHPP can induce the self-activation of Vγ9Vδ2 T cells. Besides BTN-family, NKG2D on Vγ9Vδ2 T cells can mediate activation via MICA/B and ULBP on APC or target cells. hMSH2 is another ligand activating Vγ9Vδ2 T via binding to TCR. (Created with BioRender.com. at MPIIB)

2.5 Cervical organoids: a potent *in vitro* model for research and medicine discovery

2.5.1 From traditional cell culture to organoids

In the preclinical phase of drug discovery, cell lines and animal models have been the most commonly used and important models. However, even when a new drug has shown robust efficacy in the preclinical phase, an extremely high failure rate is frequently encountered at the clinical phase (Atkins et al.,2020). This problem has prompted researchers to rigorously examine new preclinical models. To compensate for the cell line models, Meritxell Huch tried the long-term culture of primary and liver stem cells, which retain the genetic features of the particular individual, but still lack the original morphological information of the parent tissue (Huch et al.,2015). With regards to it, several 3D *in vitro* models were consequently developed

and their adequate translatability to the clinic was exploited (Antill-O'Brien et al.,2019; Ozcelikkale et al.,2017;Horvath et al.,2016)

Over the last two decades, organoids established by Hans Clevers, have been developed into a potent tool for drug discovery (Clevers et al.,2014;Nakamura and Sato,2018). Organoids can be cultured from either induced pluripotent stem cells (iPSCs) or organ-specific adult stem cells with a growth factor cocktail that can maintain undifferentiated stem cells in the basal layer, while inducing differentiation into various specific cell types to reaggregate and replicate the architecture of the original tissue. The first generation of organoid models consisted only of epithelial cells, and reproduced the epithelial structure of the tissue without stromal, vascular and immune cells (Zhao et al.,2022). This shortcoming has been overcome by developing various co-culture models and recapitulating the interplay between different cells and even unraveling host tissue-pathogen interactions (Pollen et al.,2023). The next generation of advanced organoid-based model is the organoid chip, which integrates multiple organoids on a single chip (Zhao et al.,2022). This chip, which can reproduce the functions of organs of the whole body, opens up a wide range of basic translational and clinical research prospects, such as deciphering the heterogeneous composition of tissues and measuring not only the drug effect but also the side effects for other important organs (Liu et al.,2021;Vunjak-Novakovic et al.,2021). Organoids are also amenable to cutting-edge experimental technologies such as CRISPR-Cas9 gene editing and can be efficiently subjected to live imaging (Mboko et al.,2022;Saorin et al.,2022).

2.5.2 Cervical organoids and their applications

Cervical organoid cultures, especially cervical cancer organoid, can be generated from adult stem cells of cervical tissue biopsies and resections. To maintain long-term stemness, a fibroblast feeder layer providing stromal signals, is used to support the cervical adult stem cells isolated from cervical tumors (Llames et al.,2015). After harvesting, adult stem cells are capable of further differentiation and organoid formation with proper growth factors (Liu et al.,2020;Zhao et al.,2022). The histological structure of cervical organoids derived from the same piece of tissue can vary significantly and represent the parental histology features: ecto-cervical organoids contain mainly stratified squamous layers, while endo-cervical organoids show the characteristics of columnar monolayer (Chumduri et al.,2021). Chumduri et al. generated long-term expandable organoids from ecto- and endo-cervical tissues in the presence or absence of Wnt agonists, primarily demonstrating the Wnt independence of the ecto-cervical organoid culture (Chumduri et al.,2021). They showed differentiation potential toward an ectocervical phenotype, including cell movement from the basal to superficial layers, accompanied by cell differentiation and flattening (squamification) by activating the CAMP

pathway (Chumduri and Turco,2021). The squamous stratified epithelium is characterized by the expression of cytokeratins including KRT5, KRT14 and KRT17, which are distinct from those that characterize the endocervix epithelium such as KRT8, KRT7, and KRT18 (Chumduri et al.,2021;Herfs et al.,2012). The endo- or ecto-cervical organoids can not only recapitulate the histological structure but also faithfully replicate the original tissue gene expression pattern as determined by their gene expression profiles (Chumduri et al.,2021;Lõhmussaar et al.,2020). This indicates that cervical organoids can be employed for some types of analyses that require large numbers of cells with faithful replication of original heterogeneous tissue. It furthermore indicates that organoids can be confidently used as an *in vitro* model for the investigation of immunotherapeutic co-culture and infection.

Organoids are increasingly being utilized in medicine discovery. It has been reported that colorectal cancer patients derived organoids have been used for the cytotoxic effect evaluation of CAR-NK92 (Yuki et al.,2020). This organoid-immune cell co-culture system could be used to evaluate the discriminate response of T cell with different CARs against normal or cancer organoids. Co-culture of patient-derived tumor organoids with autologous TILs mimics the *in vivo* process of TIL migration to the tumor, meanwhile TIL tumor cytotoxic function can be tested as well (Kong et al.,2018). Furthermore, organoids also represent a potential *in vitro* model to validate the function of checkpoint inhibitors (e.g., PD-1, CTLA-4, LAG-3, TIM-3, and VISTA) and the efficacy of combinatorial treatments conducted in clinical immunotherapy trials (Noordhoek et al.,2016;Xinaris et al.,2015). The effects of hormones on cervical biology were studied by treating cervical organoids with hormones and a functional response to estrogen and progesterone was observed, which replicates *in vivo* changes of cervix during pregnancy and the menstrual cycle (Alzamil et al.,2021). In addition to acting as an immune responder, organoids can reflect the host's response to a microbial invasion. Stefanie Koster et al. modeled the co-infection of HPV and Chlamydia with cervical organoids and revealed the transcriptome changes induced by HPV and/or Chlamydia invasion (Koster et al.,2022). Their global transcriptomic analysis demonstrated that HPV E6E7 and C. trachomatis elicit distinct host cell transcriptional programs promoting stemness and preneoplastic molecular phenotypes (Koster et al.,2022). Overall, the organoid system thus exerts an important tool for revealing carcinogenic or disease mechanisms and new medicine discoveries (Figure 4).

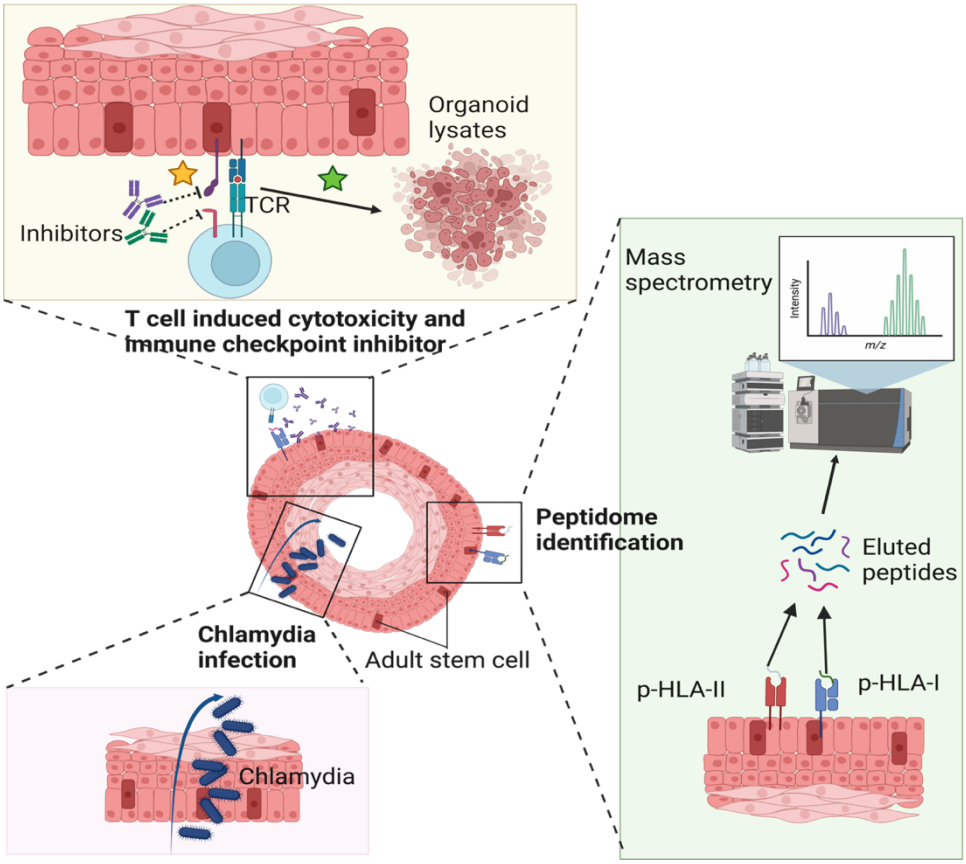

Figure 4. Ectocervical organoid and application. The ectocervical organoid resembles the *in vivo* structure of the ectocervix. The adult stem cell is located in outside layers, thereafter the stem cells initiate differentiation towards inside layers. Faithful recapitulation of the cervical tissue molecular heterogenicity suggests the possibility of tumor-associated antigens (TAA) screening based on cervical organoids. The TAA peptides can be identified by analyzing eluted HLA-restricted peptidome in organoids. The *in vivo* process of chlamydia invasion and infection of the cervix can be also mimicked in the cervical organoid model. The organoid-T cell coculture model can be effectively utilized for the killing effect and immune checkpoint modulation evaluation. (Created with BioRender.com. at MPIIB)

2.6 Goals of the thesis

The cervix is essential for protecting the upper reproductive system from infection and other extrinsic risks. Its function is also important for fertilization and embryo development. Cervical lesions are mainly caused by HPV and other sexually transmitted bacteria such as Chlamydia trachomatis. Cervical cancer is a persistent, high-risk, HPV-associated disease. To deeply explore the mechanism of infection and carcinogenesis of the cervix, Thomas F. Meyer, Cindrilla Chumduri, and the colleagues successfully established cervical organoid models, which constituted the basis of this project.

The first aim of this project was to establish healthy, HPV+, and cancerous cervical organoids. Thereafter the recapitulation of *in vivo* architecture and molecular characteristics was described. The second aim was to detect tumor-associated antigens and epitopes in cervical cancer organoids through multi-omic analysis. The final objective was to establish a Vγ9Vδ2 T cell and organoids co-culture model for visualizing and evaluating cytotoxic effects against the healthy, HPV+, and cancerous cervical organoids and to provide a potent personalized tool for testing additional modulators in the future.

3 MATERIALS AND METHODS

3.1 Materials

3.1.1 Buffers and chemicals

Table 1. Buffers

buffer	component	concentration
Phosphate buffered saline (PBS)	NaCl	137 mM
	KCl	2.7 mM
	KH_2PO_4	1.8 mM
	Na_2HPO_4 x 2 H_2O	10 mM
	ad H_2O, pH 7.4	
PBST	PBS	
	Tween 20	0.05% (v/v)
Paraformaldehyde 3.7%	H_2O at 60°C	900 mL
	Paraformaldehyde	3.7g
	10xPBS	100 mL
	pH 7.4	
Tris-acetate EDTA buffer (TAE) (10x)	Tris base	242 g (40 mM)
	Acetic acid	57.1 mL (40 mM)
	0.5 M EDTA (pH 8.0)	100 mL (1 mM)
	ad H_2O	1 L
Tris buffered saline (TBS)	NaCl	137 mM
	KCl	2.7 mM
	Tris base	25 mM
	ad H_2O	
TBST	TBS	
	Tween 20	0.1% (v/v)
Immunofluorescence buffer (IFB)	BSA	1% (w/v)
	FCS	2% (v/v)
	Tween 20	0.1% (v/v)
	in 1xPBS, sterile filtered	
IF blocking buffer	BSA	3%
	Goat serum	1%
	Triton-X-100	0.2%
	Tween-20	0.1%
	in 1xTBS	

IF permeabilization buffer	glycine Triton X-100 Tween-20 in 1x TBS	0.1 M 0.2% 0.1%
IF washing buffer	Triton-X100 Tween-20 in 1x TBS	0.1% 0.2%
Collagenase Type II solution	collagenase II HBSS	100 mg 200 mL
Poly-HEMA solution	Poly (2-hydroxyethyl methacrylate) 100% Ethanol	1.4g 40 mL

Table 2. Chemicals

Chemical	**Cat. #**	**Manufacturer**
GeneRuler 1 kb DNA Ladder	SM0312	Thermo Scientific
Taq reaction buffer	B9014SVIAL	NEW ENGLAND BioLabs
Taq DNA Polymerase 5,000 Units/mL	M0273AVIAL	NEW ENGLAND BioLabs
GeneRuler 50bp DNA Ladder	SM0371	Thermo Scientific
MgCl2	A351H	Promega
DNA gel loading dye (6X)	R0611	Thermo Scientific
dNTPs	R0182	Thermo Scientific
LE agarose	840004	Biozym
Axygen® Sealing Film for Quantitative Real-Time PCR (qPCR)	800038	Stem Cell
SYBR® Green I	S9430-1ML	Sigma-Aldrich
Paraformaldehyde	P087	Carl Roth
2-Propanol	1.096.342.511	Merck

Ethanol	1.009.832.511	Merck
Target retrieval solution (10x)	S1699	Dako
Tris base	A1086.5000	AppliChem
Glycine	3908	Carl Roth
Triton-X100	3051	Carl Roth
Tris-Cl	9090	Carl Roth
NaCl	3957	Carl Roth
Tween-20	P9416	Sigma
EDTA	X986	Carl Roth
Goat serum	GOA-1A	Capricorn
SYBR™ Safe Nucleic Acid Gel Stain	S33102	Invitrogen
Fluoromount-G	SBA-0100-01	Southern Biotech
Hoechst 33342	H1399	Thermo Fisher
Bovine serum albumin (BSA)	3854	Carl Roth
Propidium iodide (PI)	25535-16-4	Sigma-Aldrich
Cell recovery solution	47743-696	Corning
Poly (2-hydroxyethyl methacrylate)	P3932-10G	Sigma-Aldrich

3.1.2 Cell culture reagents and media

Table 3. Cell culture reagents and supplements

Reagent	**Cat.#**	**Manufacturer**
Fetal Calf Serum	F7524-500ML	Sigma

DPBS	14190250	Gibco
Collagenase II (0.5 mg/mL)	C2-28	Biochrom
DMEM	10938-025	Gibco
Sodium pyruvate	S8636	Sigma
L-Glutamine	25030-024	Gibco
0.05% (wt/v) Trypsin-EDTA	25300-096	Gibco
Penicillin/Streptomycin	15070063	Gibco
RPMI 1640	11875093	Gibco
Collagen type I	C3867	Sigma
Matrigel	11543550	Corning
Cryo SFM	C-29910	Promo cell
Advanced DMEM/F12 (ADF)	12634	Gibco
Glutamax (100X)	35050-038	Gibco
HEPES	15630-056	Gibco
TrypLE Express	12604013	Gibco
Hydrocortisone	H0888-1G	Sigma
Forskolin	F6886	Sigma
N-Acetyl-L-cysteine	A9165	Sigma
Nicotinamide	N0636	Sigma
N2 Supplement 100x	17502048	Gibco
B27 supplement (50X)	17504044	Gibco
TGF-β inhibitor (A83-01)	Cay9001799	Cayman Chemicals

ROCK inhibitor (Y-27632 dihydrochloride monohydrate)	Cay10005583	Cayman Chemicals
Human Noggin	120-10C	Peprotech
Human EGF	AF-100-15	Peprotech
Human FGF10	100-26-25	Peprotech
Ficoll-Hypaque	Biocoll L 6113/5	Biochrom
Human IL-2	-	Novartis
Zoledronic acid	-	Novartis
Bromohydrin pyrophoshate (BrHPP)	IPH1101	Innate Pharma

Table 4. Cell culture media

Medium	**Components**	**Volume/Concentration**
ADF++	Advanced DMEM/F12	500 mL
	GlutaMax	5 mL
	HEPES	6 mL
D+++	DMEM	500 mL
	Na-pyruvate	5 mL
	L-Glutamine	5 mL
	hiFBS	50 mL
R+	RPMI1640	500 mL
	hiFBS	50 mL
R+++	RPMI1640	500 mL
	hiFBS	50 mL
	human IL-2	100 IU/mL
	zoledronic acid	50 uM
M5+FSK	ADF++	9.275 mL
	P/Strep 10000 U/mL	100 µl
	Hydrocortison (50 µg/mL)	100 µl
	hEGF(100 µg/mL) 1:10-10µg/mL	10 µl
	FGF10 (100 µg/mL)	10 µl

hNoggin (100 µg/mL)	10 µl
TGFbeta inhibitor-1000x (0.5 mM)	40 µl
NAC (500 mM)	25 µl
B27-50X	200 µl
N2 supplement- 100x	100 µl
Nicotinamid (NIC) 1 M	100 µl
Rock Inhibitor (3 mM)	30 µl
FSK stock (10 mM)	10 µl

3.1.3 Antibodies

Table 5. Antibodies

Primary antibody	**Cat.#**	**Manufacturer**	**Host**	**Reactivity**	**Application**	**Dilution**
Cytokeratin 5-Alexa488	ab193894	Abcam	rabbit	human	IF	1:300
EpCAM	2929S	Cell Signaling	mouse	human	IF	1:800
Ki67	ab16667	abcam	rabbit	human	IF	1:200
BTN3A1	ab236289	Abcam	rabbit	human	IF	1:100
HLA-ABC-PE	555553	BD Biosciences	mouse	human	FACS	1:150
PD-L1-APC	374513	Biolegend	mouse	human	FACS	1:20
Vγ9-AF488 (clone 7A5)	-	in-house	mouse	human	FACS	1:100
TCR Vδ2-FITC (IMMU 389)	IM1464	Beckman Coulter	mouse	human	FACS	1:100
CD107a-PE	555801	BD Biosciences	mouse	human	FACS	1:100
CD3-APC	340440	BD Biosciences	mouse	human	FACS	1:100
anti-BTN3A (clone 103.2) antagonistic mAbs	-	Imcheck	mouse	human	inhibitory	5 ug/mL

anti-BTN2A1 (clone 7.48) antagonistic mAbs	-	Imcheck	mouse	human	inhibitory	5 ug/mL
Secondary antibody						
IgG (H+L) AlexaFluor® 647	711-606-152	Dianova	Donkey	Rabbit	IF	1:150
IgG(H+L) Cy3	115-165-146	Dianova	Goat	Mouse	IF	1:150
Antibodies for immunoaffinity chromatography						
pan-HLA-I-specific antibody W6/32	In-house	University of Tübingen, Department of Immunology	-	-	immunoaffinity chromatography	-
HLA-DR-specific antibody L243	In-house	University of Tübingen, Department of Immunology	-	-	immunoaffinity chromatography	-
pan-HLA-II-specific antibody Tü39	In-house	University of Tübingen, Department of Immunology	-	-	immunoaffinity chromatography	-

3.1.4 Primers

Table 6. Primers for reverse transcription and quantitative PCR.

Gene name	Primer Sequence (5’ – 3’)
GAPDH (Koster et al.,2022)	F: 5’-GGT ATC GTG GAA GGA CTC ATG AC-3’
	R: 5’-ATG CCA GTG AGC TTC CCG TTC AG-3’
HPV16 (Herfs et al.,2012)	F: 5’-AGC TGT CAT TTA ATT GCT CAT AAC AGT A-3’
	R: 5’-TGT GTC CTG AAG AAA AGC AAA GAC-3’
HPV18 (Herfs et al.,2012)	F: 5’-CGA ACC ACA ACG TCA CAC AAT-3’
	R: 5’-GCT TAC TGC TGG GAT GCA CA-3’

All primers were obtained from Metabion or Sigma and diluted to 10 µM. Abbreviations:
F = forward, R = reverse.

3.1.5 Organoid lines and cell lines

Table 7. Organoid lines

Sample No.	HPV status	Disease/ clinical condition	Normal or diseased
hc40	Negative	Normal cervical tissue from an ovarian cancer patient undergoing radical hysterectomy	healthy
hc48	negative	Healthy Ecto and Endo	healthy
hc63	negative	Healthy hysterectomy strips	healthy
hc40e6e7	HPV16 positive	hc40 with HPV16 E6E7 oncogene integration	HPV positive
hc48e6e7	HPV16 positive	hc48 with HPV16 E6E7 oncogene integration	HPV positive
hc63e6e7	HPV16 positive	hc63 with HPV16 E6E7 oncogene integration	HPV positive
hc88	HPV16 positive	squamous cell carcinomas (SCC)	cancer
hc89	HPV16 positive	squamous cell carcinomas (SCC)	cancer
hc90	HPV16 positive	squamous cell carcinomas (SCC)	cancer
hc91	HPV18 positive	squamous cell carcinomas (SCC)	cancer

Table 8. Cell lines

Cell line	Source	Description
3T3-J2 cells	A kind gift from Craig Meyers; Howard Green laboratory, Harvard, University, RRID: CVCL_W667	Irradiated 3T3-J2 cells were used as fibroblast feeder cells for maintaining the stemness of cervical 2D stem cells
Daudi	ATCC	The Daudi cell line is composed of B lymphoblasts from a Burkitt's Lymphoma patient. It can be recognized and attacked by Vγ9Vδ2 T
End1/E6E7	ATCC	The endocervical cell line (End1/E6E7) consists of normal endocervical cells but with HPV16 E6E7 expression

HeLa	ATCC	HeLa is a cervical adenocarcinoma cell line which contains HPV18 sequence

3.1.6 Commercial kits

Table 9. Commercial kits and their application

Kit	**Cat.#**	**Manufacturer**	**Application**
QIAmp DNA Mini Kit	51306	QIAGEN	DNA extraction
AllPrep DNA/RNA Mini Kit	80204	QIAGEN	RNA and DNA extraction
CellTrace™ CFSE Cell Proliferation Kit	C34554	Invitrogen	Organoid tracing and labelling
NucRed™ Dead 647 ReadyProbes™ Reagent (TO-PRO-3 iodide)	R37113	Invitrogen	Viability assays
AB Power SYBR® Green RNA-to-CT™ 1-Step Kit	4389986	Thermo fisher	qRT-PCR
PKH67 Green Fluorescent Cell Linker Kit for General Cell Membrane Labelling	PKH67GL-1KT	Sigma-Aldrich	Cell membrane labelling

3.1.7 Software, instruments, consumables

Table 10. Software and applications

Software	**Company**	**Application**
Prism 9	GraphPad	Data processing
Excel 2019	Microsoft	Data processing
word 2019	Microsoft	Documentation
PowerPoint 2019	Microsoft	Presentation and image processing
ImageJ	Fiji/Open source	Image processing
StepOne Software v2.3	Thermo Fisher Scientific	RT-qPCR analysis
ZEN blue software v3.5	Zeiss	Image acquisition
EndNote 20	Clarivate Analytics	Literature management
Rstudio	Rstudio, Inc	Bioinformatic analysis
FlowJo 10.5.0	TreeStar, USA	FACS analysis

Table 11. Instruments

Equipments	**Manufacturer**
Inverted system microscopes IX50	Olympus
Inverted system microscope DM HC	Leica
TCS SP-E and SP-8 confocal microscopes (Leica)	Leica
CLSM 780confocal microscope	Zeiss
Powerful, Advanced Research Level ECHO Microscope	ECHO
SYBOT-1000 & CYTOMAT 2 & CELLAVISTA 4	SYNENTEC
FACSCantoTM II	BD
Real-Time PCR System	Applied Biosystems
StepOnePlus™ Master Cycler Gene Amp® PCR System 9700	Thermo Fisher
Agarose gel electrophoresis chamber easy cast	BioRad
Power Pack 300	BioRad
Power Pack P25	Biometra
NanoDrop 1000 UV/Vis spectrophotometer	Kisker
G2565CA high-resolution laser microarray scanner	Agilent Technologies
pH meter	Mettler-Toledo
Balances	Sartorius
Biological safety cabinet Herasafe (Thermo Scientific)	Thermo Fisher
Heracell 240i CO2 incubators (Thermo Scientific)	Thermo Fisher
Freezer Forma	Thermo Fisher
Refrigerator Comfort NoFrost	Liebherr
Paraffin Rotation Microtome HM315	Microm
Tissue processor TP1020	Leica
Waterbath 1083	GFL
Shaking platform 3006	GFL
Megacentrifuge 2.0 R	Heraeus Instruments
Centrifuges 5810R, 5417C and 5415R	Eppendorf
Mini centrifuge C1301	Labnet
Mini vortexer	VWR
Thermomixer comfort	Eppendorf
Single channel pipettes	Pipetman

Table 12. Consumables

Consumables	Manufacturer	Cat.#
T25/75/150-cm2 tissue culture flasks	TPP	90 026/076/151
12/24/96-well tissue culture plates	TPP	920 12/24/96
Low Volume 384-well Black/Clear Flat Bottom Polystyrene TC-treated Microplate	Corning	3542
96-Well, Cell Culture-Treated, V-Shaped-Bottom Microplate	Corning	3894
15/50-ml conical centrifuge tubes	TPP	910 3/10
0.5/1.5/2.0-ml eppendorf tubes	NeoLab	E-23 13/06/07
10/200/1000-µl ART barrier pipette tips	Thermo Scientific	10098960/ 10029040/10313272
20/100-µl PP filter tips	Nerbe Plus	07-662-8300/07-642-8300
5/10/25-ml serological pipettes	TPP	940 /05/10/24
0.22 µm Vacuum filtration system “rapid”-Filtermax	TPP	99505
0.22 µm Sartorius MinisartR sterile filters	Thermo Scientific	10730792
C-Chip disposable hemocytometer	Kisker Biotech	M-NZ
Bemis Parafilm “M”	Thermo Scientific	11762644
5/10/20-ml B Braun solo cone Luer syringes	Braun	12752637
25 mm, 0.4 mm Sterican single-use 21 G syringe needles	Carl Roth	X134.1
Glass slides	Thermo Scientific	J3800AMNZ
Coverslips	Marienfeld Superior	101172

3.2 Cell and organoid culture

3.2.1 3T3-J2 culture and irradiation

The 3T3-J2 cell line was provided by Craig Meyers; Howard Green Laboratory, Harvard University, (RRID: CVCL_W667) and 3T3-J2 are required for monolayer ectocervical epithelial cell culture.

3T3-J2 cells were defrosted and seeded in T75 cell culture flasks in D+++ medium then incubated at 37 °C and 5% CO^2 in a humidified incubator. When the cells were approximately 80% confluent, they were split with pre-warmed Trypsin-EDTA and digested for 5 min until the cells detached from the surface. The cells were re-suspended with 10 mL D+++ medium and counted, followed by irradiation with 30 Gy on ice in a Gammacell 40 Exactor. After irradiation, 1 million irradiated 3T3-J2 were seeded per T25 flask and incubated for a minimum of two hours, until all cells were attached to the surface.

3.2.2 Stem cells isolation from ectocervical cancer tissue

Human cervical specimens were obtained from volunteers undergoing standard surgical procedures by Mandy Mangler (Department of Gynecology, Charité University Hospital, Campus Virchow Clinic, and August Viktoria Klinikum Berlin), approval for experimental usage of the tissue samples was provided by the Charité ethics committee (EA1/059/15) and informed consent was obtained from all donors. Within 2-3 hours after removal, samples were transferred to the lab. Before the sample arrival, T25 flasks were coated with collagen I, which was diluted with PBS 1:100, for 1 h at 37 °C and washed three times with PBS before use. The samples were washed with PBS in a sterile 10 cm petri dish and further chopped into small pieces using sterile scissors and forceps. 5 mL pre-warmed 0.5 mg/mL Collagenase type II was well-mixed with the tissue pieces in a 15mL tube on an orbital shaker at 180 rpm for 2.5 h at 37 °C. The mixture was pelleted at 1000 rpm for 7 min (4 °C), and the supernatant was discarded. The pellet was again digested into single cells with 5 mL TrypLE for 15 min at 37 °C on the orbital shaker. The cell suspension was pipetted up and down 5 times, 5 mL ADF++ added, then pipetted up and down 5 times again. If there was any tissue left, it was allowed to be settle. The supernatant was passed through a 40 µm cell strainer and collected in a 50 mL falcon tube. The settled tissue was digested again until almost all the tissue dissociated into single cells. The pellet was collected and expanded on a coated T25 flask in M5+FSK medium.

3.2.3 2D cervical stem cell lines culture

Passage 0 epithelial cells were cultured without irradiated 3T3-J2 monolayer and seeded in a Collagen I coated T25 flask. After most epithelial cells attached to the surface, the medium was refreshed every 3-4 days intervals until the cells achieve 80-90% confluence. The cells were then split at a ratio of 1:2. For passage 0, after removing the medium, the cells were rinsed thrice with PBS. Subsequently, they were dissociated with 1 mL of TrypLE per T25 flask for 10 minutes at 37°C. The cells detached from the flask surface were then suspended in 10 mL of ADF++ in a 15 mL Falcon tube. Following centrifugation at 400xg for 4 minutes at 4°C, the cell pellet was resuspended in M5+FSK and seeded onto an irradiated 3T3-J2 layer. From

passage 1, the epithelial cells were cultured on irradiated 3T3-J2 layer and the medium was refreshed every other day. At 80%-90% confluence, the cells were enzymatically detached twice. First, 0.5mL TrypLE was added to detach the irradiated 3T3-J2 feeder cells (1min, 37 °C). Thereafter the cervical epithelial cells were detached with another 1 mL of TrypLE for 10 min (37 °C).

3.2.4 3D cervical organoid lines cultured from 2D stem cell lines

Ectocervical epithelial cells were prepared for organoid culture, as described above, the number of epithelial cells was counted. A certain number of cells was centrifuged (400xg for 4 min at 4 °C) and the supernatant was discarded. Matrigel was added to the cell pellet to achieve a final concentration of ~20,000 cells/ 50 µL Matrigel. Matrigel domes were then seeded in the center of each well of a pre-warmed 24-well plate. The plate was then placed in the incubator for 20 min until the Matrigel was polymerized. 500 µL of pre-warmed M5+FSK was added to each well and the medium was refreshed every 3-4 days.

To propagate organoids, the organoid cultures were split every 1-2 weeks at a 1:3-1:5 ratio, according to the size and density of the organoids. The medium around the Matrigel was first discarded and the Matrigel domes were dissolved with 1 mL cold PBS. The mixture was then collected in a 15 mL Falcon tube and centrifuged (400 g for 5 min at 4 °C). The organoid pellet was collected and digested with 1 mL pre-warmed TrypLE at 37 °C for 15-20 min, in a shaking water bath followed by vortexing, to break it down further. The suspension was disrupted further by drawing up and returning it through a needle 5 times, ending up with single cells. The suspension was centrifuged again with 4 mL cold ADF++ at 1000xg for 5 min (4 °C) and the cell pellet was resuspended in Matrigel and repeated the incubation.

3.2.5 Freezing and thawing of cervical 2D stem cell and 3D organoid lines

To prepare cryostocks of 2D epithelial cells, the cells were first dissociated and counted as previously described. After centrifuging, the pellet was resuspended with Cryo-SFM at a final concentration of 1 million cells/mL. The cell suspension was then distributed into cryotubes (0.5 mL/tube) and transferred into a Mr. Frosty®.

For 3D organoids cryostock preparation, the organoids should not be older than five days (preferably two to three days old). The organoids from 2 to 3 wells (for each cryostock) were released from the Matrigel with cold PBS. After the organoid pellet was collected, it was resuspended with 500 µL Cryo-SFM, transferred into a cryotube, and put into a Mr. Frosty® containing isopropanol. The cryostocks from 2D and 3D were kept at -80°C for 24 hrs before being transferred to a liquid nitrogen tank.

In order to thaw the cryostocks, whilst keeping most of the cells and organoids alive, the cryotubes were quickly defrosted in a 37 °C water bath until there was only a small piece of ice remaining. The cells were then transferred to 15 mL Falcon tubes, to which 10 mL of pre-warmed ADF++ medium was gradually added and mixed thoroughly. The cells were then centrifuged (400xg for 4 min at 4 °C). 2D epithelial cells were seeded on an irradiated feeder layer with M5+FSK. 3D organoids were directly resuspended in Matrigel and cultured in a 24-well plate.

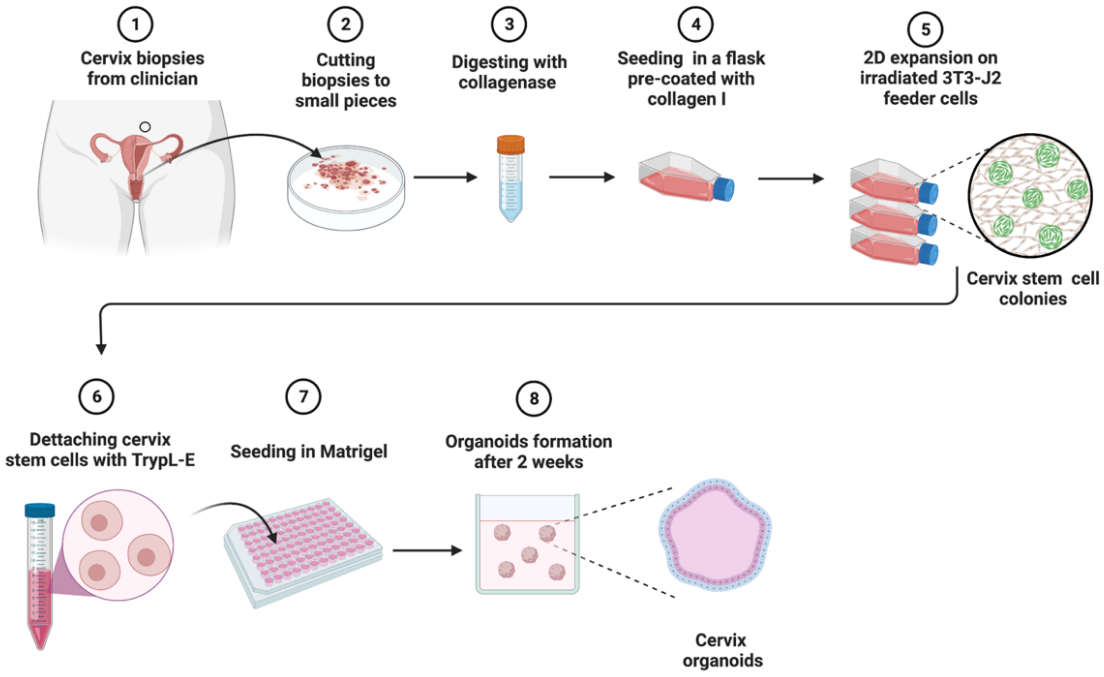

Figure 5. Ectocervical stem cell and organoid cultivation. The ectocervical biopsies are diced finely and digested with collagenase II. The resulting cell mixture is seeded in a coated-T25 tissue culture flask with M5+FSK medium. After 1-2 weeks, the surviving stem cells usually become more than 70% confluent and are split onto an irradiated feeder layer. Apart from direct utilization, the stem cells can be seeded in Matrigel droplets forming organoids. Normally 2 weeks later, the cervix organoids are ready to be harvested. (Created with BioRender.com. at MPIIB)

3.3 Immunofluorescence assays

A 15 mL falcon tube was pre-rinsed with 10% BSA in PBS. Organoids from 2-3 wells were collected in the prepared tube and washed once with cold PBS. They were then incubated on ice for 30 min with cell-recovery solution, followed by another wash with PBS. The organoids were allowed to settle by gravity and the supernatant was discarded. Organoids were fixed with pre-warmed 4% PFA for 30 min at room temperature and washed twice with PBS. Prior to staining, the organoids can be stored in PBS at 4 °C.

The fixed organoids were firstly permeabilized with permeabilization buffer for 30 min followed by 2h blocking. A primary antibody cocktail was prepared with blocking buffer, and organoids were stained with primary antibodies at 4°C overnight. The next day, the organoids were washed four times with washing buffer, thereafter, stained with secondary antibodies for 2h at room temperature and washed again. Following on, they were stained with fluorochrome-conjugated antibodies against Krt5 and Hoechst for 2h at room temperature. The organoids were then washed three times. After the final wash with deionized water, organoids were mounted with Fluoromount-G. The mounting suspension drop was dispensed at the center of a glass slide and a coverslip was placed over it. Finally, the coverslip was sealed with nail polish. The resulting slides can be stored long-term for subsequent image examination with a confocal microscope.

3.4 RNA techniques

3.4.1 RNA isolation

To prepare enough samples for RNA isolation, 3-well organoids of each line were harvested and thereafter the exaction was processed according to the AllPrep DNA/RNA Mini Kit (QIAGEN) manufacturer's protocol. All steps after sample collection were done under Rnase free condition. The purity and concentration of RNA samples were measured and the A260/ A280 absorbance ratio should be around 2. The RNA samples were stored at -80 °C for qRT-PCR and RNA sequencing.

3.4.2 Quantitative real-time polymerase chain reaction (qRT-PCR)

After the organoid RNA extraction, the AB Power SYBR® Green RNA-to-CT™ 1-Step Kit (Thermo Fisher) was used for qRT-PCR reaction. In addition to the RT enzyme with the reverse transcriptase and Rnase inhibitors, the kit contains the nucleic acid stain SYBR® Green Taq DNA-Polymerase and dNTPs. During the elongation phase of the PCR, the SYBR® Green bound to the DNA groove, at which point the relative mRNA expression was measured via calculating the SYBR® Green fluorescence signal. The intensity of the fluorescence signal is proportional to the amount of double-stranded DNA. Each reaction requires SYBR® Green 12.5 µL, RT mix 0.2 µL, primer pair 0.5 µL (final concentration 200 nM) and RNAse free water 1.8 µL. When the reaction was completed (with the PCR program set as below), melting curve analysis was performed to verify amplicon specificity. The gene expression was calculated using the ΔCT method, by calculating exceeded the value of the fluorescence signal compared to GAPDH (housekeeping gene), using the formula below:

ΔCt= Ct (HPV)-Ct (GAPDH)

qRT-PCR Program

30 min 48 °C (reverse transcriptase)

10 min 95 °C (inactivation of Rtase and activation of Taq)

15 s at 95°C
60 s at 60°C
} 40 cycles

Melting curve:

15 sec 95°C

15 sec 60°C

15 sec 95°C

3.4.3 Analysis of RNA sequencing

RNA sequencing was performed at the Max Planck Genome Centre, Cologne, using Illumina HiSeq3000. PolyA enrichment was applied to all samples. For each sample, 50 M single-end reads (150 bp) were generated. The assessment of raw sequence read quality was conducted using FastQC. Subsequently, reads were aligned to the human reference genome (assembly GRCh37) utilizing the splice-aware aligner STAR (v2.7) in two-pass mode. To map reads to genes, quality GTF files obtained from Gencode (version 28) were employed through FeatureCounts, thereby obtaining a raw count matrix. Within this matrix, genes exhibiting no expression across samples were filtered out. Thereafter, differential gene expression analysis was performed using DESeq2 (v1.32.0) in R. The data quality control and pre-analysis were done by Hilmar Berger from the MPIIB Department of Molecular Biology. Genes were ranked according to their log2 fold change relative to healthy controls, followed by gene set enrichment analysis (GSEA) performed through the fgsea method within the clusterProfiler R package (v4.0.5). The biological function enrichment was analyzed via the Database for Annotation, Visualization, and Integrated Discovery (DAVID, 2021), focusing on GO Biological Process (C5-BP). Heatmaps depicting gene expression levels measured in transcripts per million (TPMs) were generated using the “pheatmap” package (v1.0.12). Volcano plots were generated using “ggplot2” package (v3.4.0), while circos plots were generated using “Goplot” and “dplyr” packages.

3.5 Peptidome analysis

3.5.1 HLA immunoaffinity purification

Peptidome data was generated and pre-analyzed by Marcel Wacker. HLA-I and HLA-II peptides were isolated using column-based immunopurification as previously described (Wacker et al.,2023). The frozen cervical organoid samples containing $1x10^8$ cells were incubated in the lysis buffer containing a 3-[(3-cholamidopropyl) dimethylammonio]-1-propanesulfonate (CHAPS) (Panreac AppliChem, Darmstadt, Germany) shaking for 1 hour. Thereafter, the lysate was sonicated (with at least 150 W of ultrasonic power, 50% pulse length, 2 minutes) and subsequently incubated for 1 hour. Lysates were cleared by centrifugation at maximum speed (3100 x g), followed by sterile filtration through a 5 µm filter (Merck Millipore, Darmstadt, Germany). To prepare the sepharose beads coupled with either the pan-HLA class I–specific mAb W6/32 or the pan-HLA class II–specific mAbs Tü-39 coupled, 1 mg W6/32 or Tü-39 mAb was attached to 40 mg beads (cyanobromide-activated sepharose 4B, Cytiva Sweden AB, Uppsala, Sweden) suspended in 1 ml PBS. The chromatography setup comprised two connected columns (Econo Column® Chromatography Columns 0.5 cm × 5 cm BioRad, München, Germany), with the upper and lower column designated for the mAb W6/32 and mAbs Tü-39 coupled cyanobromide-activated sepharose beads, respectively. The sample was circulated overnight through this column system at 4 °C. Affinity columns were then rinse for 30 min with PBS followed by a 1-hour wash with double distilled water. Four times acid elution was performed afterwards with intermittent drying of the matrix. In initial elution, 150 µL of 0.2% (v/v) trifluoro acetic acid (TFA) and 50 µL of 10% (v/v) TFA were used, with subsequent elution using 150 µL of 0.2% (v/v) TFA in the last 3 repeats. The incubation time of acidic elution was 15 minutes for each time. All eluates were mixed and then filtered with 3 kDa and 10 kDa ultracentrifuge filters (Amicon Ultra 0.5 centrifugal filter unit 3 or 10 kDa, Merck Millipore, Billerica, USA) for HLA class I and HLA class II peptides, respectively, and stored at -80°C. Prior to Mass spectrometry (LC-MS/MS) analysis, the filtrates were concentrated via lyophilization, followed by purification and desalting steps using a ZipTip C18 pipette tip (15 µm particle size, 200 Å pore size, 0.6 µl volume, Merck-Milipore, Darmstadt, Germany). After binding peptides to the C18 ZipTip, the tip was rinsed with 0.1% (v/v) TFA. Peptides were subsequently eluted with 32% (v/v) ACN in 0.2% (v/v) TFA. The effectiveness of the 0.1% (v/v) TFA washing solution (termed desalting) was also assessed for peptide loss. The desalting and final sample volumes were concentrated with vacuum centrifugation and adjusted to 25 µl with 1% (v/v) ACN in 0.05% (v/v) TFA for subsequent LC-MS/MS analysis.

3.5.2 Mass spectrometric data acquisition and processing

Mass spectrometric data was acquisited as previously described (Wacker et al.,2023). Peptide separation was conducted using reversed-phase liquid chromatography (nanoUHPLC, UltiMate 3000 RSLCnano, Thermo Fisher, Waltham, Massachusetts, USA), followed by an on-line coupled Q Exactive HF mass spectrometer (Thermo Fisher). The peptide samples were loaded with a solvent mixture of 1% CAN and 0.05% TFA on a 75 µm x 2 cm Acclaim PepMap 100 C18 Nanotrap column (Thermo Fisher Scientific) at a flow rate of 4 µL/min for 10 min. The separation process was performed on a 50 µm × 25 cm PepMap RSLC C18 (Thermo Fisher Scientific) column, with a particle size of 2 µm (PepMap C18, Thermo Fisher). Samples were analyzed in three technical replicates. The samples underwent elution with a linear gradient from 3% to 40% solvent B (80 %/0.15% FA in water) at a flow rate of 0.3 µL/min over 90 min. Ionization of eluting peptides was achieved through a nanospray source and the analysis was performed in the online coupled mass spectrometer equipped with a top 35 HCD (Higher-energy C-trap dissociation) method. This setup generated fragment spectra at a resolution of 30,000. The mass range was limited to 400-650 m/z for HLA class I peptides and 400-1000 m/z for HLA class II peptides, and positive charge states 2–3 for HLA class I and 2–5 for HLA class II were selected for fragmentation.

Data processing was performed following the methodology previously outlined (Nelde et al.,2019). Integration of the database search results from the SequestHT search engine [University of Washington] against the human proteome (Swiss-Prot database, 20,279 reviewed protein sequences, September 27th, 2013) was facilitated by the Proteome Discoverer (v1.4, Thermo Fisher), employing a precursor mass tolerance of 5 ppm, fragment mass tolerance of 0.02 Da, and allowing oxidized methionine as a dynamic modification. Binding strength against nine representative HLA-I alleles (HLA-A*03:01, HLA-B*27:07, HLA-C*15:02, HLA-A*01:01, HLA-A*68:01, HLA-B*15:23, HLA-B*52:01, HLA-C*07:04, HLA-C*12:02) were predicted with NetMHCpan 4.1BA. Thresholds of IC50 and rank for strong binders were set at IC50< 500 nM and rank<1. The MHC-I peptide immunogenicity was analyzed with the Immune Epitope Database (IEDB) prediction tool, a positive score indicates a likelihood of T cell recognition and a negative score indicates that recognition is less likely.

3.6 TCGA and GEO data analysis

3.6.1 TCGA and GEO data collection

Clinical information, mRNA expression data of 292 cervical cancer patient samples (cases without complete information were excluded) were retrieved from The Cancer Genome Atlas (TCGA) via the cBioPortal (https://www.cbioportal.org/). The GSE228568 dataset consists of

three HPV16 positive cervical cancer samples and three normal samples microarray data were downloaded from the Gene Expression Omnibus (GEO; https://www.ncbi.nlm.nih.gov/geo/) was included. TCGA data was utilized for exploring the relationship between DNA repair genes expression, patient's prognosis and the tumor microenvironment (TME). GEO data was downloaded to validate whether the biology function enrichment pattern observed in organoids consist with the one in corresponding tissues.

3.6.2 DRGscore calculation and prognosis analysis

DNA repair-related genes (DRG) expression of TCGA data was constructed by LASSO-COX dimension reduction analysis using R packages "glmnet" and "survival" (Li et al.,2021;Xu et al.,2022;Xu et al.,2023). The λ value corresponding to the minimum partial likelihood deviance was selected as the optimal λ. Finally, 5 candidate genes and corresponding lambda values (RAD50: 0.12368922, OGG1: 0.0211609, SUCLA2: 0.04715829, XPA: 0.0045094, MGMT : 0.0153683) were obtained based on TCGA data. The DRGscore of each patient was calculated as follows:

DRGscore = expr RAD50 × λ RAD50 + expr OGG1 × λ OGG1 + expr SUCLA2 × λ SUCLA2 + expr XPA × λ XPA+ expr MGMT × λ MGMT.

where expr (gene) was the expression level of the gene and λ (gene) was the corresponding lambda value. Combined with the survival data, the R packages "survival" and "survminer" were employed to determine the cutoff of DRGscore and whether there is a survival difference between high/low DRGscore groups. The Kaplan–Meier curve analysis was conducted to compare the overall survival (OS) between these two groups.

3.6.3 Tumor microenvironment evaluation and prognosis

CIBERSORT method (https://cibersort.stanford.edu/) was used to quantify the infiltrating immune cell ratio of TCGA data (Luca et al.,2021). The proportion of 22 immune cells was calculated. With R package "ESTIMATE", the stromal score, immune score and ESTIMATE score were calculated (Fan et al.,2022;Feng et al.,2023). Tumor Immune Dysfunction and Exclusion (TIDE) score and tumor inflammation signature (TIS) score were used to infer the clinical response of patients to immunotherapy (Jiang et al.,2018). High TIDE scores and low TIS scores were associated with poorer immunotherapy outcomes (Huang et al.,2021). TIDEscore was calculated with an online tool (http://tide.dfci.harvard.edu/login/) and TISscore was calculated as the mean of normalized expression on a log2-scale of 18 characteristic genes (Ayers et al.,2017). The receiver operating characteristic curve analysis (Rock et al.,2016) was utilized to compare the performance of the DRGscore, TIDEscore, and TISscore

in prognosis prediction by using the package “pROC”. “ggplot2”, “ggpubr”, and “ggsignif” R packages were used to generate boxplots to display the immune cell makeup and scores, etc.

3.7 Vγ9Vδ2 T cells expansion and functional assays

3.7.1 Vγ9Vδ2 T cell expansion

Vγ9Vδ2 T cells were expanded from peripheral blood mononuclear cells (PBMCs) obtained from leukocyte concentrates of healthy blood donors using a Ficoll-Hypaque (Biochrom, Biocoll L 6113/5) density gradient according to the manufacturer’s protocol. The leukocyte concentrates, sourced from the Institute of Transfusion Medicine UKSH Campus Kiel with Ethics Approval D 434/22. The blood was diluted at a 1:2 ratio in PBS. Each 30 mL of diluted blood was gently layered onto 15 mL of Ficoll in a 50 mL falcon tube, and spun down at 2000rpm for 20 min, with the brake turned off. The resultant white layer containing the leukocytes was carefully collected into a fresh 50 mL falcon tube and washed twice with PBS to remove the residual Ficoll. Following this, the cell pellet was resuspended in complete RPMI medium for later Vγ9Vδ2 T cell expansion.

Prior to expansion, the initial Vγ9Vδ2 T cell population was checked by staining PBMC with anti-Vδ2-FITC and anti-CD3-APC. Samples with the Vγ9Vδ2 T cell percentage over 2% were accepted to be further expanded. On day one, the Vγ9Vδ2 T cells were selectively activated by stimulating PBMCs with 5 μM zoledronic acid and 100 IU/mL IL-2. In the following 14-day expansion period, 50 IU/mL IL-2 supplement was added every other day (Peters et al.,2020). After two weeks of expansion, the purity of Vγ9Vδ2 T cells was checked, and the lines were used for experiments when Vγ9Vδ2 T cells represented more than 90% of the total cell population.

3.7.2 Vγ9Vδ2 T cell co-culture with 2D cervical stem cells

Prior to the co-culture, I collected and counted different 2D cervical stem cell lines. Daudi cells were used as a positive control group. All cell lines were first counted and pelleted in 15 mL Falcon tubes by centrifuging at 1,400 rpm for 5 min. PKH67 green dye was prepared according to the manufacturer’s protocol (for $7.5x10^5$ cells 75 μL Diluent C and 0.2 μL mixture was required). Cell pellets were resuspended in this dye and mixed well. After incubation in the dark at room temperature for 4 min, 7 mL R+ medium was added and incubated for a further 1 min to stop the staining. The cells were then pelleted by centrifuge once more. In order to remove the leftover PKH67, it was necessary to transfer the resuspended cells to new Falcon tubes before the final two washes. After counting the cells, they were resuspended with the proper volume of R+++ medium for a cell concentration of $2x10^5$ cells/ mL. Vγ9Vδ2 T cells

were also counted, and cell suspensions were prepared at the final concentration of $2x10^6$ cells/mL (E: T 10:1).

Three different conditions were set up to compare the cytotoxicity effect: organoid lines (negative control), organoid lines co-cultured with Vγ9Vδ2 T cells, and organoid lines co-cultured with BrHPP activated Vγ9Vδ2 T cells. 50 µL organoid cells were added in each well, thereafter mixed with 50 µL Vγ9Vδ2 T cells in the presence or absence of BrHPP. R+++ medium was added to maintain an equal volume of liquid in all the wells. The co-culture lasted for 4 hrs. Following this, the cells were stained with PI for 10min (4°C) and analyzed using flow cytometry.

Cervical cancer cell cytotoxicity effect was calculated using the formula:

Cytotoxicity= 100− [(% of living epithelial cells in co-culture with γδ T cells/% of living epithelial cells without γδ T cells) × 100] (Sacchi et al.,2018)

3.7.3. Flow cytometry analysis

To investigate the cytotoxic effect against organoids and the expression of CD107a of Vγ9Vδ2 T, cells were harvested after co-culture, transferred into 96-V bottom plates, and then washed with wash buffer. The cells were then stained with PI, or other fluorochrome-conjugated monoclonal antibodies directed against the interested surface molecules, and incubated for 30 min at 4 °C. The cells were washed twice, using wash buffer, then resuspended in wash buffer. Cells were immediately loaded on the FACS Canto II flow cytometer. At least 10,000 events were collected for the analysis of the different surface molecules. Data were then analyzed with FlowJo v.10.

3.7.4 Vγ9Vδ2 T cell co-culture with cervical organoid lines

Prior to co-culture, a flat-bottom 384 well-plate (black with clear bottom, Corning) was coated with Poly-2-hydroxyethyl methacrylate (poly-HEMA; Sigma, P3932) dissolved in 100% ethanol, following the method previously described (Kuroda et al., 2013). 30 µl poly-HEMA solution was added in each well, followed by swirling for 10 min using a plate rotator and left to dry overnight under the culture hood. Prior to use, the plate was washed with PBS.

Organoid lines were cultured for approximately seven days, while the Vγ9Vδ2 T cell population was expanded for 14 days, according to the established protocols. Matrigel was dissociated using 11 mL of cold PBS and the resulting organoid suspension was collected in a 15 mL Falcon tube. Thereafter, 1 mL of the organoid suspension was extracted and digested into single cells using TrypLE, with the count of single cells used to estimate single-cell equivalents

for the rest of organoids. The organoids underwent three washes with cold PBS before being collected and stained with Celltrace CFSE according to the supplier's protocol. Following this, Vγ9Vδ2 T cells were added at E:T = 10:1 (effectors were Vγ9Vδ2 T cells, targets were organoid lines). In the respective conditions, "Dead cells" were boiled for 10 min at 95°C prior to the start of the experiment, and cisplatin-treated cells served as positive control for cell death. Vγ9Vδ2 T cells were non-activated or activated without/with 300 nM BrHPP, 10 µL of Nucred Dead 647 was incorporated to distinguish between dead and live cells, and the plate was promptly measured under the CELLAVISTA 4 automated cell imager in combination with the SYBOT X-1000 equipped with the CYTOMAT 2 C-LiN system (all SYNENTEC).

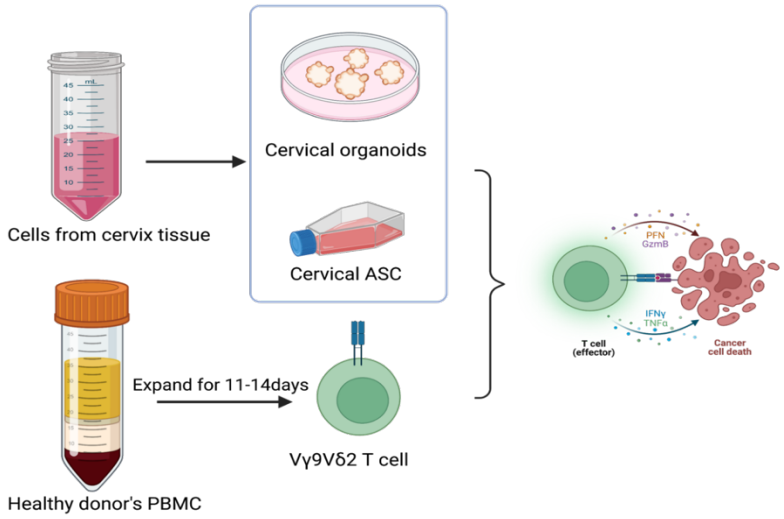

Figure 6. Assessment framework for Vγ9Vδ2 T cell cytotoxic impact on cervical organoids. Cervical organoids derived from adult stem cells—representing healthy, HPV-positive, and cancerous tissues—were cultured using established protocols. Concurrently, Vγ9Vδ2 T cells were selectively proliferated using zoledronic acid and interleukin-2 to achieve over 90% purity. Post-coculture, cytotoxic effects were quantitatively assessed through flow cytometry and qualitatively via live cell imaging. (Created with BioRender.com. at MPIIB)

3.8 Microscopy and image analysis

3.8.1 Live-cell imaging of co-culture

Measurements and imaging acquisition of Vγ9Vδ2 T cell and cervical organoid co-culture were conducted using the CELLAVISTA 4 automated cell imager in combination with the SYBOT X-1000 equipped with the CYTOMAT 2 C-LiN system (all SYNENTEC) as previously described (Dong et al.,2023). Wells were monitored every hour over a 24-hour period. Afterwards, fluorescence data and images were extracted using YT-Software (SYNENTEC GmbH) employing the Real Cytoplasm (2F) application. The settings were adjusted to detect

all organoids in the green channel and followed by analysis of the average intensity of yellow and red signals within each spheroid area. Different channel settings were used. Exciter: Blue (475/28) – Emission filter: Green Filter 530nm (530/43), Exciter: Green (529/24) – Emission filter: Amber Filter 580nm (607/70), Exciter: Red (632/22) – Emission filter: Far Red Filter 670nm (685/40).

3.8.2 Light and fluorescence microscopy

Phase contrast and brightfield images were taken with a 4x or 10x objective using the OLYMPUS IX50. Images were contrast adjusted and scale bars were added using FIJI. Fluorescence images were taken with a fluorescence microscope (ECHO® Microscope).

3.8.3 Confocal microscopy

With assist of David Holthaus, confocal images were obtained after IF staining with a 10x, 40x or 63x oil objective using a Zeiss cLSM 880 microscope, equipped with Plan-Apochromat 20x/0.8 M27 and C-Apochromat 40x/1.20 water M27 objectives and analyzed with ZEN blue software and ImageJ version 1.52a.

3.9 Statistical analysis

All violin plots depicted the median with Tukey whiskers. Statistical significance was determined using a Two-Way ANOVA with Tukey's correction for multiple testing. For comparisons other than the violin plots, two-tailed Student´s t-test with mean ±SD (standard deviation) was employed. Descriptive statistics were also included. Basic calculations were performed using MS EXCEL 2023 (Microsoft). Figures were plotted using Prism 9 (GraphPad) or R (v4.2.2). A p-value <0.05 was considered statistically significant, with asterisks indicating the following p values: ns for not significant, * for p<0.05, ** for p<0.01, *** for p<0.001, **** for p < 0.0001.

4 RESULTS

4.1 Cervical organoids replicate the morphological and transcriptomic characters of cervical tissue

4.1.1 Establishment and characterization of cervical cancer organoid lines

In addressing the challenge of acquiring adequate cervical tissue samples for diverse *in vitro* assays, our laboratory has successfully pioneered the establishment of a robust culture protocol for patient-derived cervical organoids. This advancement is documented in our peer-reviewed publications (Gurumurthy et al.,2022;Koster et al.,2022). Our methodology is distinct from traditional organoid cultivation techniques, primarily through the incorporation of 3T3-J2 feeder cells. These feeder cells are a rich source of extracellular matrix components—such as type IV collagen, laminin, various glycoproteins, interstitial procollagens, fibronectin, and hepatocyte growth factor—which collectively create an optimal milieu for the proliferation of primary cervical cells (Alitalo et al.,1982;Ligaba et al.,2015).

Utilizing the developed methodology, I successfully generated four new cervical cancer organoid lines. Following the isolation of primary cervical cancer cells from four unique parental tissues, these cells were initially cultured on collagen-I-coated flasks (Figure 7A left). After the 0 passage, they were transferred onto a layer of irradiated 3T3-J2 feeder cells (Figure 7A right), facilitating further growth before encapsulation in Matrigel domes to form cervical organoids. I noted that within a week, cervical epithelial cells formed proliferative colonies, eventually replacing the apoptotic feeders (indicated by light spots in Figure 7A, right). Remarkably, no discernible differences in the rates of proliferation and colony formation were observed under optical microscopy between the healthy, HPV+, and cancer primary cells (Figure 7B, upper).

For subsequent growth into organoids, the epithelial cells were cultivated in M5+FSK medium, which contains critical growth factors. Unlike the Clevers' group medium for ectocervical organoids (Lõhmussaar et al.,2021), our protocol intentionally omits R-spondin-1 due to its observed inhibitory effect on ectocervical organoid proliferation (Chumduri et al.,2021;Lõhmussaar et al.,2021). Among the organoid lines previously established by Stephanie Koster, six cervical organoid lines—including three healthy and three HPV16 E6E7-transformed (HPV+) lines—along with four newly cultivated cervical cancer lines, are poised for further investigative assays. In the various cervix organoid lines, we observed subtle variations in three-dimensional spheroid architecture under optical microscopy (Figure 7B, lower).

4.1.2 Verification of HPV16/18 expression in cervical organoid lines

As demonstrated in the studies, HPV16 and HPV18 play a significant role of in cervical carcinogenesis (Bordigoni et al.,2021;Fan et al.,2020;Layman et al.,2020). I assessed the HPV status across ten organoid lines using quantitative real-time PCR (qRT-PCR). Controls expressing various levels of HPV16 and HPV18, including End1, and HeLa cells, were used to measure HPV16 and HPV18 level in organoids. The ΔCT method quantified HPV expression relative to GAPDH, with lower ΔCT values indicating higher expression levels. This analysis confirmed the presence of HPV16 E6 E7 oncogenes in three organoid lines derived from cervical cancer (Cancer1-3) and in all three HPV+ lines. Uniquely, the Cancer4 organoid line was identified as harboring HPV18, reflecting the distinct incidences of HPV16 and HPV18 in cervical cancer pathology (Figure 7C) (Ahmed et al.,2017).

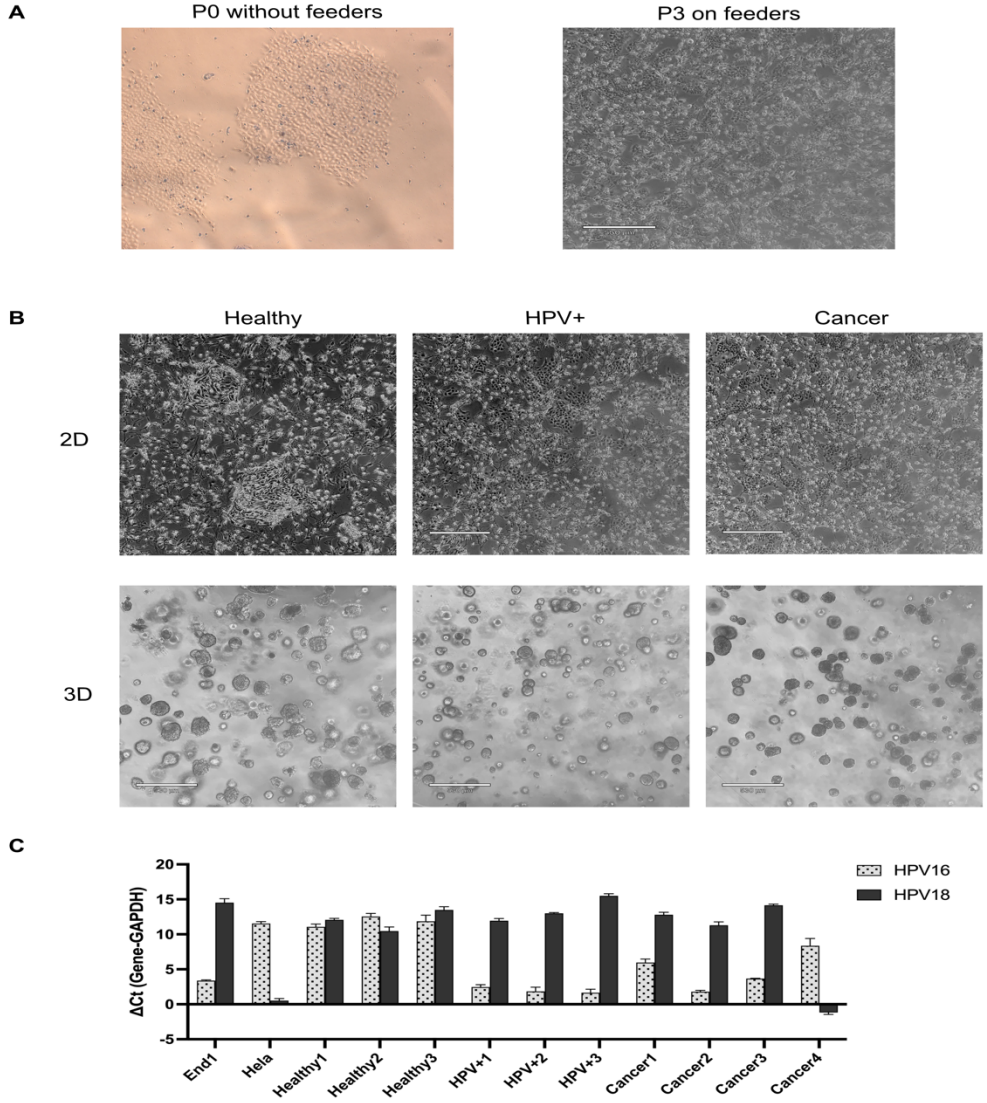

Figure 7. Ectocervical organoid cultivation and HPV16 E6E7 assessment.

A) Primary cervical cell colonies at passage 0 (P0) were formed on collagen I-coated flasks (left). Subsequent passages (P3) involved expansion on a layer of irradiated feeder cells (right). Visible bright spots within the 2D primary cell cultures indicate feeder cells undergoing detachment.
B) Representative brightfield images illustrating both two-dimensional (2D) primary cell cultures and three-dimensional (3D) organoids derived from healthy, HPV+, and cancerous tissues. In the 2D culture system, following primary cell attachment, emerging colonies progressively outgrew and supplanted the feeder cells, expanding into the surrounding spaces. In 3D cultures, single cells proliferated and self-organized into spheroidal organoids within one to two weeks, with diameters ranging from 60 to 100 micrometers. Under optical microscopy, no marked morphological differences were observed among healthy, HPV+, and cancer organoids.
C) Quantitative real-time PCR (qRT-PCR) analyses were conducted, with ΔCt (HPV16/18-GAPDH) values normalized against GAPDH as the reference gene. End1 cells served as a positive control for HPV16, and HeLa cells as a positive control for HPV18 detection. All three healthy organoids were HPV-negative. Integration of HPV16 oncogenes E6E7 was confirmed in all three HPV+ organoid samples and in Cancer organoids 1, 2, and 3. The Cancer 4 organoid line exhibited integration of HPV18.

4.1.3 The cervical organoids exhibit a faithful reproduction of the structural polarity in tissue

Within one to two weeks of culture, the primary cells gave rise to organoid structures in Matrigel dome. These organoids progressed from simple epithelial formations to complex structures with distinct basal and apical polarities that reflect the architecture of the tissue of origin. Significantly, in HPV+ and cancerous organoids, the proliferation marker Ki67 exhibited a diffuse expression throughout all cellular layers (Figure 8B, HPV+, cancer), deviating from the confined expression to basal and parabasal layers observed in healthy organoids (Figure 8B, healthy). This pattern effectively mirrors the proliferative gradients found in clinical biopsies (Figure 8A), indicating a loss of cellular growth control characteristic of neoplastic transformation. In the organoids derived from cervical tissue, KRT5, a cytoskeletal protein indicative of ectocervical origin (Eckert and Rorke,1989), exhibited a stratification that closely emulates the epithelial layers found in native cervical tissue, as demonstrated in Figure 8. Comprehensive details on the ectocervical organoid cultures are elaborated in prior studies (Gurumurthy et al.,2022;Koster et al.,2022). This atypical proliferation pattern, a hallmark of altered structural polarity, is emblematic of oncogenic transformation. It highlights the utility of our cervical organoid models for probing the molecular mechanisms underpinning cervical carcinogenesis.

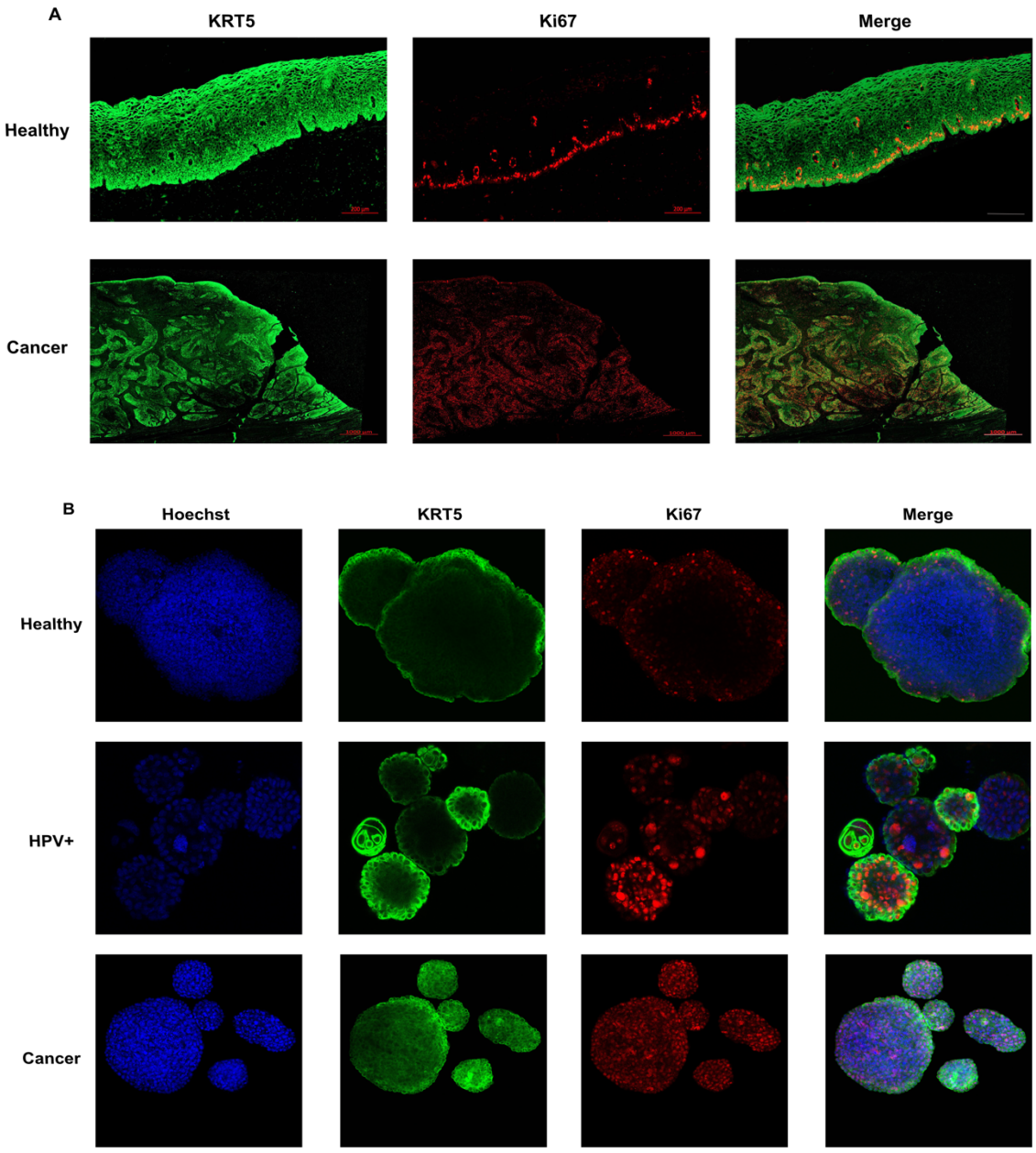

Figure 8. Immunofluorescence analysis of cervical epithelium and organoids.

A) Representative immunofluorescence images contrasting healthy ectocervical tissue with ectocervical squamous carcinoma (SCC). The epithelium was labeled with cytokeratin 5 (KRT5, green fluorescence) to demarcate structural cells, alongside Ki67 (red fluorescence), marking proliferative cell populations. Tissue IF images were acquired by Volker Brinkmann from MPIIB.

B) Representative immunofluorescence images of cervical organoids from healthy, HPV-transformed (HPV+), and cancerous origins. Nuclear staining was achieved with Hoechst (blue fluorescence), with additional labeling for KRT5 (green fluorescence) and Ki67 (red fluorescence) to illustrate cellular composition and proliferative activity. IF images were acquired with assistance of David Holthaus from IKMB.

4.2 Transcriptomic characters of cervical organoid and tissue

4.2.1 Transcriptomic shifts in HPV-associated cervical carcinogenesis

Cervical carcinogenesis is closely associated with persistent high-risk HPV infection. By comparing transcriptomic profiles of healthy, HPV+, and cancer-derived organoids, I dissected the genetic alterations facilitating cervical transformation. Moreover, upregulated genes in these HPV-positive (HPV+) and cervical cancer organoids may encode tumor-associated antigens (TAAs) recognizable by T cells, potentially activating anti-tumor immune responses (Otter et al.,2019). I initially extracted RNA from healthy, HPV+, and cancerous cervical organoid lines for RNA sequencing. Hilmar Berger from MPIIB's Molecular Biology Department conducted data preprocessing and screening for differentially expressed genes (DEGs) using the STAR (v2.7) aligner, aligning sequences to the human reference genome (GRCh37). Gene mapping was performed with FeatureCounts, utilizing GTF files from Gencode (v28) to obtain raw counts. Non-expressed genes were removed from this raw count matrix, and DESeq2 (v1.32.0) in R (v4.0.5) was applied to identify differentially expressed genes.

In total, HPV+ and cancer-derived organoid lines exhibited 927 and 1735 genes with increased expression, respectively (Figure 9A upper, red, blue), while 173 and 1402 genes were notably decreased in expression (Figure 9A lower, red, blue). In my comparative analysis with the GEO dataset (GSE228568) (Figure 9A, T1(green)), I discovered extensive differential gene expression in cervical cancer: 5,066 genes were upregulated and 3,102 were downregulated. Notably, there were 517 upregulated and 211 downregulated genes shared between the organoids and actual cervical cancer tissues, highlighting the backdrop of tissue-specific genetic variation and cellular complexity (Figure 9A).

4.2.2 Expression gradient of DNA repair genes in HPV progression to cervical cancer

Integration of high-risk human papillomavirus (HR-HPV) into the host genome disrupts the function of DNA damage and repair genes, contributing to the development of persistent HPV infections and cervical cancer (Gusho and Laimins,2021). Gene Set Enrichment Analysis (GSEA) corroborates that genes involved in DNA repair pathways are predominantly active in HPV+ (Figure 9C lower) and cervical cancer (Figure 9C, upper). For a more nuanced interpretation of gene expression trends, I generated heatmaps using 'pheatmap' R package. These visual representations delineate the differential expression profiles associated with DNA damage-repair pathways across healthy, HPV-infected, and malignant cervical organoid models. The heatmap shown in Figure 9B revealed pronounced overexpression of DNA

damage-repair genes in cancerous compared to healthy organoids, with HPV+ organoids exhibiting intermediate expression patterns.

To further elucidate the crucial DNA repair-related genes, I crafted an additional heatmap profiling 41 essential DNA repair genes. This heatmap underscores their varying expression across healthy, HPV-positive, and cancerous organoid lines, with genes like MSH2, MCM-family proteins, BRCA1, BRCA2, and EXO1 standing out (Figure 9D). These genes are acknowledged for their pivotal roles in DNA repair and cellular stress signaling pathways (Ciccia and Elledge,2010) and cancer transformation. The mutation of DNA mismatch repair (MMR) genes MLH1, MSH2, MSH6 and PMS2/1 play an important role for Lynch syndrome, formerly known as Hereditary Non-Polyposis Colorectal Cancer (HNPCC), identification (Antill et al.,2015). Furthermore, the MCM protein family, markedly upregulated, is known for prognostic relevance and as potential therapeutic targets in various cancers (Yu et al.,2020). Overall, the gradation in DNA repair-related gene expression indicated their unique and significant role in the transition from HPV infection to cancerous transformation.

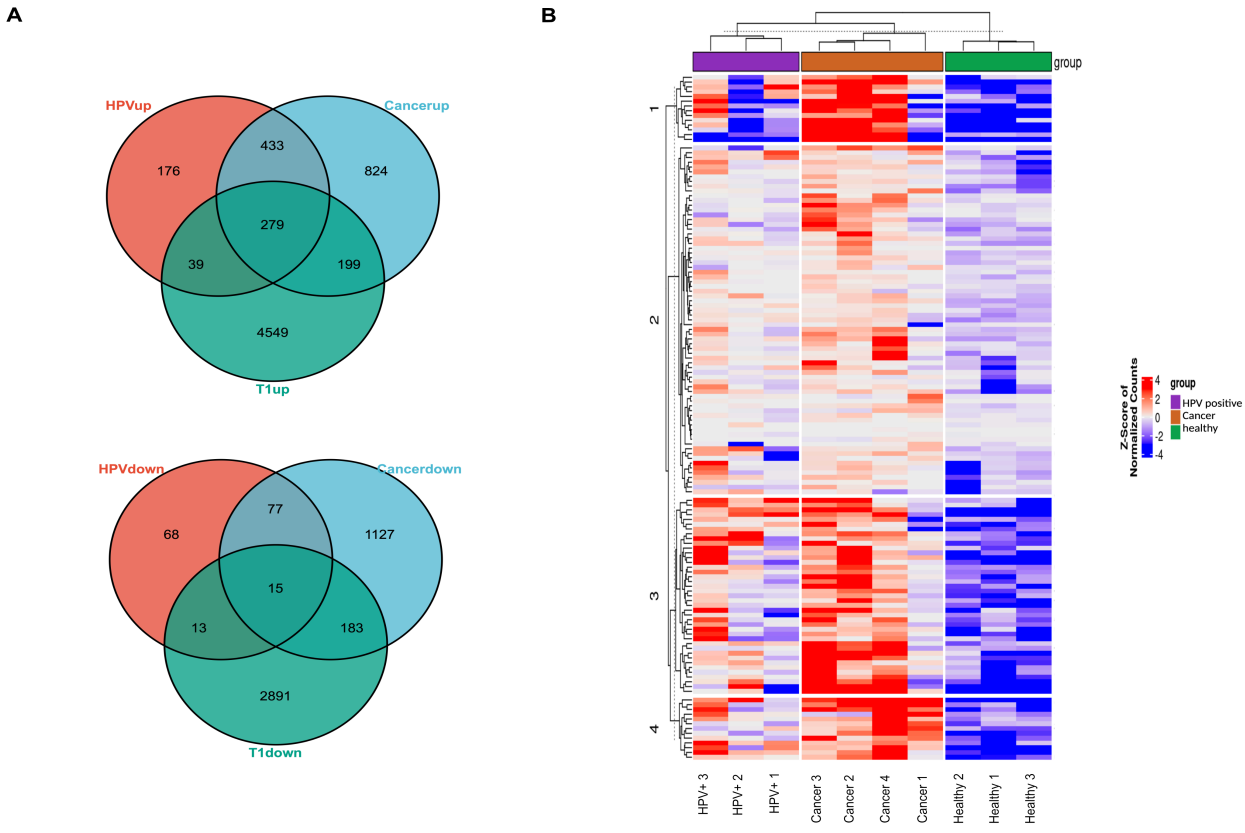

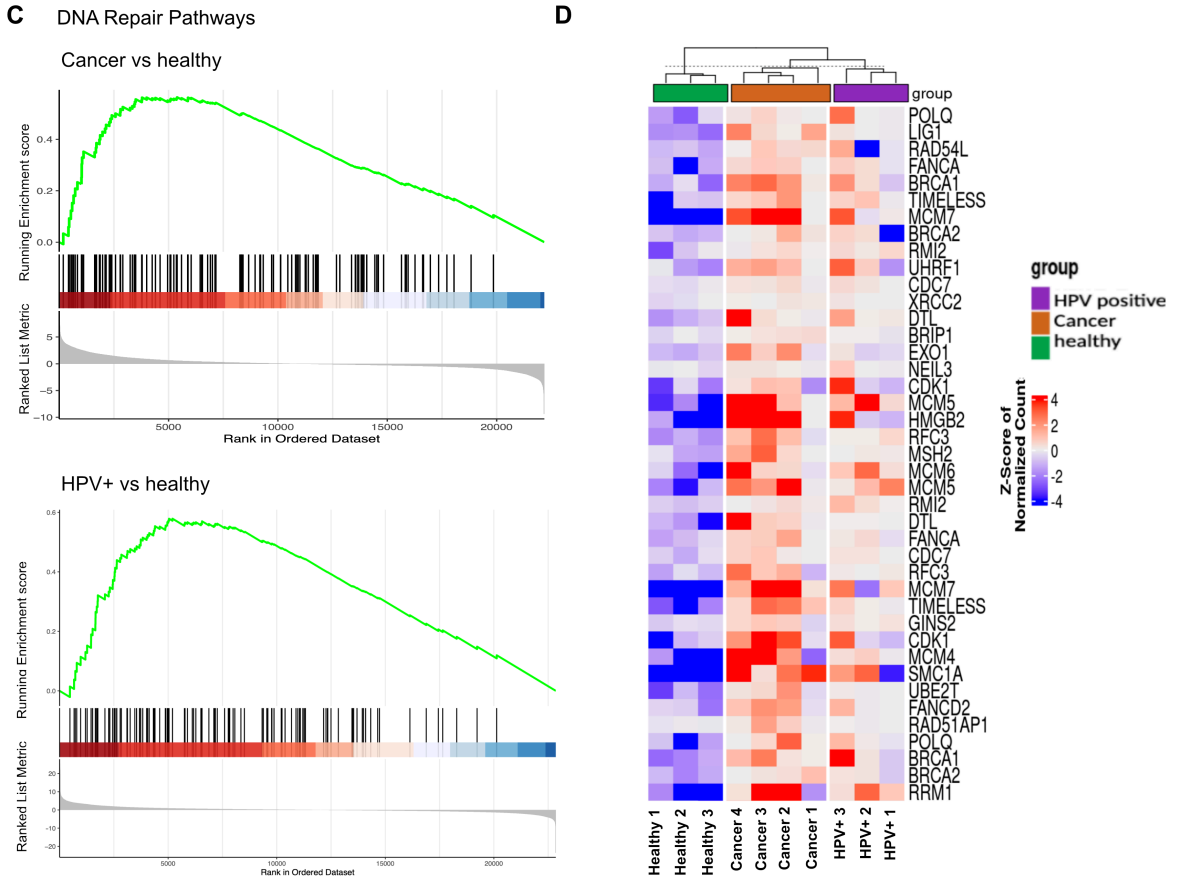

Figure 9. Transcriptomic analysis of cervical organoid and tissue.

A) Venn diagrams depict shared and unique up/down-regulated gene expression among HPV+, cancerous organoid lines, and cervical cancer tissues (compare to healthy tissues). Upregulated genes are indicated in the upper diagram, while downregulated genes appear in the lower diagram.

B) A heatmap illustrated the expression profiles of DNA damage-repair genes across healthy, HPV+, and cancerous organoid lines, with expression levels normalized to transcripts per million (TPM) and indicated by a z-score gradient from high (red) to low (blue).

C) Enrichment analysis of DNA repair genes. The bars illustrated gene set enrichment within DNA repair pathways, contrasting HPV+ (lower) and cancer (upper) organoids with healthy ones. Red bars denote upregulated genes involved in DNA repair, while blue bars indicate downregulated genes relative to healthy organoid benchmarks.

D) Comparative heatmap of DNA repair gene expression. This heatmap visualized the expression levels of 41 DNA repair-related genes across healthy, HPV+, and cancer organoid lines. Expression data, normalized to transcripts per million (TPM) and presented as z-scores, range from high (red) to low (blue), delineating the differential gene expression profiles among the organoid types.

4.2.3 Augmentation of DNA repair pathways in HPV-associated cervical carcinogenesis

For a comprehensive analysis of Gene Ontology (GO) Biological Process (BP) enrichment in dysregulated genes from HPV+ and cancerous organoid lines, as well as cervical cancer tissues, I utilized the DAVID database for annotation. Volcano plots were generated via the 'ggplot2' R package to visualize significant GO BP changes. I applied a stringent False Discovery Rate (FDR<0.05) and a log2 fold change threshold (|log2FC| ≥ 1.5), identifying notably enriched processes. Among these, cell division, cell cycle, and DNA repair processes were consistently upregulated across all samples, as depicted in Figure 10A with red arrow.

The aforementioned results prominently feature DNA repair genes and processes. Further elucidation of DNA repair mechanisms was achieved through enrichment analysis of ten specific repair pathways (Double-strand break repair via homologous recombination, DNA synthesis involved in DNA repair, DNA-dependent DNA replication, DNA repair, Regulation of DNA repair, Nucleotide-excision repair, Mismatch repair, Double-strand break repair, Double-strand break repair via nonhomologous end joining, Regulation of double-strand break repair via homologous recombination), with results presented in circos plots produced using 'Goplot' and 'dplyr' packages (Figure 10B). A similar enrichment pattern was observed in HPV+, cancer organoids and cervical cancer tissue datasets. And the differential expressed genes (DEGs) were significantly enriched in three DNA damage repair processes including DNA repair (GO:0006281), double-strand break repair (GO:0006302), and double-strand break repair via homologous recombination (GO:0000724) processes (Figure 10B). Moreover, in HPV+ organoids, more down-regulated genes (blue dots) were enriched in double-strand break repair (GO:0006302), and double-strand break repair via nonhomologous end joining (GO:0006303) compared to the ones in cancer organoids and tissues (Figure 10B). This observed uniform pattern of enrichment across groups underscored the significant role of these pathways in cervical oncogenesis.

In summary, this comprehensive transcriptomic analysis has confirmed increased DNA repair activity in both HPV-positive and cancerous organoid samples and the enrichment of DNA repair genes highlights their potential importance in the evolution of cervical cancer. By incorporating further peptidome analysis, the role of DNA repair genes in cervical cancer—particularly their involvement in generating tumor-associated antigens—can be clarified. Integrating additional peptidome analysis could allow the role of DNA repair genes to be elucidated, such as the source of tumor-associated antigens (TAAs) in cervical cancer.

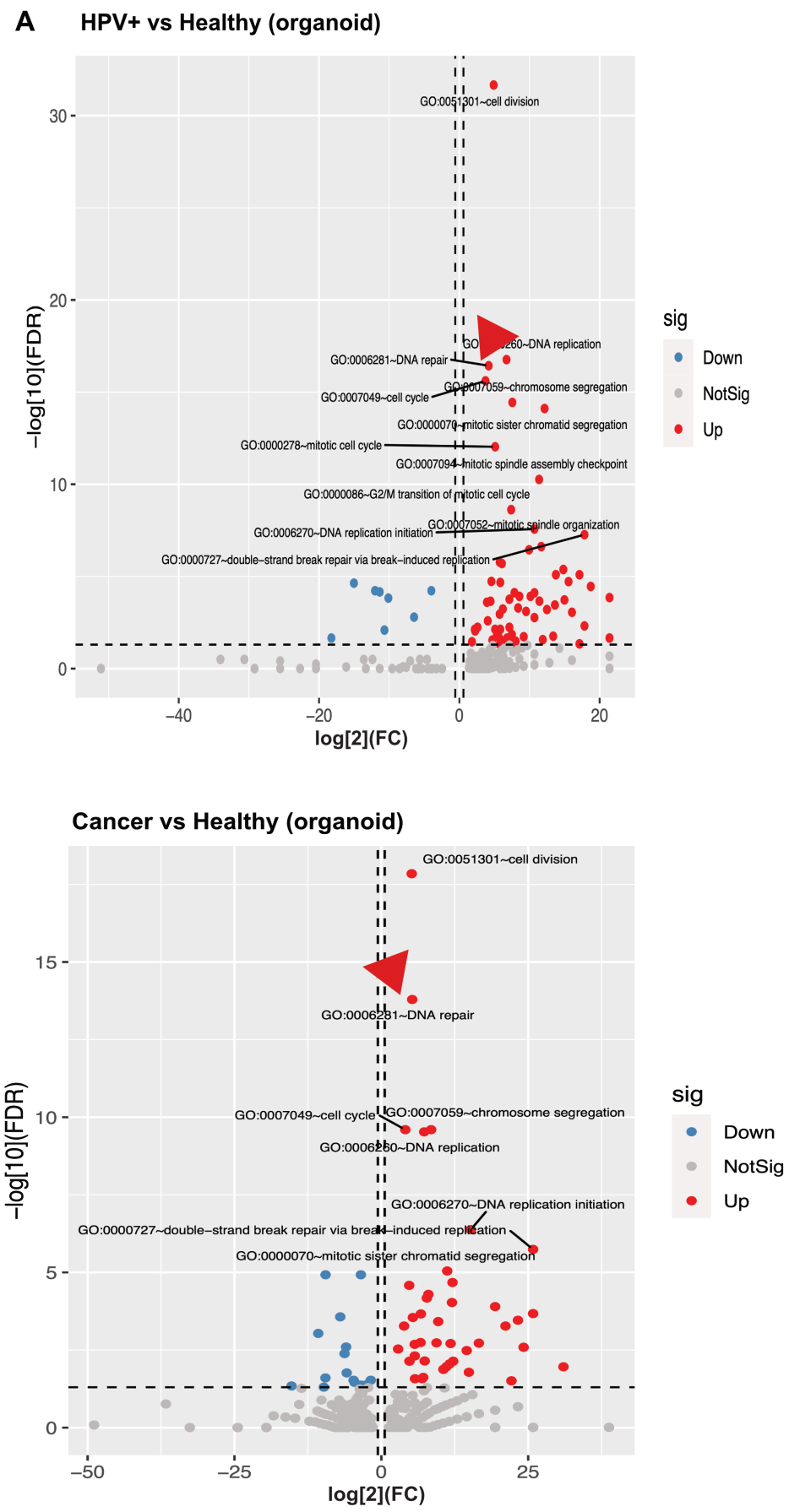
A
HPV+ vs Healthy (organoid)
GO:0051301~cell division
GO:0006281~DNA repair
GO:0007049~cell cycle
GO:0007059~chromosome segregation
GO:0000070~mitotic sister chromatid segregation
GO:0000278~mitotic cell cycle
GO:0007094~mitotic spindle assembly checkpoint
GO:0000086~G2/M transition of mitotic cell cycle
GO:0007052~mitotic spindle organization
GO:0006270~DNA replication initiation
GO:0000727~double-strand break repair via break-induced replication
−log[10](FDR)
log[2](FC)
sig
Down
NotSig
Up
Cancer vs Healthy (organoid)
GO:0051301~cell division
GO:0006281~DNA repair
GO:0007049~cell cycle
GO:0007059~chromosome segregation
GO:0006270~DNA replication initiation
GO:0000727~double-strand break repair via break-induced replication
GO:0000070~mitotic sister chromatid segregation
−log[10](FDR)
log[2](FC)
sig
Down
NotSig
Up

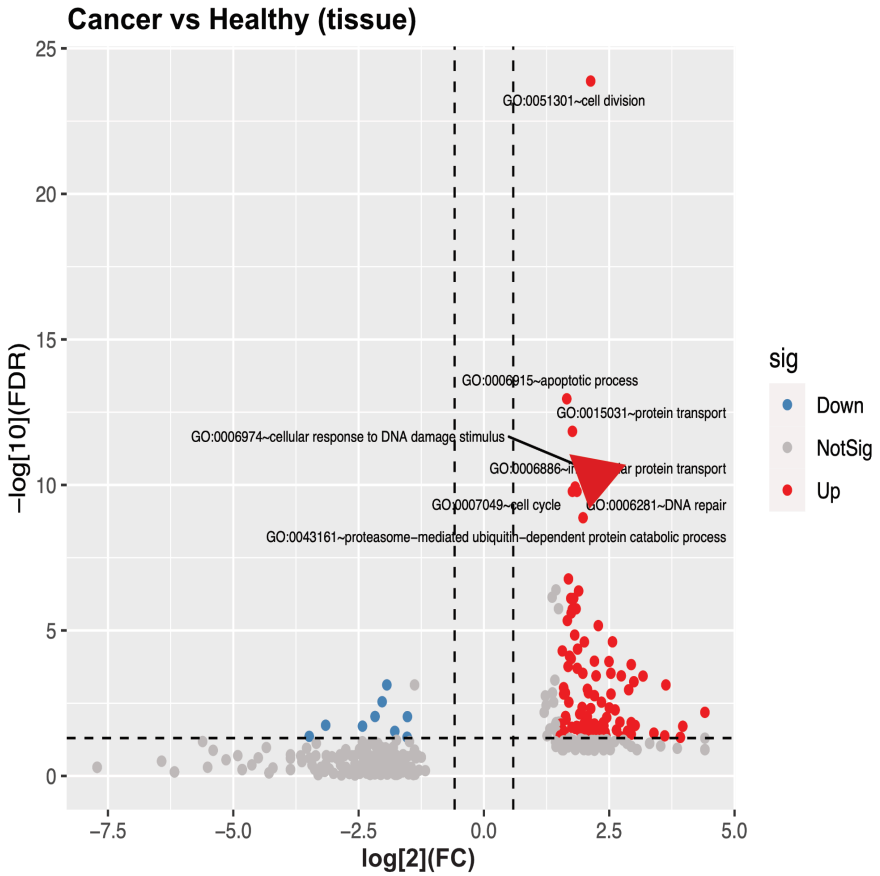

B

ID	Description
GO:0000724	double−strand break repair via homologous recombination
GO:0000731	DNA synthesis involved in DNA repair
GO:0006261	DNA−dependent DNA replication
GO:0006281	DNA repair
GO:0006282	regulation of DNA repair
GO:0006289	nucleotide−excision repair
GO:0006298	mismatch repair
GO:0006302	double−strand break repair
GO:0006303	double−strand break repair via nonhomologous end joining
GO:0010569	regulation of double−strand break repair via homologous recombination

HPV+ vs healthy (organoid)

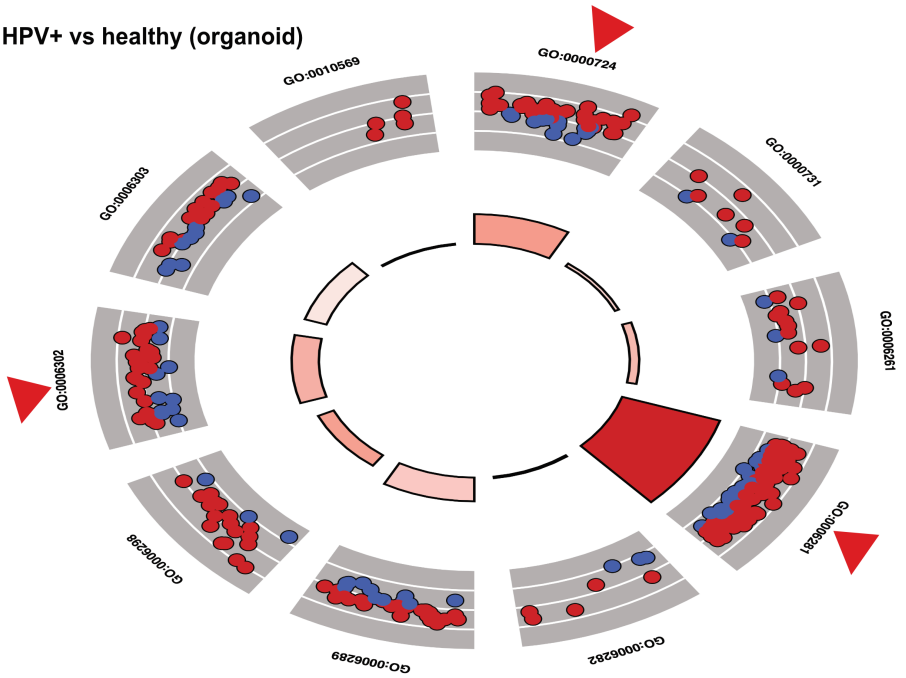

Cancer vs healthy (organoid)

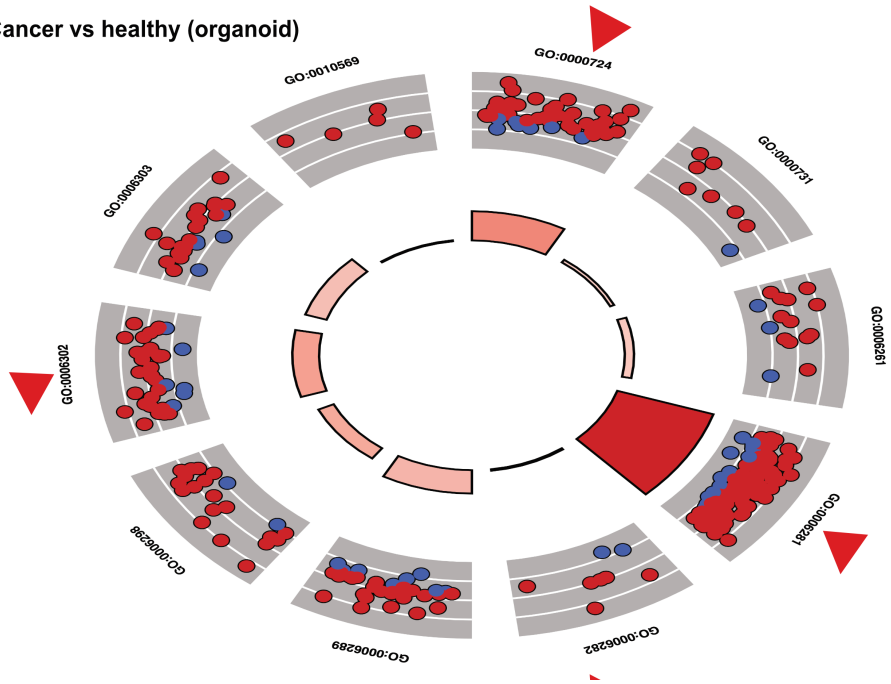

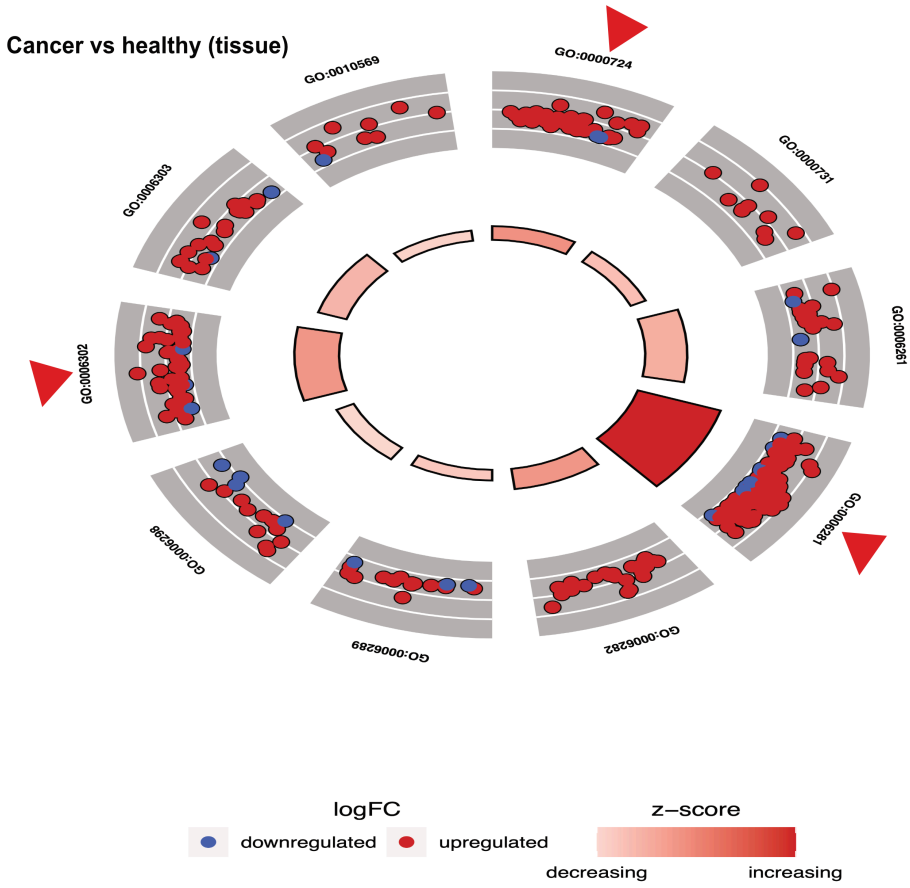

Figure 10. Enhanced functional enrichment of DNA repair genes in HPV+ and cancerous cervical organoids.

A) Volcano plots revealed enriched GO biological processes in the studied groups (HPV+vs healthy organoid, cancer vs healthy organoid, cancer vs healthy tissue), using a threshold of FDR<0.05 and |log2 fold change| ≥ 1.5. Significant upregulations (FDR<0.05, log2FC ≥ 1.5) are marked in red, and downregulations (FDR<0.05, log2FC ≤ -1.5) in blue.

B) Enrichment analysis of 10 specific DNA repair processes was visualized, where red and blue dots within each DNA repair process denote up- and down-regulated genes, respectively. The z-score corresponded to the enrichment within DNA repair processes. The table includes the corresponding Gene Ontology (GO) identifiers.

4.3 DNA repair gene-derived epitopes as potential tumor-associated antigens in cervical cancer

4.3.1 Characteristics of HLA-I/II-restricted peptide repertoires across four cervical cancer organoid lines

DNA repair deficits and HPV-related gene impairments can drive critical genomic changes, resulting in the expression of neoantigens and TAAs in cervical cancer (De Mattos-Arruda et al.,2020;Ma et al.,2018). These antigens are processed and presented on the cell surface bound to HLA molecules, forming a repertoire of non-self-peptides recognizable by the

immune system, thus initiating an immune response against HPV-infected or cervical cancer cells (Wang et al.,2020). RNA sequencing is commonly employed to identify neoantigen and TAA-derived peptides, but advancements in multi-omics have made mass spectrometry an invaluable tool for peptidome characterization. By using HLA immunoaffinity purification, peptides bound to HLA molecules can be isolated into a candidate antigen pool for validation.

For each cervical cancer organoid sample comprising 1.0 x 10^8 cells, a comprehensive harvest was performed. Marcel Wacker from Tübingen University executed the peptide elution and subsequent data acquisition. The analysis yielded a diverse spectrum of HLA-I/II-restricted peptides across four distinct cervical cancer organoid lines. A total of 6,515 HLA-I-restricted peptides were cataloged, distributed among the lines as follows: 2,824 in Cancer1, 1,679 in Cancer2, 1,628 in Cancer3, and 384 in Cancer4 (Figure 11A, red). In addition, we identified 719 HLA-II-restricted peptides, with Cancer1 contributing 153, Cancer2 contributing 199, Cancer3 contributing 140, and Cancer4 contributing 227 (Figure 11A, blue). Predominantly, HLA-I-restricted peptides ranged from 8-12 amino acids (Figure 11B, red), whereas the HLA-II-restricted peptides demonstrated a broader length variance of 8-25 amino acids (Figure 11B, blue).

Venn diagrams were then constructed to demonstrate the peptide diversity among the organoid lines. Notably, a mere 6 HLA-I peptides (Figure 11C, upper) and 34 HLA-II peptides (Figure 11C, lower) were common to the four lines, whereas Cancer 2 and Cancer 3 shared 1,367 HLA-I-restricted and 84 HLA-II-restricted peptides. Due to an anomalously low peptide count, Cancer 4 was omitted from further analysis.

HLA genes are highly polymorphic within the human genome, with over 35,000 allotypes spanning HLA-A, -B, and -C subfamilies (Amini et al.,2019). To delve deeper into peptide binding affinities and immunogenic potential, Hilmar Berger identified the HLA-allotypes present in the four cervical cancer organoid lines, detailed in Table 13. The HLA alleles HLA-A01:01, HLA-A03:01, HLA-A68:01, HLA-B27:07, HLA-B52:01, HLA-C12:02, and HLA-C*15:02 were prevalently observed across all four cervical cancer organoid lines studied.

Table 13. HLA allotypes of the four cervical cancer organoid lines

Sample	**HLA-A1**	**HLA-A2**	**HLA-B1**	**HLA-B2**	**HLA-C1**	**HLA-C2**
Cancer 1	A*03:01	A*03:01	B*27:07	B*27:07	C*15:02	C*15:02
Cancer 2	A*01:01	A*68:01	B*52:01	B*15:23	C*07:04	C*12:02
Cancer 3	A*01:01	A*68:01	B*52:01	B*15:23	C*12:02	C*07:04
Cancer 4	A*02:01	A*03:01	B*07:02	B*07:02	C*07:02	C*07:02

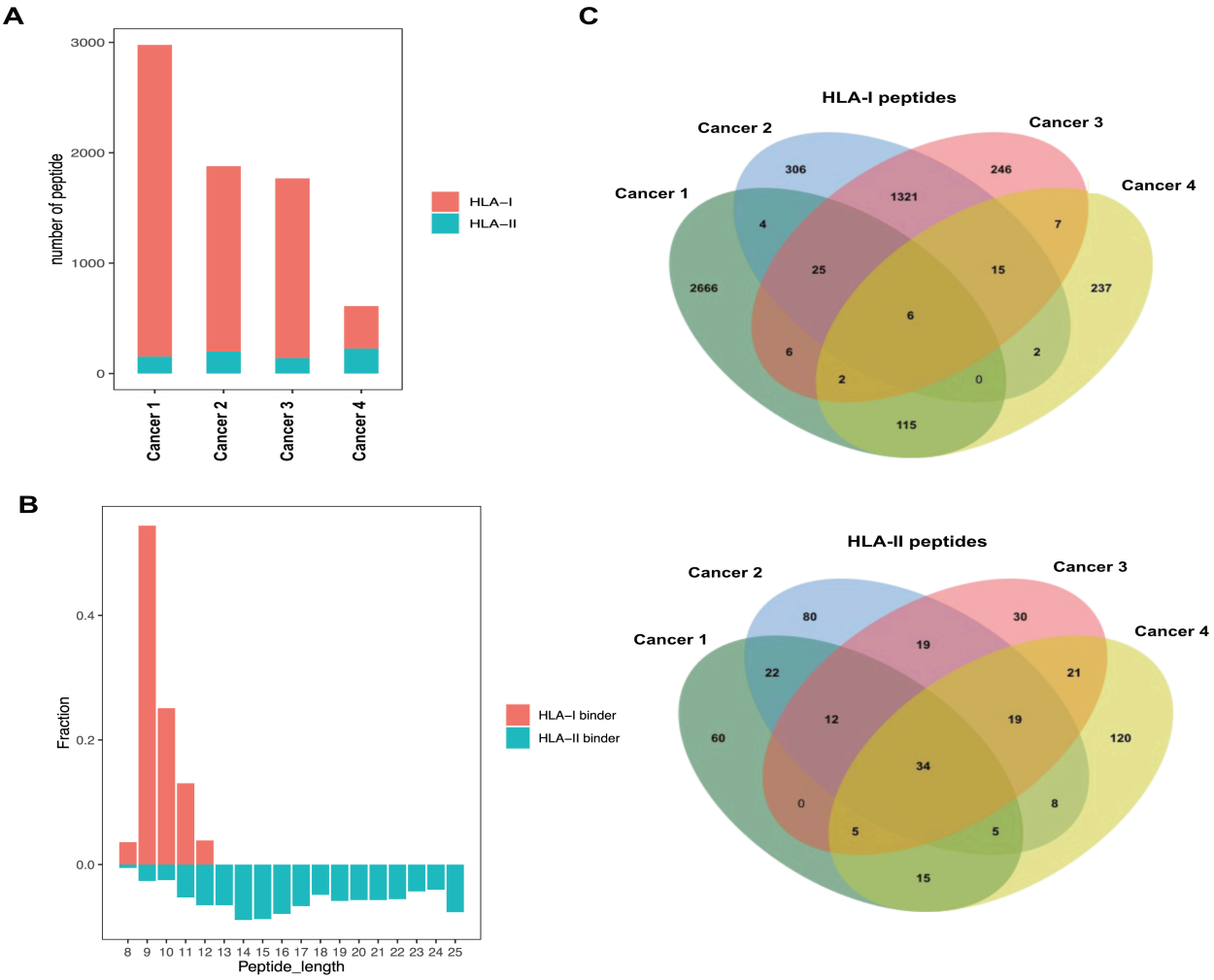

Figure 11. Peptidome profile of HLA ligands in cervical cancer organoids.

A) Mass spectrometry was employed to identify HLA-I/II-restricted peptide sequences from the four cancer organoid lines. Within the bar plot, the quantity of peptides bound to HLA-I and HLA-II depicted by red and blue bars, respectively.

B) This bar plot illustrated the distribution of peptide lengths for the whole HLA-I and HLA-II-restricted peptide repertoires from the four organoid lines. Peptide lengths were indicated on the x-axis, with HLA-II peptide lengths reflected on the negative scale, and the y-axis showed the proportion of peptides at each length.

C) The Venn diagram visualized the commonality among peptides presented by HLA-I (upper) and HLA-II (lower) across the four cancer organoid lines.

4.3.2 Identification of highly immunogenic peptides within HPV-positive cervical cancer organoids.

TCR recognition of foreign peptides presented by HLA molecules is crucial for the subsequent T cell activation and immune response. Assessing TCR recognition involves evaluating factors such as binding angles, cofactor necessity, kinetic rates of association and dissociation, stability, and the detailed nature of the interaction (Edwards et al.,2012;Gagnon et al.,2006). These factors collectively contribute to the binding affinity. While certain studies suggest that a high-affinity TCR-pHLA (peptide-HLA complex) interaction may not always activate T cells, a consensus exists that a higher binding affinity generally promotes T cell activation (Holler and Kranz,2003;Stone et al.,2009;Tian et al.,2007). Binding affinity can be quantified using various techniques, including surface plasmon resonance (SPR) for 3D affinity, computational docking simulations like TCRFlexDock, and tetramer assays (Pierce and Weng,2013). Moreover, computational tools are increasingly used to pre-screen potential peptide targets from vast libraries, enhancing efficiency while reducing costs and time. Popular tools such as NetMHC, NetMHCpan, MHCflurry, and resources from the Immune Epitope Database (IEDB) can be utilized to predict peptide-HLA binding affinities and immunogenicity based on peptide sequences and HLA allotype variations. In this study, the predictive metrics of binding affinity (IC50 in nanomolar) and the percentile rank scores serve as indicators to gauge the likelihood of binding (Paul et al., 2013).

In this study, I focused on peptides originating from genes overexpressed in HPV-associated and cancerous organoid lines. The initial analysis involved mapping the overlap between overexpressed genes in HPV-associated and cancerous organoids and the HLA-I/II-restricted peptide repertoire across cancer1-3 organoid lines, which was illustrated via the Venn diagrams in Figure 12A-C. Overlapping of overexpressed genes and HLA-I-restricted peptides was observed (315 in cancer1, 92 in cancer2, and 40 in cancer3), with a noted scarcity of overlaps within HLA-II peptides (Figure 11A-C). Subsequent to this finding, I focused exclusively on HLA-I-restricted peptides for further analysis regarding binding affinity and immunogenic potential. Utilizing the IEDB's immunogenicity prediction tool, I identified highly immunogenic peptides exceeding a MHC-I Immunogenicity score > 0 (IEDB.imm). Further, binding affinities were calculated using NetMHCpanBA4.0, selecting strong binders with IC50 values below 500 nM and rank scores under 1. The distribution of these strong versus weak binders was visually represented in Figure 12D with red and blue bars, respectively, revealing those strong binders to HLA-A01:01, HLA-A03:01, HLA-A68:01, HLA-B27:07, and HLA-C*15:02 comprised less than 10% of the total identified peptide repertoire (Figure 12D).

4.3.3 Detection of conserved residues among high affinity HLA-I peptides

HLA Class I molecules are composed of a constant β2-microglobulin chain and a variable heavy chain, the latter containing α1, α2, and α3 domains. These domains form a peptide-binding groove with specificity dictated by a series of pockets unique to each HLA allotype (Papadaki et al.,2023). T cell receptor (TCR) recognition hinges on the interaction between its complementarity-determining regions (CDRs) and the polymorphic residues of the α1 and α2 helices of the HLA-I molecule, as well as the presented peptide's residues (Papadaki et al.,2023). Notably, TCR specificity primarily arises from the CDR3's interaction with the peptide (Szeto et al.,2020). Variations in the chemical properties of the pockets in the HLA-I heavy chain lead to distinct peptide repertoires being presented; often, the peptides' second and terminal residues are conserved among those that bind to a common HLA molecule (Szeto et al.,2020).

To elucidate the amino acid patterns of peptides with strong binding affinities, sequence motifs were analyzed. These motifs represent conserved and information-rich patterns that are essential for the interaction between peptides and their corresponding receptors. In the motif logos, the prevalence of specific amino acids at each position is depicted by the relative size of letters, with the height indicating the frequency of occurrence (Andreatta et al.,2017; Sricharoensuk et al.,2022). Motif patterns of the identified potent binding peptides were delineated utilizing GibbsCluster 2.0. The resulting motifs for the peptides presented by five HLA-I allotypes (HLA-A*0301, HLA-C*1502, HLA-B*2707, HLA-A*0101, HLA-A*6801) highlighted conserved residues, particularly at the second and C-terminal positions (Table 14), aligning with findings of the previous study (Szeto et al.,2020). Predominantly, amino acids consist of the high immunogenic peptides, such as Arginine (R), Lysine (K), Tyrosine (Y), Phenylalanine (F), Leucine (L), Valine (V), Asparticacid (D), Isoleucine (I), and Threonine (T) were favored at the anchor positions for these five HLA allotypes (Figure 12E, Table 14). Specifically, HLA-A0301 and HLA-A6801 shared anchor residues at C-terminal, while HLA-C1502 and HLA-B2707 showed commonality at the C-terminus (Table 14). The detailed anchor residue patterns for these allotypes were cataloged, reflecting the allotype-specific anchor residue characteristics and suggesting a potential for cross-presentation, which is crucial for immune surveillance (Di Marco et al.,2017).

Table 14. Anchor residues of the HLA-I allotypes

Position	HLA-A*0301	HLA-C*1502	HLA-B*2707	HLA-A*0101	HLA-A*6801
1	-	R,K	-	-	-
2	L,I,V	T,S	R,K	T,S	V,T
3	-	-	-	D,E	-
C-terminus	K,R	L,I,V	L,I,V	Y,F	K,R

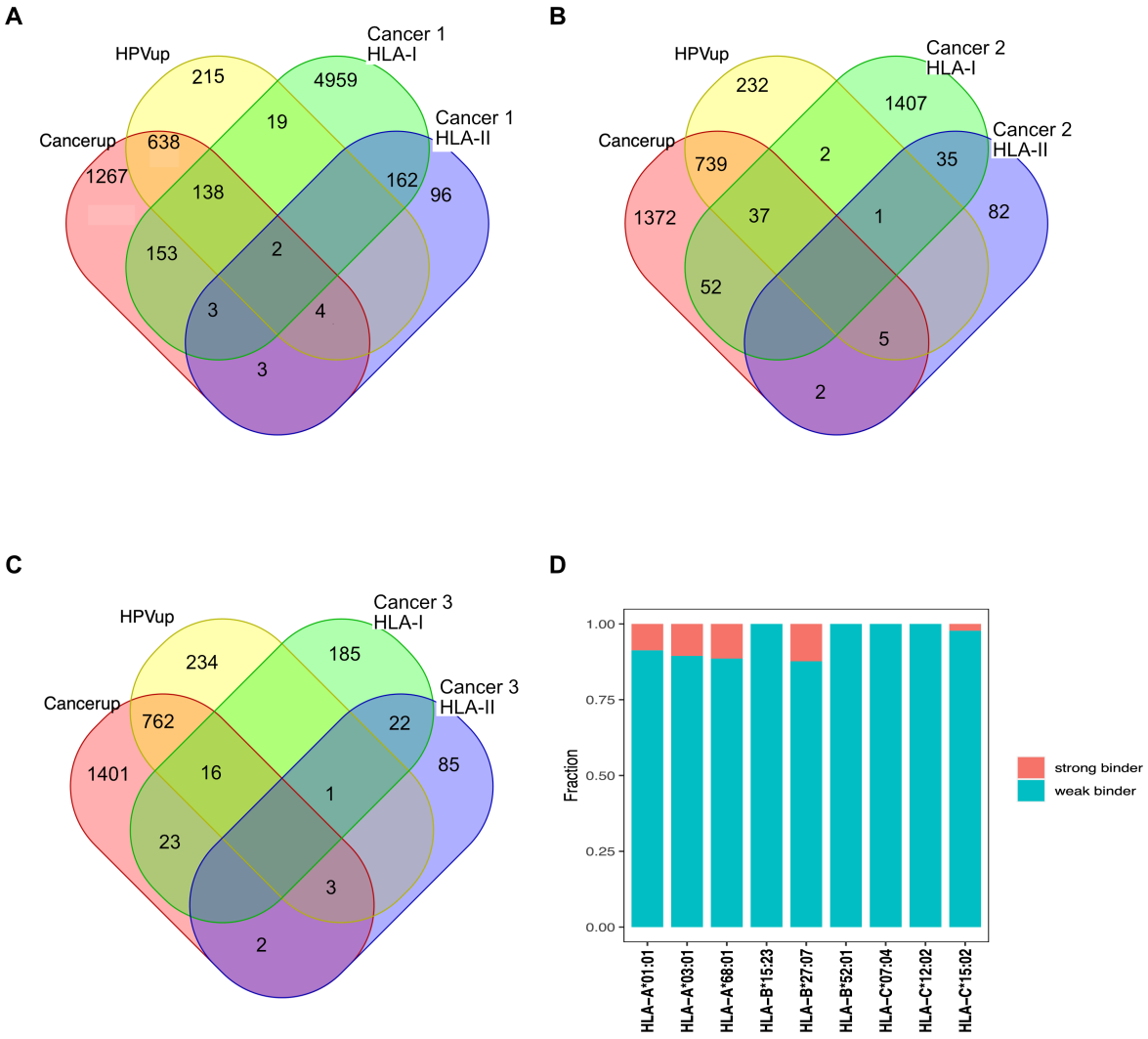

E

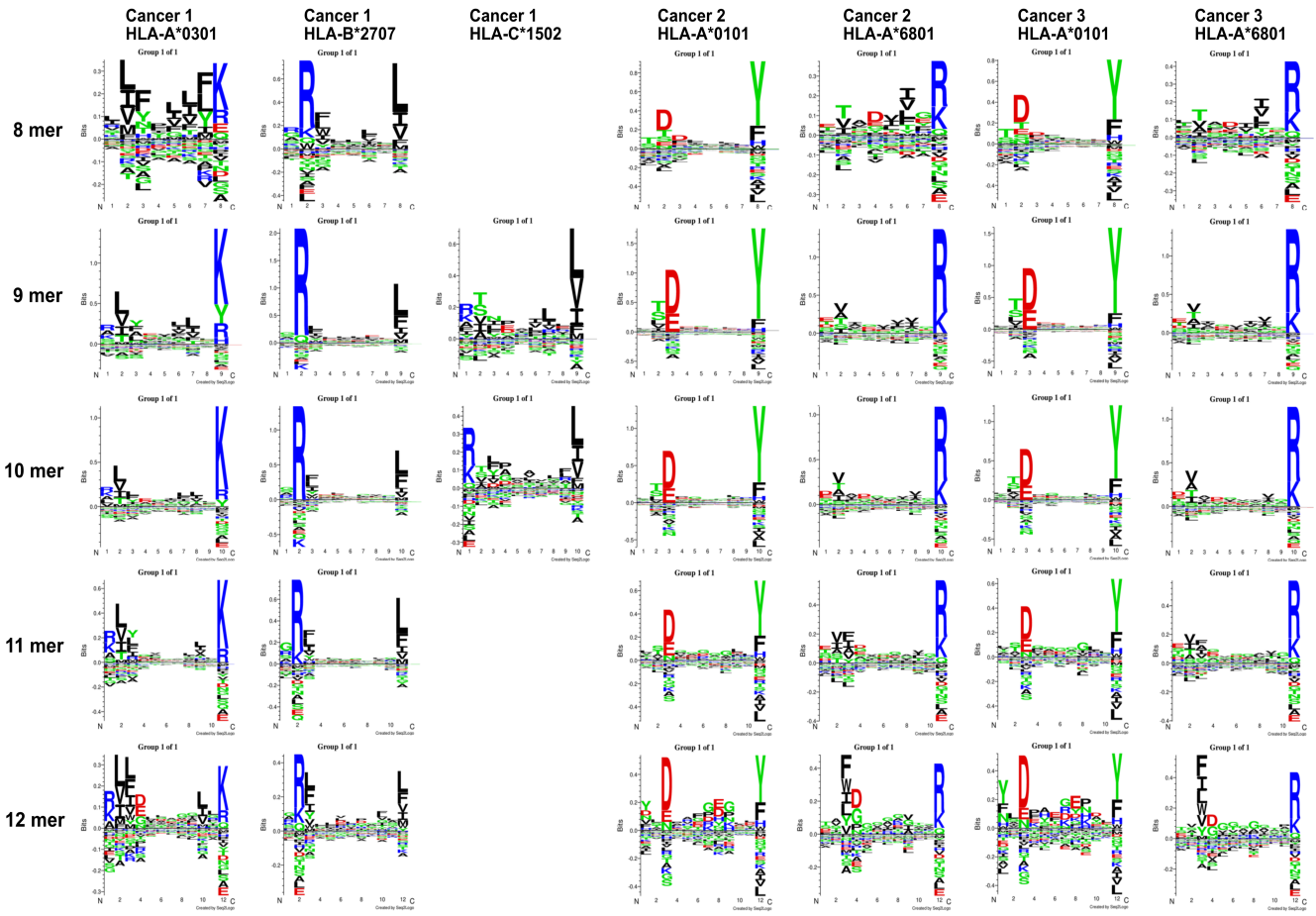

Figure 12. Characterization of binding motifs in high-affinity epitopes.

A-C) Venn diagrams depict the intersection of HLA-I/II-restricted peptides derived from cervical cancer1-3 organoid lines (designated as Cancer1/2/3 HLA-I/II) with the overexpressed genes in HPV and cancer organoids (notated as HPVup/Cancerup). The repertoire of HLA-Class I-restricted peptides coinciding with the genes that demonstrated elevated expression levels was advanced to further analysis to assess their immunogenicity and HLA-binding affinity.

D) The peptides with high immunogenicity (an immunogenicity score > 0) were subsequently selected for assessment of their binding affinity. The plot illustrated the proportion of peptides that exhibit either strong (red) or weak (blue) binding affinities to HLA-I allotypes, with strong binders defined by IC50 < 500 nM and a rank score < 1 using NetMHCpanBA4.0.

E) Motif analysis of the strong binders: GibbsCluster 2.0 algorithm facilitated the delineation of sequence motifs for strongly binding peptides (8-12 amino acids in length) associated with HLA-A03:01, HLA-B27:07, HLA-C15:02 in cancer1, and HLA-A01:01, HLA-A*68:01 in cancer2 and cancer3. Specifically, the C-terminal anchor residues K, and R were shared by HLA-A*0301 and HLA-A*6801. L,V, and I were identified at position 2 of peptides binding to HLA-A*0301. HLA-C*1052 and HLA-B*2707 shared L,V,I at C-terminus and R, K were beared at position 2 of the HLA-B*2707 restricted peptides, but at position 1 of the HLA-C*1502 peptides. T and S were shared by position 2 of the peptides on both HLA-C*1502 and HLA-A*0101. In the HLA-A*0101 peptides, position 3 and C-terminus were dominated by D, E and Y, F respectively.

4.3.4 Prominent DNA repair enrichment within high immunogenic HLA-I peptide repertoire

To annotate the biological processes and functions of the peptides with high immunogenic, these peptides were aligned with the Gene Ontology (GO) Biological Process (BP) database. The resulting dot plots illustrate the top 20 enriched GO BPs within the peptide repertoire, factoring in p-value significance and the frequency of gene occurrence in each process (Figure 13). The size of each dot corresponds to the number of genes enriched in a biological process, and the brightness of blue signifies the p-value, with darker blue indicating lower p-values. Notably, processes like cell division, cell cycle, and DNA repair were prominently represented in the high immunogenic HLA-I peptide repertoire (Figure 13), corresponding to the transcriptomic discoveries. This alignment underscores the critical role of the relevant genes involved in these processes. The observed enrichment of DNA repair-related genes at both the transcriptome and peptidome levels supported a hypothesis: the overexpression of DNA repair-related genes might result in an increased translation of DNA repair-related antigens. These antigens, when persistently exposed to immune cells, may impact the immune response and induce the sustained expression of immune-checkpoint molecules in the tumor microenvironment (TME) (Angelosanto et al.,2012). Beyond cell division and DNA repair, the HLA-I-restricted peptides are also implicated in protein phosphorylation, inhibition of apoptosis, innate immune response, and antiviral defense (Figure 13), which are processes known to regulate the dynamics of cervical cancer development and immune-mediated eradication (Riera Romo, 2021).

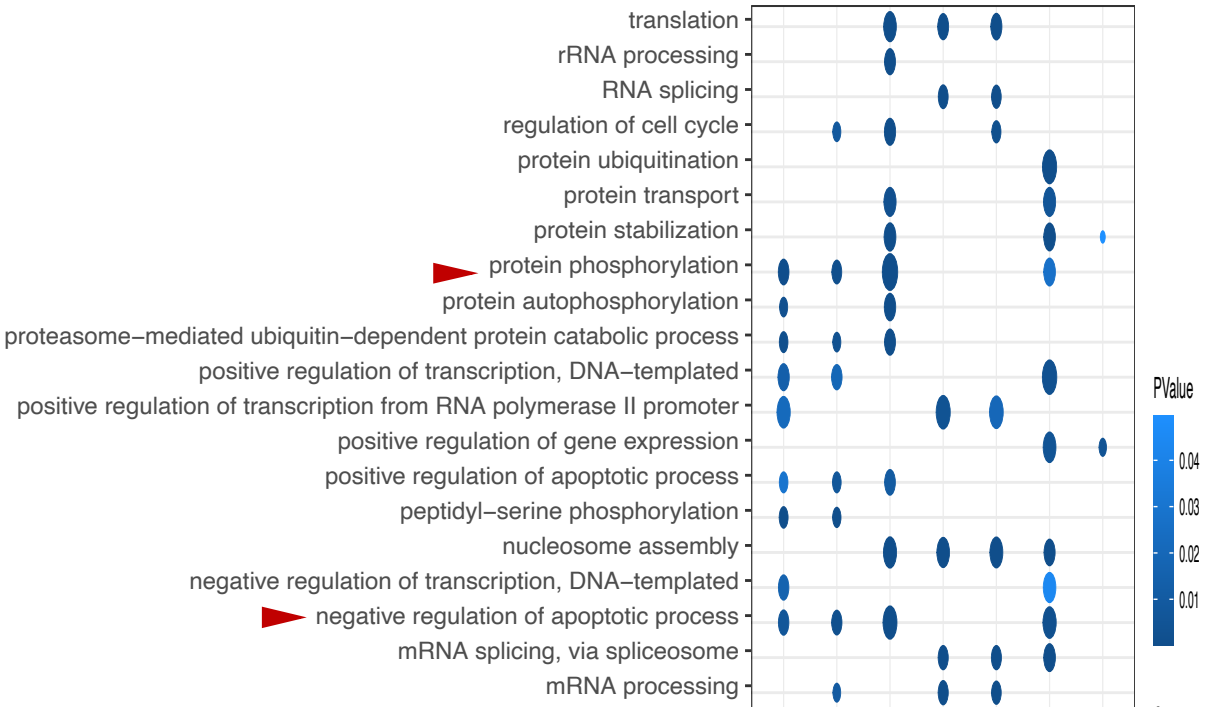

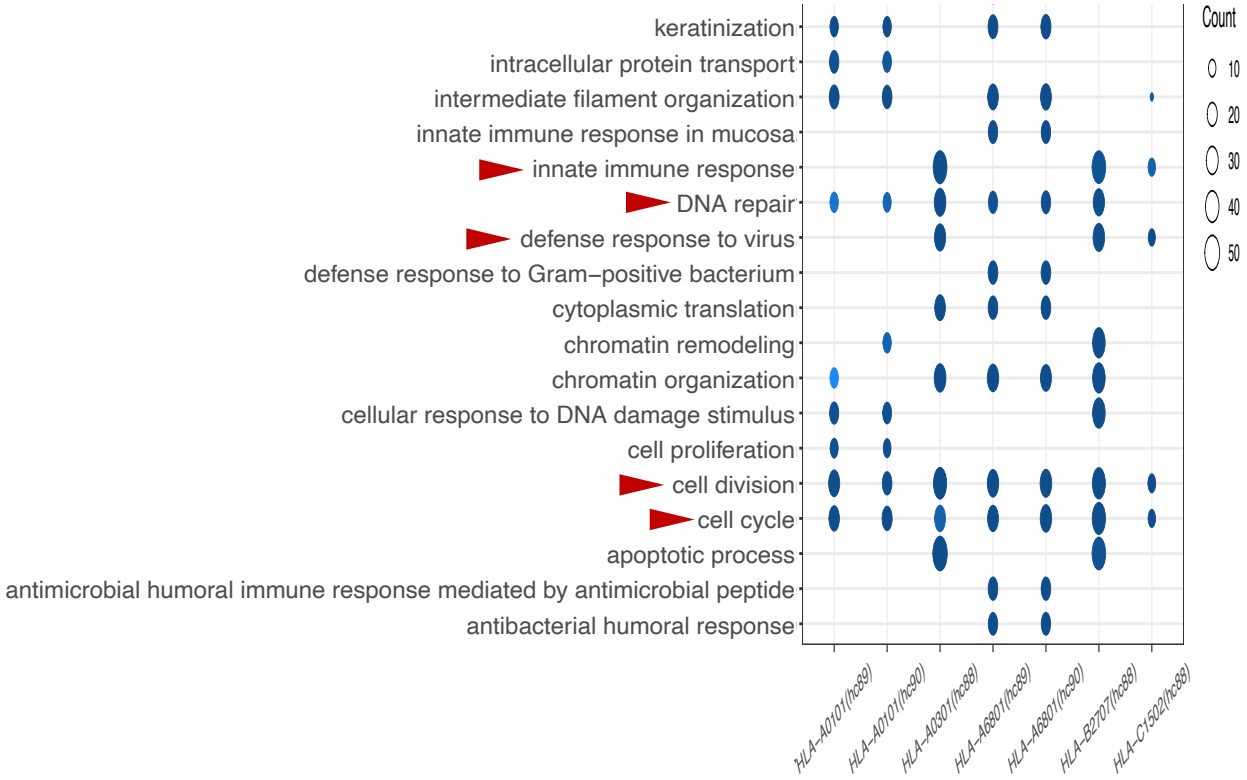

Figure 13. Functional enrichment analysis of high immunogenic HLA-I peptide repertoire.
A dot plot visualization of the top 20 significantly enriched biological processes within the high immunogenic HLA-I-binding peptide repertoire derived from the three cervical cancer organoid lines (cancer1-3). Among the top 20 GO biological processes, peptides enriched in cell division, cell cycles and DNA repair processes were displayed by HLA-I molecules across all cancer organoids. The magnitude of each dot is proportional to the quantity of genes, with a larger size indicating a greater number of genes involved. The intensity of the blue brightness indicates the level of statistical significance, with darker blue representing lower p-values.

4.4 High correlation of DNA repair gene signature with patient prognosis and tumor microenvironment regulation in cervical cancer

4.4.1 Implications of DNA Repair Gene signature (DRGscore) for prognostication in cervical cancer

The transcriptomic profiling of organoid cultures and the analysis of GEO cervical tissue datasets have yielded insights into the role of DNA repair genes in cervical carcinogenesis. Notably, robust DNA repair mechanisms are operational during the malignant transformation of cervical cells (Helleday et al.,2008;Prati et al.,2018). A deficiency in DNA repair processes leads to the accumulation of somatic mutations and increases the efficacy of treatments such as immune checkpoint inhibitors, chemotherapy, and radiation therapy (Volkova et al.,2020; Zhu et al.,2021; Zhu et al.,2016). Thus, I posited that a DNA repair gene signature could

predict patient prognosis in cervical cancer, leading to the construction of a DRGscore for further analysis.

4.4.1.1 Formulation of DRGscore employing LASSO-Cox regression modelling

The concept of a gene signature refers to a distinct expression pattern across a set of genes that enables to define a natural ranking of samples and classify the samples in unsupervised way (Cantini et al.,2017). In my research, I utilized the TCGA-CESC dataset, which includes transcriptomic and clinical information from 304 cervical cancer patients, to construct a DNA repair gene (DRG) signature. This signature was developed by incorporating the top 100 well-characterized DNA repair genes identified through GeneCards. I employed the least absolute shrinkage and selection operator (LASSO-COX) regression analysis for dimensionality reduction to formulate the DRG signature (DRGscore). In 1997, Robert Tibshirani introduced this novel method for variable selection and shrinkage in Cox's proportional hazards model (Tibshirani,1997;Yang et al.,2022). This approach, now widely adopted, facilitates the selection of predictive variables associated with overall survival (OS) time and generate gene signatures indicative of prognostic outcomes (Tibshirani,1997;Yang et al.,2022). The optimal penalty parameter (λ) for the LASSO model was determined by selecting the λ associated with the minimum partial likelihood deviance, utilizing the “glmnet” and “survival” packages in R (Li et al.,2021;Xu et al.,2022;Xu et al.,2023) (Figure 14A). Subsequently, five candidate genes and their respective λ values (λ (RAD50): 0.12368922, λ (OGG1): 0.0211609, λ (SUCLA2): 0.04715829, λ (XPA): 0.0045094, λ (MGMT): 0.0153683) were integrated to construct the DRGscore for each patient. Utilizing the “survival” and “survminer” R packages, defined a cutoff value for the DRGscore at 0.07 to categorize patients into high or low DRGscore groups. The DRGscore exhibited a strong prognostic ability for overall survival (OS), revealing a profound survival disparity ($p<0.0001$) between the two groups, with patients in the low DRGscore cohort experiencing a more favorable prognosis (Figure 14B).

4.4.1.2 Enhanced prognostic predictive power of DRGscore over TIDEscore and TISEscore

Two prognostic metrics, the Tumor Immune Dysfunction and Exclusion (TIDE) score and the Tumor Inflammation Signature (TIS) score, are known to predict clinical responses to immunotherapy (Jiang et al.,2018). It has been observed that elevated TIDE scores and diminished TIS scores correlate with suboptimal outcomes following immunotherapy (Huang et al.,2021). To evaluate the prognostic predictive efficacy of DRGscore relative to TIDEscore and TISscore, I employed the same TCGA-CESC dataset to compute these three scores and subsequently appraised their prognostic accuracy using receiver operating characteristic (ROC) curve analysis (Rock et al.,2016), with reference to patient overall survival (OS) times.

Employing the R packages “pROC,” “ggplot2,” and “ggpubr,” I generated the ROC curves and calculated the Area Under the Curve (AUC). The analysis confirmed that the DRGscore, with an accuracy of 62.9%, outperforms both the TIDEscore (54.6%) and the TISscore (58%) in prognostic prediction (as shown in Figure 14C). Intriguingly, the DRGscore demonstrated superior predictive power for patient prognosis when contrasted with the other two scores related to immunotherapy.

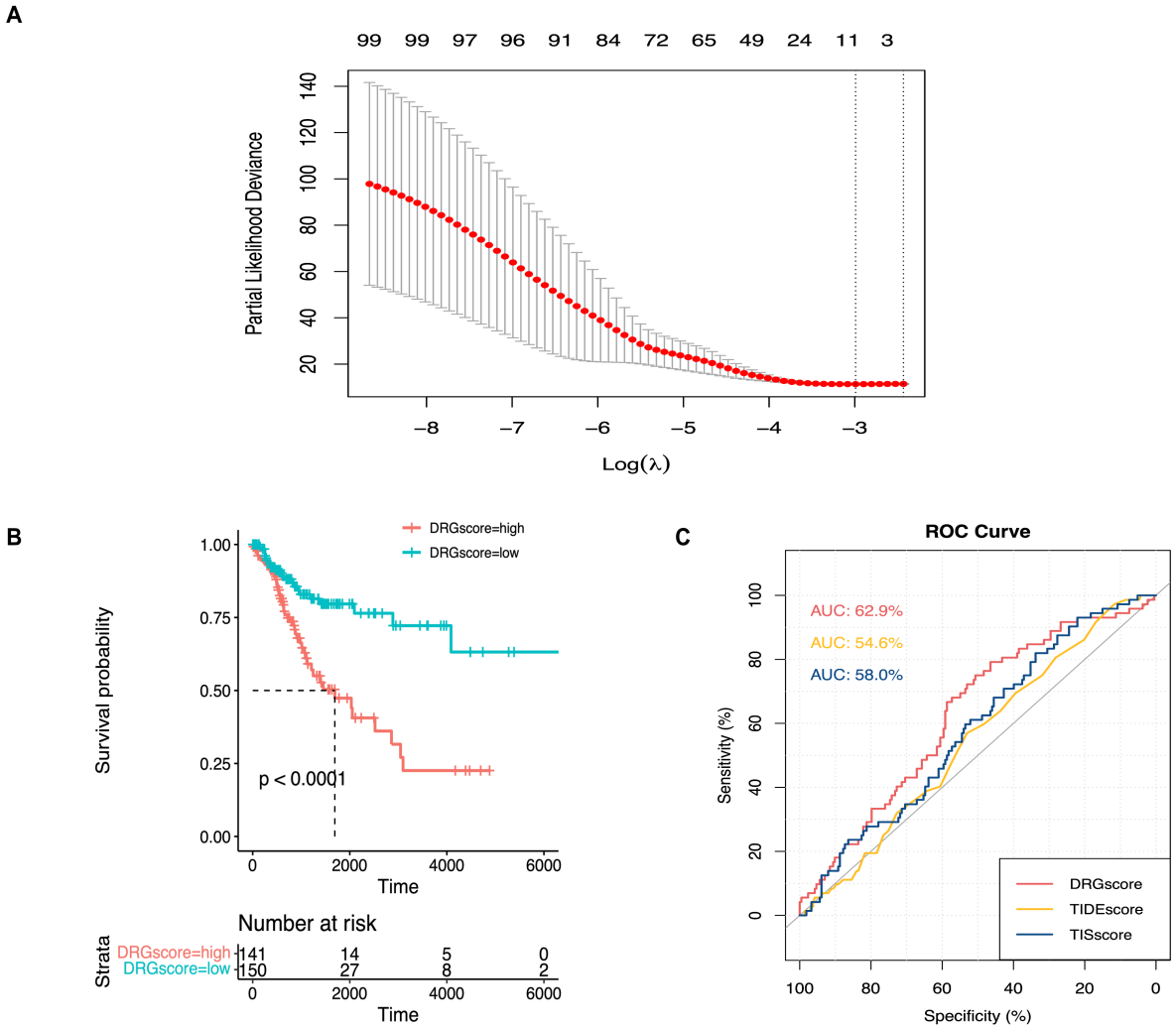

Figure 14. Assessment and prognostic comparison of DRGscore in cervical cancer.

A) This panel presented the application of the least absolute shrinkage and selection operator (LASSO) Cox regression analysis to derive a DNA Repair Gene (DRG) signature. Displayed was a plot from a 10-fold cross-validation procedure to determine the optimal penalty parameter (λ) based on the minimum criteria. The plot illustrated the relationship between the partial likelihood deviance and the logarithm of λ, with dotted vertical lines indicating the optimal λ corresponding to the minimum criteria and one standard error from this minimum. The number of retained variables at each given λ is denoted along the upper x-axis.

B) The Kaplan-Meier survival curves differentiated between patients with high and low DRGscore values within the TCGA-CESC cervical cancer cohort. The plot's lower segment enumerates the count of surviving patients at various time points post-diagnosis, segregated into the two DRGscore strata. Statistical significance was determined using two-tailed Student´s t-test with mean ±SD, a p-value <0.05 was considered statistically significant.
C) This section compared the prognostic utility of the DRGscore, TIDEscore, and TISscore for cervical cancer patients within the TCGA-CESC cohort, utilizing receiver operating characteristic (ROC) analysis. The efficacy of each scoring method in predicting patient outcomes is visualized through the ROC curves and quantified by the Area Under the Curve (AUC).

4.4.2 Strong correlation between DRGscore and tumor environment alterations

The tumor microenvironment (TME) is pivotal in shaping tumor development, progression, and therapeutic outcomes, characterized by its dynamic and complex cellular architecture. Apart from the tumor cells, the TME includes a variety of cellular components such as stromal cells, endothelial cells, and immune cells, along with growth factors, cytokines secretion, and different immune checkpoints expression. Together, these components can either drive or hinder tumor growth, highlighting the multifaceted influence of the TME on cancer dynamics.

4.4.2.1 Correlation between multiple immune cell subsets in TME and patient prognosis

Immune cells are crucial elements within the tumor microenvironment (TME), playing a dual role that varies based on context. Tumors are classified into two types based on the presence and distribution of immune cells within the TME: "hot" tumors, characterized by immune cell infiltration, and "cold" tumors, which lack immune cell presence in the TME. The presence of CD8 and CD4 T cells, B cells, Dendritic cells and NK cells within the Tumor Microenvironment (TME) is generally associated with a favorable prognosis and can aid in predicting responses to Immune Checkpoint Inhibitors (ICIs) (Del Prete et al.,2023;Gentles et al.,2015). To explore the impact of multiple immune cell subgroups on cervical cancer patient prognosis, the CIBERSORT algorithm, developed by researchers at Stanford, which is accessible via an online platform (https://cibersort.stanford.edu/), was employed to assess the proportions of 22 types of infiltrating immune cells within the TCGA-CESE RNA-seq data (Luca et al.,2021). Employing the "survival" and "survminer" R packages, Kaplan-Meier survival curves were generated to distinguish patients based on high and low proportions of various immune cell subgroups. Among the 22 types of infiltrating immune cells, B cells, CD8+ T cells, activated CD4+ T cells, and both activated and resting Dendritic Cells (DCs) showed a positive correlation with favorable prognoses in patients with cervical cancer (Figure 15). However, a higher presence of resting CD4+ T cells in the TME was associated with a poorer prognosis (Figure 15D). This observation aligns with the previously demonstrated prognostic landscape

of tumor-infiltrating immune cells across various human cancers (Anderson and Simon,2020; Del Prete et al.,2023; Gentles et al.,2015)

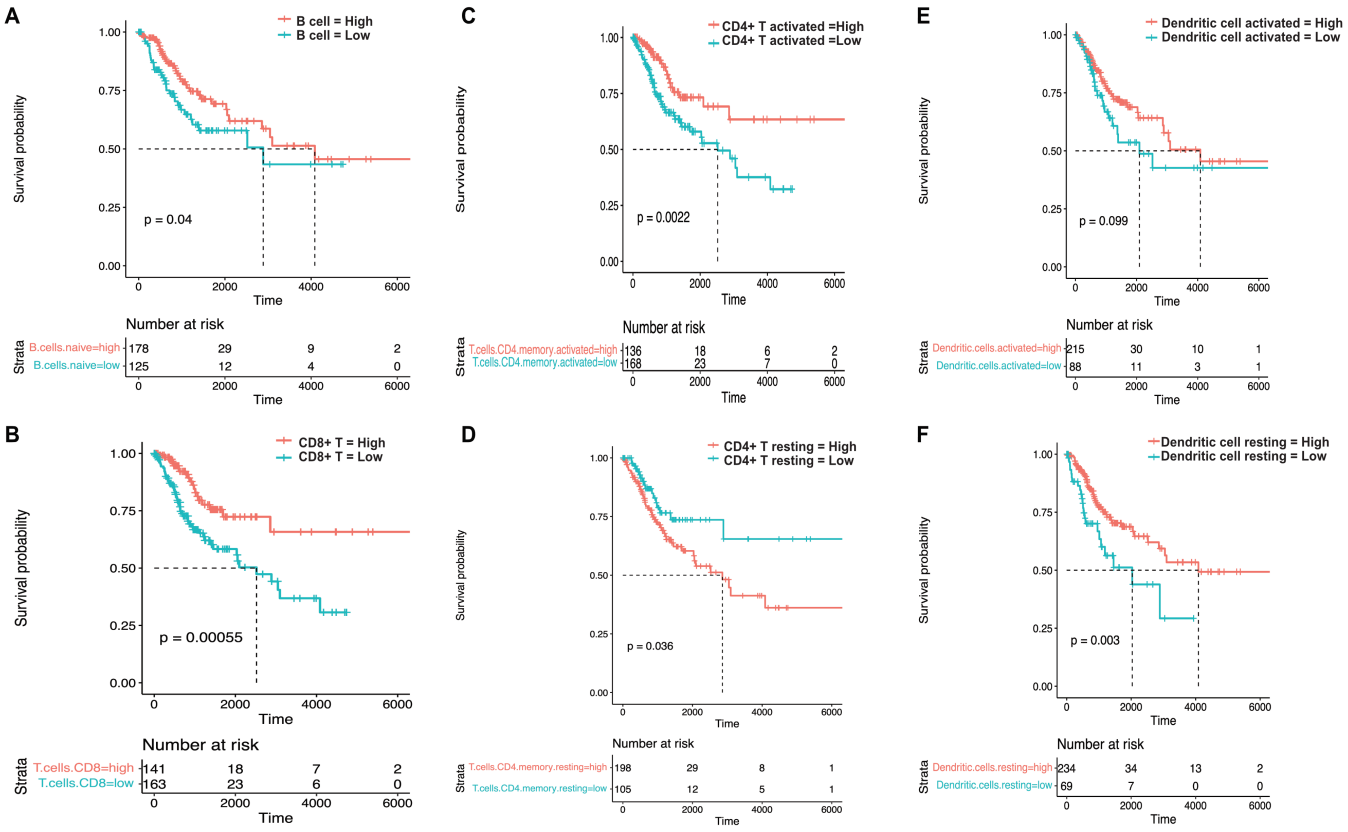

Figure 15. Analysis of prognostic significance of multiple immune cell subsets.
A-F) Kaplan-Meier survival analyses correlate the proportions of B cells (A), CD8+ T cells (B), activated CD4+ T cells (C), resting CD4+ T cells (D), activated Dendritic cells (E) and resting Dendritic cells (F) within patient survival outcomes in the TCGA-CESC cervical cancer cohort. Red represents the group with a larger proportion of the six immune cell subsets, while blue indicates the group with a smaller proportion of these cell subsets. Statistical significance was determined using two-tailed Student´s t-test with mean ±SD, a p-value <0.05 was considered statistically significant.

4.4.2.2 Differences in immune cell infiltration and immune checkpoint expression between groups categorized by DRGscore in cervical cancer

DNA repair dynamics have emerged as critical modulators of the TME, influencing both the efficacy of immune checkpoint inhibitors and the composition of immune cells within the TME (Duan et al.,2019;Lama-Sherpa and Shevde,2020). Moreover, a strong correlation has been observed between DNA repair insufficiency and both tumor mutation burden and neoantigen prevalence (Qing et al.,2021). Building on the findings above that demonstrated a significant correlation between various immune cell subsets and cervical cancer patient prognosis, the

capacity of the DRGscore to serve as an indicator for immune cell alterations within the TME and as a stratification aid for therapeutic direction is a crucial question that warrants further investigation.

To further explore this aspect, I utilized the "ESTIMATE" R package to derive microenvironmental scores from the TCGA-CESC dataset. I calculated stromal, immune, and ESTIMATE scores for the dataset (Fan et al.,2022;Feng et al.,2023). Drawing on the identified profile of 22 types of infiltrating immune cells, the 304 patients in the TCGA-CESC dataset were categorized into groups with high and low DRGscores, using a threshold DRGscore of 0.07. Subsequently, each patient's proportion of 22 types of infiltrating immune cells and the microenvironmental scores including stromal score, immune score, ESTIMATE score, were determined and compared across the DRGscore groups. Notably, a higher prevalence of CD8+ T cells, γδ T cells, and regulatory T cells (Tregs) was observed in the TME of the low DRGscore group, whereas the high DRGscore group exhibited an increase in M0 macrophages and resting CD4+ T cells (as shown in Figure 16A). To elucidate the relationships among DRGscore, microenvironmental scores, and immune cell infiltration, Figure 16B depicts the correlations, with red and blue indicating positive and negative associations, respectively, and dot size representing the significance level. DRGscore negatively correlated with microenvironmental scores and the presence of CD8+ T cells, M1 macrophages, activated CD4+ memory T cells, and γδ T cells, while positively correlating with M0 macrophages, affirming its potential as a negative prognostic indicator for immunotherapeutic outcomes (Figure 16B). Significant differences in the expression of three well-known immune checkpoints on T cells (CTLA-4, LAG-3, PD-1) and two expressed on cervical cancer cells (Galectin-9, HVEM) were observed between the high and low DRGscore groups (Figure 16C).

Overall, the DRGscore serves as a valuable indicator for assessing TME cell composition, and patient prognosis. A lower DRGscore correlates with a more favorable prognosis and a positive response to immunotherapy, marked by a higher presence of effective immune cells within the TME and increased expression of immune checkpoints. For patients with high DRGscores, employing DNA repair inhibitors may impair DNA repair activity, potentially enhancing the efficacy of subsequent treatments akin to those used in the low DRGscore cohort. Additionally, discovering the significant difference in infiltrating γδT cells between the high and low DRGscore groups was intriguing. Given that the presence of γδT cells in the TME is considered a positive indicator for cancer patient prognosis(Nabhan et al.,2023). I intended to explore the cytotoxic efficacy of γδT cells against cervical cancer cells.

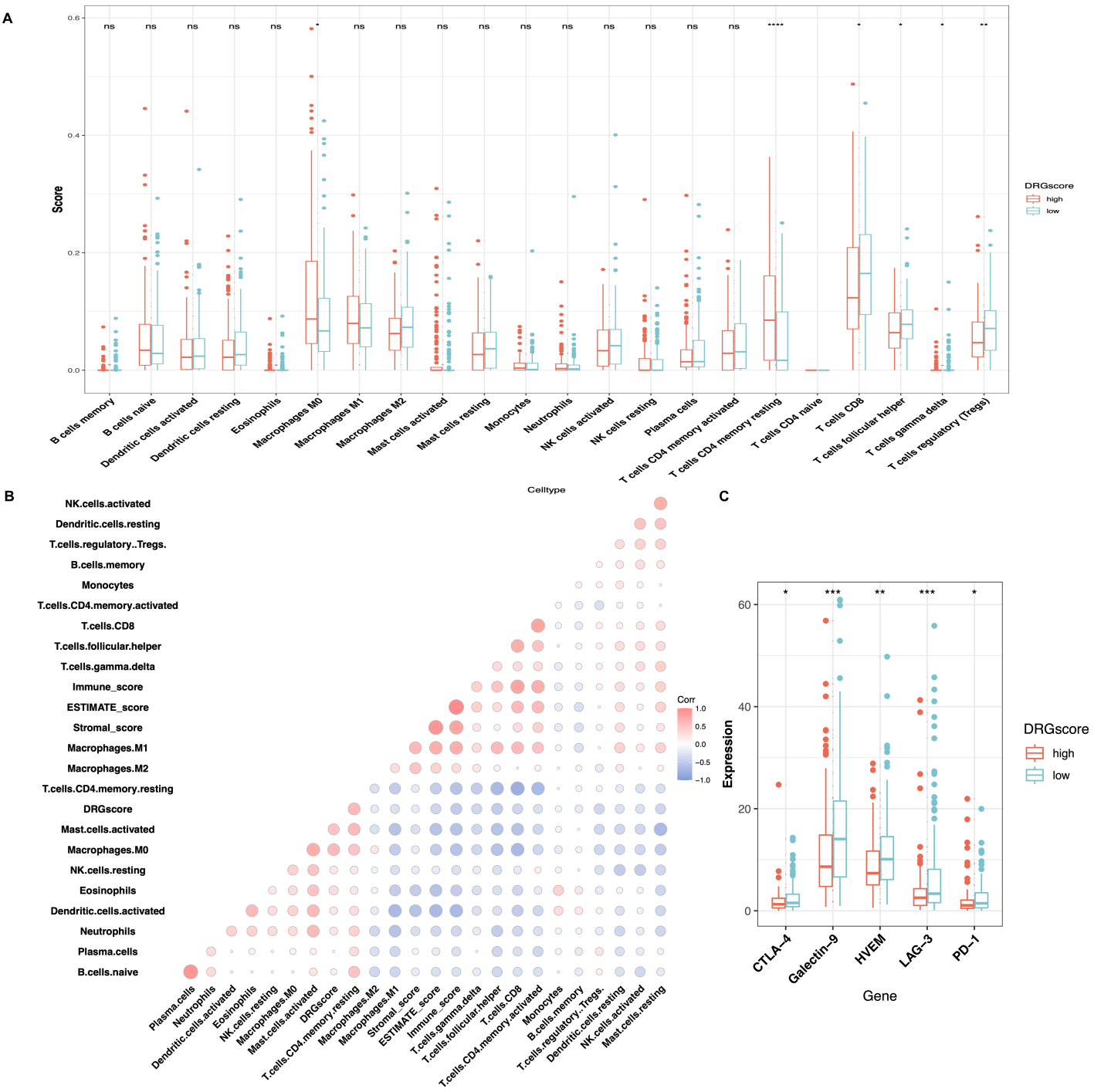

Figure 16. Assessment of immune landscape associated with DRGscore in the TCGA cervical cancer cohort.

A) The CIBERSORT algorithm quantitatively assesses the composition of 22 types of immune cells infiltrating the tumor microenvironment, comparing high versus low DRGscore patient groups. High DRGscore group is in red, low DRGscore group is in blue. Statistical significance was determined using two-tailed Student´s t-test with mean ±SD, 'ns' for not significant; * for p<0.05; ** for p<0.01; *** for p<0.001; **** for p<0.0001.

B) Correlations between DRGscore, immune cell populations and microenvironmental scores from the TCGA-CESC dataset are depicted, with color coding indicating the direction of correlation (red for positive, blue for negative) and dot size inversely related to the p-value.
C) Differential expression levels of immune checkpoints (CTLA-4, LAG-3, PD-1, Galectin-9, HVEM) are examined across patient groups with contrasting DRGscores. High DRGscore group is in red, low DRGscore group is in blue. Statistical significance was determined using two-tailed Student´s t-test with mean ±SD, 'ns' for not significant; * for p<0.05; ** for p<0.01; *** for p<0.001.

4.5 Vγ9Vδ2 T cells exhibit cytotoxicity against HPV+ and cervical cancer organoids

γδ T is an important T cell subset that kills tumor or infected cells in an HLA-independent manner (Kabelitz et al.,2020). Vγ9Vδ2 T cells are the major γδ T subset distributed in human blood and have been applied in clinics, which shed light on allogeneic T cell therapy development for cancer patients. Vγ9Vδ2 T cells were thus exploited in our study.

4.5.1 Efficient *in vitro* expansion of Vγ9Vδ2 T cells using zoledronate and IL-2 co-stimulation

Given the HLA-independent mechanism of Vγ9Vδ2 T cells, these allogeneic cells emerge as a viable option for immunotherapy in cancer treatment. The critical issue for adopting allogeneic Vγ9Vδ2 T cells in adoptive immunotherapy is the procurement of a sufficient number of efficacious cells, alongside confirming their clinical safety and effectiveness. Typically, γδ T cells can be obtained for therapeutic usage via *in vivo* patient stimulation or through *in vitro* expansion before infusion back into patients (Kunzmann et al.,2012;Nussbaumer and Koslowski,2019). Various agents, including zoledronate, recombinant IL-2, IL-15, IL-18, and vitamin C, have been examined to enhance expansion efficiency and purity (Peters et al.,2020). Currently, the combination of zoledronate and recombinant IL-2 is favored for optimizing *in vivo* and *in vitro* amplification of Vγ9Vδ2 T cells.

Research by A J Nicol and colleagues has shown that a higher yield of Vγ9Vδ2 T cells can be achieved from healthy donors than from cancer patients, and the initial frequency of these cells is crucial for the purity of the expanded population (Nicol et al.,2011). Accordingly, I assessed the baseline proportion of Vγ9Vδ2 T cells in donor PBMCs using Vγ9-AF488 and CD3-APC staining, targeting a threshold above 2%. The cells were then cultured with 50 IU/mL IL-2, added bi-daily, commencing with a mixture of 50 μM zoledronic acid and 100 IU/mL IL-2. Following an 11-14 day expansion period, the proportion of Vγ9Vδ2 T cells was reassessed. Due to individual variability in initial percentage and cell vitality, the purity of the expanded Vγ9Vδ2 T cells ranged from 90% to 96.4% (Figure 17). Peripheral blood mononuclear cells (PBMC) from all six donors successfully yielded Vγ9Vδ2 T cell populations with a purity surpassing 90%, meeting the stipulated criteria for subsequent experimental procedures.

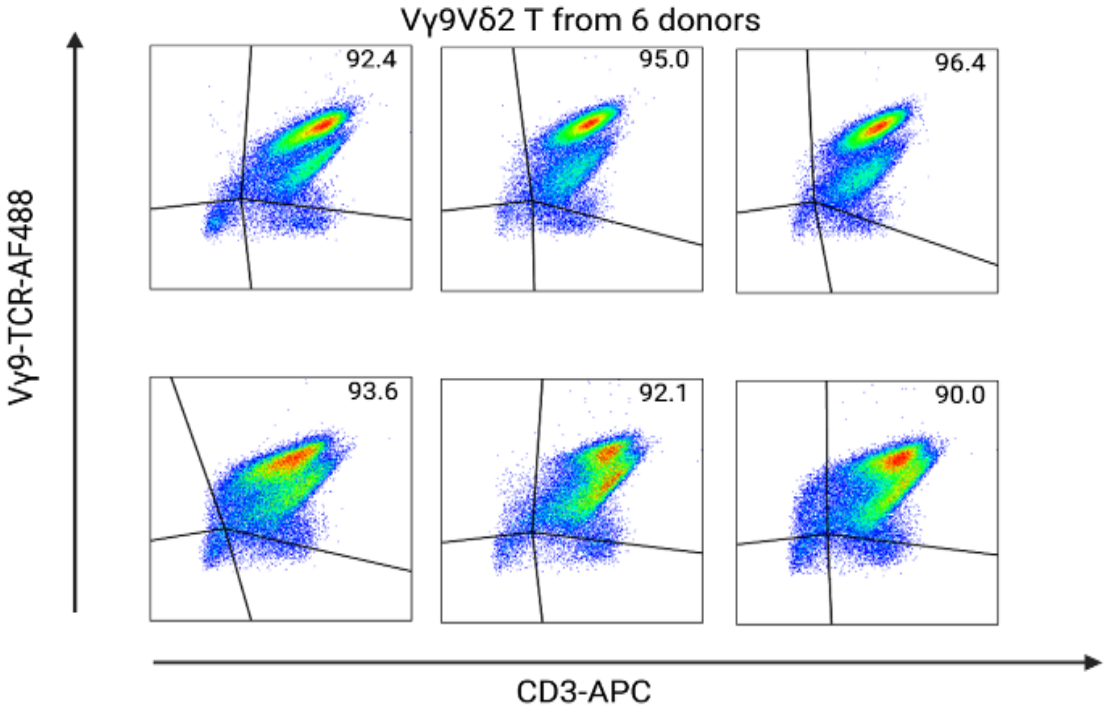

Figure 17. Efficiency of Vγ9Vδ2 T *in vitro* expansion.

Peripheral blood mononuclear cells (PBMCs) from six healthy donors, each with a Vγ9Vδ2 T cell proportion exceeding 2% of the total CD3+ cells, were incubated with 50 μM zoledronate (ZOL) and 100 IU/mL interleukin-2 (IL-2) on day one. Subsequently, 50 IU/mL IL-2 was supplemented bi-daily over the next 14 days. On the final day of the culture period, flow cytometry was employed to quantify the number of viable Vγ9Vδ2 T cells. Dot plots depicted the proliferation of Vγ9Vδ2 T cells in the PBMC cultures from the six donors at the conclusion of the two-week expansion protocol.

4.5.2 Selective cytotoxicity of Vγ9Vδ2 T cells against HPV+ and cancerous organoid cells

To examine the tumor-specific immune response triggered by Vγ9Vδ2 T cells, I quantified the cytotoxicity by measuring the number of deceased organoid cells post co-culture with Vγ9Vδ2 T cells. The organoid cells were stained with PKH67 for tracking via FITC fluorescence (Figure 18A). Co-incubation of Vγ9Vδ2 T cells with organoid cells occurred at effector-to-target ratios (E:T) of 0:1 and 10:1, both with and without the addition of BrHPP. The E:T ratio of 0:1 served as a negative control. The Daudi cell line, known for its ability to spontaneously activate Vγ9Vδ2 T cells due to endogenous PAgs (Fisch et al.,1990), served as a positive control sample. The cytotoxic response to Daudi was used to evaluate the activity of the Vγ9Vδ2 T cells. The cytotoxic impact was quantified using the formula 100−[(% viability in co-culture (E:T=10:1) / % viability in negative control(E:T=0:1)) × 100], based on the percentage of dead organoid cells (PI+PKH67+) post co-culture. Organoid cell death (PI+PKH67+) was specifically gated in the flow cytometry analysis (Figure 18A).

This experiment was repeated using three Vγ9Vδ2 T cell lines and eight organoid lines (2 healthy, 3 HPV+, 3 cancer). Notably, the cytotoxic effect was more pronounced in HPV+ and cancer cell groups compared to the healthy group, and the addition of BrHPP significantly amplified this effect (Figure 18B). Subsequent violin plot visualization and statistical analysis corroborated that Vγ9Vδ2 T cells, even without BrHPP stimulation, already showed a marked increase in cytotoxic activity against cancer and HPV+ cells as opposed to the minimal death observed in healthy cells (Figure 18B, -BrHPP). The inclusion of BrHPP further augmented the response, significantly intensifying the cytotoxic effects on HPV+ and cancer organoids relative to healthy counterparts (Figure 18B, +BrHPP).

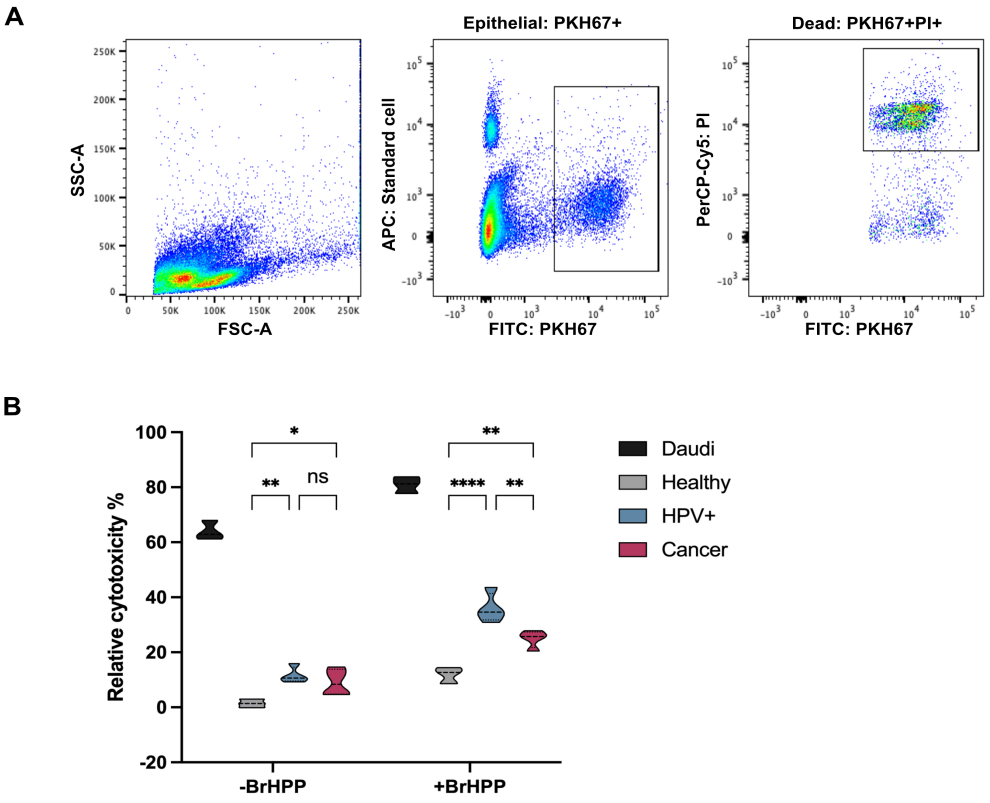

Figure 18. Vγ9Vδ2 T cell-mediated cytotoxicity directed at different organoid lines.

A) Gating strategy: Forward and side scatter estimated populations in the co-culture system. No initial gating to exclude dead cells in forward and side scatter, targeting dead organoid cell population for analysis. Organoid cells were further selected through PKH67-FITC gating, from which the death in whole organoid cells were final identified by gating on PI+PKH67+ population.

B) Violin plots illustrate the cytotoxicity against different organoid lines, quantified using the formula 100−[(% viability in co-culture/% viability in control) × 100], based on the percentage of dead organoid cells (PI+PKH67+) post co-culture, both in the presence and absence of BrHPP (+BrHPP, -BrHPP). The experiments were conducted with three independent biological and technical replicates, and statistical significance was evaluated using Two-Way ANOVA with Tukey's multiple comparisons test;

significance denoted as 'ns' for not significant; * for $p<0.05$; ** for $p<0.01$; *** for $p<0.001$; **** for $p<0.0001$.

4.5.3 Establishing a live-cell imaging model for Vγ9Vδ2 T cell cytotoxicity against cervical cancer organoid

In this section, my aim was to establish a novel *in vitro* model that would allow for the dynamic visualization of the previously identified cytotoxic interactions between organoids and Vγ9Vδ2 T cells. The objective was to directly visualize the cytotoxic effects via real-time fluorescence changes, thus necessitating a non-toxic tracer to live cells yet sensitive enough to differentiate between living and dead cells. While Hoechst is a common cell-staining agent, its permeability undermines its utility in live-cell cytotoxicity assays. Similarly, propidium iodide's ability to distinguish between late apoptotic and normal cells is compromised by its toxicity, limiting its application in live-cell imaging. Ultimately, NucRed Dead 647 ReadyProbes Reagent was selected for its minimal toxicity and cell-impermeability, emitting a red fluorescence upon binding to DNA within dead or late-stage apoptotic cells, allowing for the accurate measurement of organoid cell death during co-culture with Vγ9Vδ2 T cells. This fluorescent agent facilitated the identification of dead cells amidst the organoid cell population using an automated live-cell imaging system (SYBOT-1000 & CYTOMAT, SYNENTEC).

To initially establish the methodology, I utilized organoids derived from the cervical cancer patients. Controls included untreated organoids (indicative of spontaneous death) and those treated with cisplatin (as a positive control for induced death). In experimental setups, Vγ9Vδ2 T cells were introduced with or without BrHPP activation, and automated imaging captured the cellular changes hourly over 24 hours. A decline in the yellow signal over time was noted in all groups, with significant red fluorescence indicative of cytotoxicity appearing after four hours in all but the untreated control group (Figure 19). Particularly, organoids exposed to cisplatin or activated Vγ9Vδ2 T cells demonstrated a marked increase in dead cell signal early on, while the effect of non-activated T cells was less pronounced (Figure 19). By the 24-hour mark, some organoids had completely lysed, evidenced by intensified red fluorescence, highlighted by white arrows in the representative images (Figure 19).

This live-cell imaging methodology system not only confirms the antitumor potential of Vγ9Vδ2 T cells against cervical cancer but also underscores the efficacy of this novel co-culture model and the integrated live-cell imaging technology. Furthermore, the reproducibility of the methodology and the statistically significant differentiation among healthy, HPV+, and cancer organoids were corroborated by my colleague David Holthaus (Dong et al.,2023), who noted consistent distinctive cytotoxicity mediated by Vγ9Vδ2 T-cells across organoid lines from

healthy, HPV+, and cancerous sources, thereby reinforcing the conclusions drawn in “Result 4.5.2”.

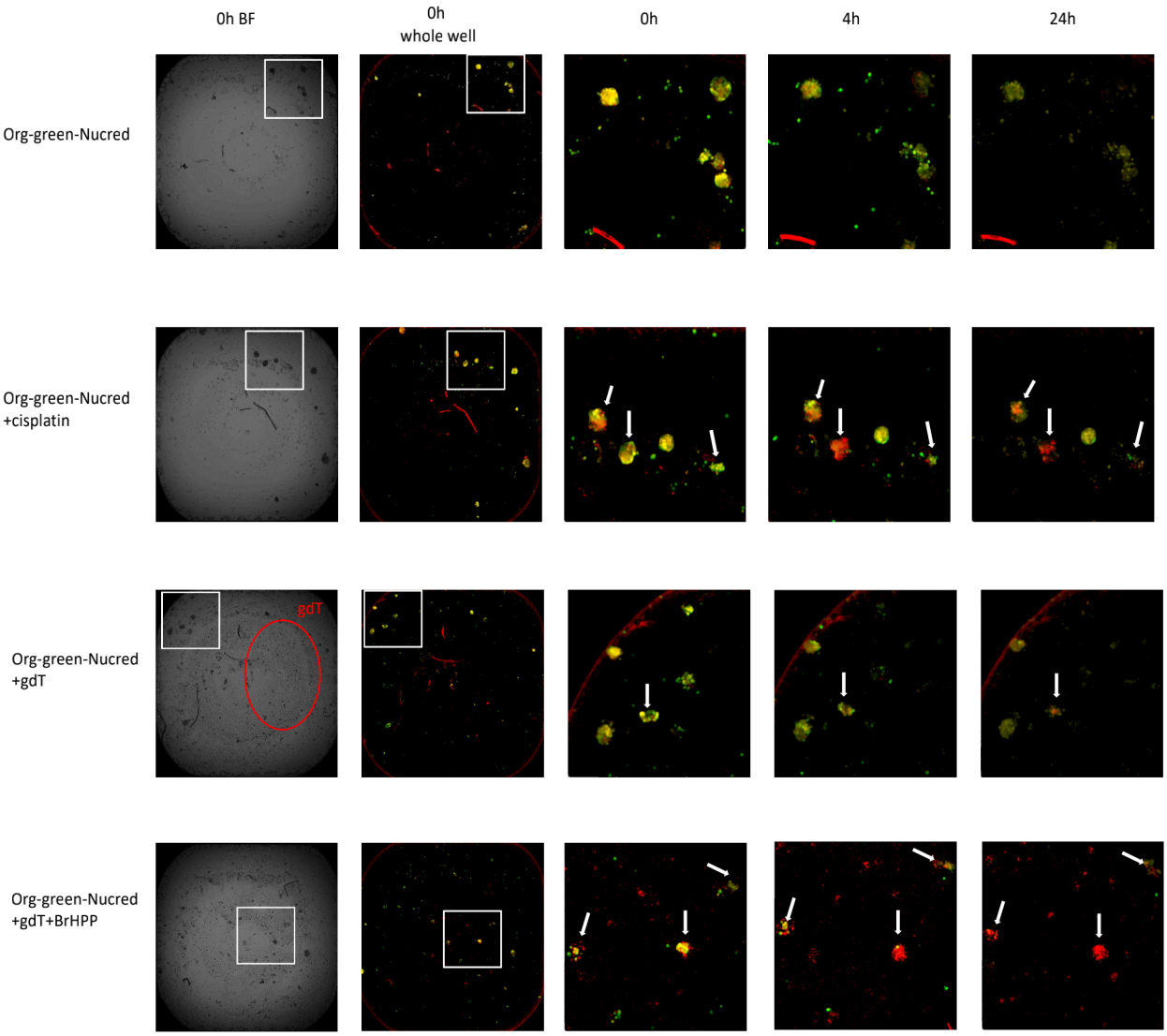

Figure 19. Representative live-cell images of Vγ9Vδ2 T cell mediated cytotoxicity against cervical cancer organoids in the co-culture system.

The series of images capture the dynamic fluorescence signal and morphological variations in cervical cancer organoids subjected to a range of treatments within a 384-microwell plate. The treatments include four conditions: Untreated organoids are depicted as the negative control (Org-green-Nucred), exposure to 200 μM cisplatin (Org-green-Nucred+cisplatin), the groups involving co-culture with Vγ9Vδ2 T cells at an effector-to-target (E:T) ratio of 10:1 (Org-green-Nucred+gdT), and co-culture with Vγ9Vδ2 T cells with supplemental BrHPP (Org-green-Nucred+gdT+BrHPP) represent the experimental focus. Staining with NucRed Dead 647 ReadyProbes Reagent differentiates live cells (yellow) from dead cells (red). Sequential fluorescence imaging captured hourly provides a temporal view of the treatment effects, with selected images displayed for time points at 0h, 4h, and 24h.

4.5.4 BTN3A and BTN2A1: crucial elements in BrHPP-induced cytotoxicity mediated by Vγ9Vδ2 T cells.

To elucidate the molecular basis for the enhanced cytotoxic effects of Vγ9Vδ2 T cells, I first examined the roles of BTN3A and BTN2A1, two key molecules implicated in the recognition and activation of Vγ9Vδ2 T cells. BTN3A1, a BTN3A isoform, is essential for Vγ9Vδ2 T cell activation due to its B30.2 domain that binds intracellular phosphorylated antigens (pAgs), triggering necessary conformational changes (Peigné et al.,2017;Sandstrom et al.,2014). BTN2A1 also plays a role in TCR activation by aiding pAg detection and directly interacting with the Vγ9 TCR (Cano et al.,2021). In the experiments, antagonist monoclonal antibodies (mAbs) against BTN3A (clone 103.2) and BTN2A1 (clone 7.48) were introduced into the co-culture at a final concentration of 5ug/mL, with organoid cells pre-treated for one hour. The anti-BTN3A mAb used does not differentiate between the BTN3A1/A2/A3 isoforms (Herrmann,2023), but BTN3A1 is known to be critical for T cell activation (Zhou et al.,2023).

After co-culture with Vγ9Vδ2 T cells, both with and without BrHPP stimulation, flow cytometry quantified the impact of antagonistic monoclonal antibodies (mAbs) by measuring the proportion of dead organoid cells (PI+PKH67+) as previously described. Violin plots, accompanied by statistical analyses, elucidated the impact of mAbs on the cytotoxicity mediated by Vγ9Vδ2 T cells (Figure 20). It clearly showed that mAbs interference did not significantly influence cell death rates in the group absence of BrHPP across four experimental mAb conditions (Figure 20A). The average values in healthy, HPV+, and cancer were calculated considering the non-significant variances in cell death (Figure 20B, -BrHPP), aiming for comparison with cytotoxicity levels in the BrHPP-stimulated group.

Interestingly, the introduction of BrHPP led to a significant reduction in cell mortality following mAb blockade, equalizing the cytotoxic levels to those observed in the absence of BrHPP. This underscores the critical role of BTN2A1 and BTN3A1 in facilitating BrHPP-induced activation of Vγ9Vδ2 T cells against cervical cancer organoids. These results reinforce that inhibiting BTN2A1 or BTN3A1 markedly diminishes cytotoxic responses upon BrHPP introduction, corroborating previous evidence that BTN3A1 and BTN2A1 are pivotal in the BrHPP-triggered activation of Vγ9Vδ2 T cells (Chen et al.,2021). Overall, the specific increase in cytotoxicity against HPV+ and cancer cells appeared to be independent of BTN3A1 and BTN2A1 recognition by Vγ9-TCR.

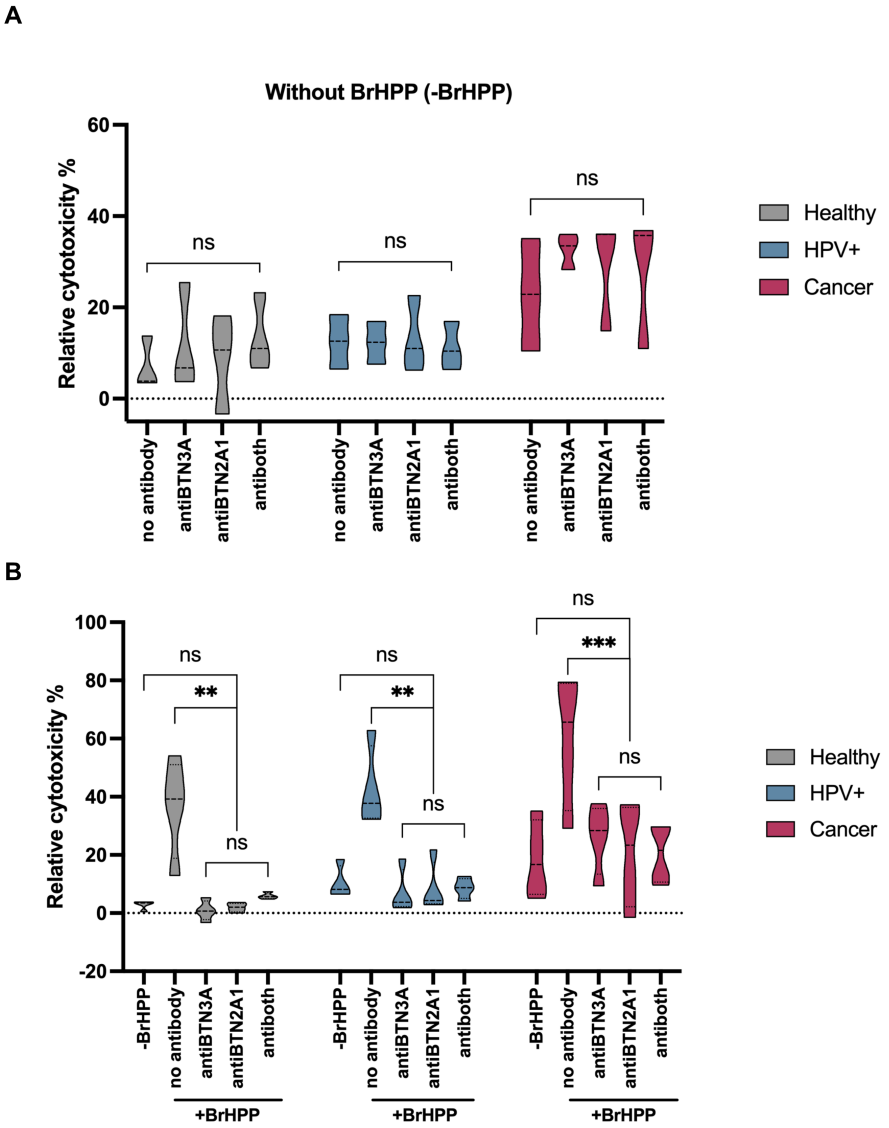

Figure 20. BTN3A and BTN2A1 antagonistic antibody modulation of Vγ9Vδ2 T-cell mediated cytotoxicity.

A) Violin plots quantify the impact of anti-BTN3A and anti-BTN2A1 mAbs on the cytotoxic effect of Vγ9Vδ2 T cells in absence of BrHPP(-BrHPP), based on the mortality rate (PI+PKH67+) of organoid cells (PKH67+) post-co-culture. Experimental groups were delineated based on four mAb treated conditions: untreated (no antibody), treated with anti-BTN3A1, treated with anti-BTN2A1, and treated with both antibodies concurrently. All these experiments were conducted with three independent biological replicates, and statistical significance was evaluated using Two-Way ANOVA with Tukey's multiple comparisons test; significance denoted as 'ns' for not significant; * for $p<0.05$; ** for $p<0.01$; *** for $p<0.001$; **** for $p<0.0001$.

B) Violin plots illustrated the effect of anti-BTN3A and anti-BTN2A1 mAbs on the Vγ9Vδ2 T cell-mediated cytotoxicity with BrHPP-stimulation (+BrHPP). Within the +BrHPP group, data across four mAb conditions are presented. A comparison between +BrHPP and -BrHPP conditions was conducted, with a single bar ahead indicating the average cytotoxicity percentage across the four mAb conditions in healthy, HPV+, and cancer groups under BrHPP deficient condition. All these experiments were

conducted with three independent biological replicates for both cytotoxicity and degranulation assays, and statistical significance was evaluated using Two-Way ANOVA with Tukey's multiple comparisons test; significance denoted as 'ns' for not significant; * for $p<0.05$; ** for $p<0.01$; *** for $p<0.001$; **** for $p<0.0001$.

4.5.5 Minor role of CD107a-marked degranulation in Vγ9Vδ2 T cell cytotoxicity targeting HPV+ and malignant organoids

Vγ9Vδ2 T cells primarily mediate their antitumor activity through two principal mechanisms: granule exocytosis, characterized by the secretion of granzyme B and perforin, and the granule-independent Fas/FasL-mediated apoptosis pathway (Li et al.,2021;Pennington et al.,2005;Schönefeldt et al.,2021). CD107a (LAMP-1), a marker indicative of cytotoxic T-cell degranulation, correlates strongly with the release of granzyme B and perforin and serves as an activation marker for Vγ9Vδ2 T cells (Bold et al.,2023). Following the findings that BTN3A and BTN2A1 are not the primary mechanisms in Vγ9Vδ2 T cell cytotoxicity distinctively against HPV+ and cancer cells, the subsequent inquiry probed into exploring the role of degranulation for this pronounced effect. To investigate CD107a mobilization, Vγ9Vδ2 T cells were co-cultured with organoid cells at a 10:1 effector-to-target (E:T) ratio, with and without the presence of BrHPP, and CD107a mobilization was monitored. Surface staining for subsequent flow cytometric analysis included anti-Vγ9 and anti-CD3 antibodies. Controls were established using Daudi cells to induce CD107a expression (positive control) and absence of target cells (negative control). Results demonstrated that CD107a expression on Vγ9Vδ2 T cells did not significantly vary post-co-culture at an E:T ratio of 10:1 across healthy, HPV+, and cancer organoid cells in the presence or absence of BrHPP (Figure 21, +/-BrHPP). However, the presence of BrHPP notably elevated CD107a expression (Figure 21, $p<0.001$), suggesting that the granule exocytosis pathway is predominantly activated by BrHPP rather than by the organoid cells themselves. This implies that the enhanced cytotoxicity observed against HPV+ and cancer organoids may be facilitated by alternative mechanisms not directly linked to degranulation.

Thus, while the precise molecular mediators of Vγ9Vδ2 T cell-induced cytotoxicity in cervical cancer remain elusive. A complex interplay of multiple ligand-receptor interactions within the HPV+/cancerous cervical organoid and Vγ9Vδ2 T cell dynamic could play a critical role, which warrants further investigation.

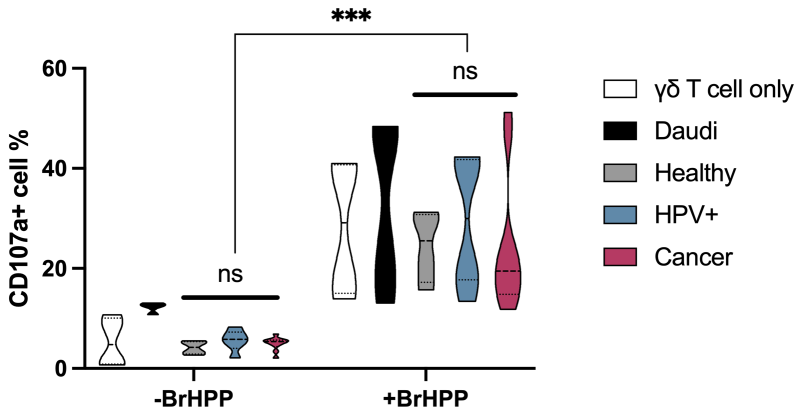

Figure 21 Assessment of Vγ9Vδ2 T cell degranulation during co-culture with cervical organoids
Violin plots represent CD107a expression on Vγ9Vδ2 T cells after co-culture with Daudi cells and various organoid lines at an E:T ratio of 10:1, with the percentage of CD107a+ Vγ9Vδ2 T cells assessed under different conditions (+/- BrHPP). The baseline CD107a expression on Vγ9Vδ2 T cells without target cells is shown as the negative control. The experiments were conducted with three independent biological replicates, and statistical significance was evaluated using Two-Way ANOVA with Tukey's multiple comparisons test; significance denoted as 'ns' for not significant; * for $p<0.05$; ** for $p<0.01$; *** for $p<0.001$; **** for $p<0.0001$.

5 DISCUSSION

This study was based on patient-derived cervical cancer organoid lines and a co-culture system with T-cells and aimed at examining the cytotoxic responses against cervical cancer at various stages of development, including healthy, HPV-positive, and cancerous states. By comparing the transcriptomic profiles of these organoids, I highlighted the significance of DNA repair genes in the transformation process of cervical cancer. This was substantiated by integrating data from the public GEO cervical tissue database. To further assess the prognostic relevance of these DNA repair genes in cervical cancer and tailor individualized treatment strategies, I developed a DNA repair gene signature (DRGscore) using the TCGA cervical cancer dataset (TCGA-CESE), demonstrating its prognostic value and informing potential immunotherapeutic strategies.

My findings also shed light on highly immunogenic HLA-I peptide repertoires that could be recognized by immune cells targeting cervical cancer. γδ T-cells, a unique subset of T-cells, targeting conserved structures on infected and malignant cells independently of HLA molecules (Kabelitz et al.,2020). My co-culture system provided evidence of the capacity of Vγ9Vδ2 T-cells to discriminate between abnormal (HPV+/cancer) and healthy organoid cells, exerting a more potent cytotoxic effect on the former. Inhibition experiments using specific antibodies identified BTN3A and BTN2A1 as pivotal elements in BrHPP-mediated Vγ9Vδ2 T-cell activation. Yet, these molecules did not seem to be the prime recognition factors of abnormal organoids. The absence of a direct link between CD107a expression and organoid recognition suggests that Vγ9Vδ2 T-cells may engage with additional, still unidentified, ligands on the surface of abnormal organoids. This presents a compelling direction for future research, especially considering potential interactions between γδ TCR and antigens associated with HPV infection and DNA repair processes such as hMSH2.

5.1 Refining *in vitro* models for cervical cancer investigation

5.1.1 Establishment of patient-derived organoids

For decades, immortal cell lines have been the cornerstone of *in vitro* cancer research due to their ease of use, ethical simplicity, and their capacity to partially recapitulate the characteristics of the diseases they model. However, their long-term cultivation can lead to genetic drift, casting doubt on the stability of their phenotype and genotype (Kaur and Dufour,2012). This is particularly problematic in cancer studies, likewise in cervical cancer, where tracing the progression from normal cervical epithelium through various stages of dysplasia, triggered by persistent high-risk HPV (HR-HPV) infection, to carcinoma is crucial. In this context, I made use of patient-derived organoids representing healthy, HPV-infected,

and cancerous cervical states to accurately chart the transformation associated with cervical cancer onset and progression. These organoids not only precisely emulate the healthy ectocervical epithelium's polarity but also the chaotic architecture characteristic of dysplasia and carcinoma. Specifically, in healthy organoids, proliferative cells (marked by Ki67 expression) are predominantly situated in the basal and parabasal layers and undergo differentiation towards the upper layers. In stark contrast, HPV-positive and cancerous organoids display pervasive Ki67 expression across all cellular strata, mirroring the disrupted tissue organization seen in disease states.

A critical advantage in my study was that I cultivated the isolated primary cervical cells on an irradiated feeder layer in order to maintain the stemness and the differentiation capacity of the cervix tissue-derived stem cells. Using this method, cells begin to self-organize into organoids once seeded in a Matrigel dome and acquire increased propagation capacity better than organoids generated by conventional strategies. This novel method seemed to be superior as compared to the direct formation of organoids from tissue-derived primary cells in Matrigel (Clevers et al.,2014;Nakamura and Sato,2018).

5.1.2 Establishment of organoid-T cell coculture model

While organoids serve as an advanced model that mimics original tissue characteristics, they are composed exclusively of epithelial cells and, thus, lack the interaction with other cellular components, diminishing the representation of tissue complexity (Baniahmad,2021; Kretzschmar,2021). Traditionally, xenograft mouse models, which preserve both the tumor cells and the surrounding microenvironment, have been the gold standard for exploring cancer progression and evaluating therapeutic interventions in pre-clinical settings (Yamaguchi and Perkins,2018). However, the translation of these models to successful human treatments remains disproportionately low (Atkins et al.,2020), likely due to the substantial genetic divergence between rodents and humans, the challenges in accurately emulating human diseases, and the variability in tumor heterogeneity (Chen et al.,2023;Horvath et al.,2016).

In response to these challenges, human organoid co-culture systems have been refined to bridge species-specific genetic gaps and to provide insights into cell-to-cell interactions, immune response mechanisms within cancers, and metastatic behaviors (Yuan et al.,2022). Yet, existing methodologies, such as air-liquid interface (ALI) cultures (Boccellato et al.,2019) and static Matrigel domes supplemented with various cell types, have their limitations in simulating the intricate interplay between organoids and other cellular subsets due to constraints on direct cellular contact and mobility.

To address these limitations and specifically to investigate T-cell cytotoxic effects on organoids, I developed a suspension organoid-T cell co-culture system that facilitates immediate interaction between T-cells and organoids. Employing an automated live-cell imaging platform and the non-toxic fluorescent dye NucRed Dead 647, this system enables continuous real-time tracking of T-cell-mediated cytotoxicity by capturing changes in fluorescence signals indicative of cell death. This innovative approach, integrating live cell imaging with organoid co-culture, constitutes a potent investigational tool for probing cellular dynamics, lymphocyte migration, and the impact of adoptive cell therapy in a controlled physiological tissue environment (Yuki et al.,2020; Kong et al.,2018;Koster et al.,2022；Dong et al.,2023).

5.2 Role of DNA repair signature in HPV carcinogenicity and therapy in cervical cancer

5.2.1 DNA damage and repair dynamics in HPV-positive cervical cancer

DNA, though inherently stable, is susceptible to damage from both internal and external sources such as ultraviolet light, ionizing radiation, and chemotherapeutic agents, and even microbe induced damage leading to chromosomal and DNA strand breaks (Alhmoud et al.,2020;Dziubańska-Kusibab et al.,2020). These damages are usually swiftly rectified to maintain genomic integrity. However, inadequate DNA repair mechanisms, resulting in persistently damaged or incorrectly repaired DNA, are crucial in driving genomic anomalies and mutations that can impair cellular functions (Jackson and Bartek,2009). Deficiencies in DNA repair, particularly within tumor suppressor genes or oncogenes, are known contributors to the development of cancer (Basu,2018).

In the context of HPV-positive cervical cancer, the integration of the HPV genome into the chromatin of host cervical cells induces substantial DNA stress, amplifying the DNA damage response (Albert and Laimins,2020; Prati et al.,2018). This necessitates highly active DNA repair processes to counteract such damage (Zhou and Elledge,2000). The stable integration of the HPV genome leads to persistent high-level expression of E6 and E7 oncogenes, pivotal events in the transformation of HPV-infected cells, progression to dysplasia, and ultimately the onset of cervical cancer (Williams et al.,2011). Interestingly, my transcriptomic analyses of HPV+ and cervical cancer organoids and tissues corroborate the upregulation of DNA repair pathways and the genes involved, highlighting the intricate relationship between viral infection and host genomic stability.

5.2.2 DNA repair implications in cervical cancer therapy

The efficacy of DNA repair mechanisms in cervical cancer patients exhibits significant heterogeneity. Within the context of cervical cancer, factors such as mutational burden, tumor

microenvironment (TME), and response to therapy are all influenced by the efficiency of DNA repair mechanisms (Chabanon et al.,2021;Karzai et al.,2018). A high mutation burden typically arises from poor DNA repair following severe genomic damage, which, paradoxically, may enhance the capacity of endogenous T cells to recognize neoantigens (Pearl et al.,2015). This recognition is crucial for the elimination of cancer cells and increases the overall immunogenicity of the tumor by promoting the infiltration of effective immune cells and the expression of immune checkpoints within the TME (Chabanon et al.,2021;Nastasi et al.,2020).

Conversely, robust DNA repair activity can lead to increased resistance to chemoradiotherapy. This resistance can be mitigated by the use of poly (ADP-ribose) polymerase inhibitors (PARPi), which impede DNA damage repair pathways (Das et al.,2023;Zhu et al.,2016). In addition to cervical cancer, Human Papillomavirus (HPV) infection is also an etiological agent for head and neck cancer (Galati, L et al.,2022). There is a marked discrepancy in molecular profiling and prognostic outcomes between HPV-positive and HPV-negative oropharyngeal Squamous Cell Carcinoma (OPSCC) patients (Egawa N.,2023). In HPV-positive OPSCC, the molecular mechanisms underlying HPV integration and its subsequent effects on tumor progression and response to therapy parallel those observed in HPV-positive cervical cancer (Tabatabaeian, H et al.,2024). Similar to cervical carcinoma, activation of the ATR and other DNA repair signaling cascades are observed in HPV-positive OPSCC (Kono, T et al.,2020) Furthermore, the application of PARP inhibitors has been shown to potentiate the chemosensitivity and radiosensitivity in this subset of OPSCC patients (Tabatabaeian, H et al.,2024). These findings underscore the importance of investigating the role of DNA repair mechanisms in the pathogenesis of HPV-induced diseases.

In this study, to evaluate the impact of DNA repair on cervical cancer prognosis, a DNA repair gene signature (DRGscore) was constructed using the TCGA cervical cancer dataset. Higher DRGscores are indicative of stronger DNA repair capabilities. Analysis of the TME revealed that the low DRGscore group exhibited a higher presence of effective immune cells and fewer suppressive elements compared to the high DRGscore group, establishing a negative correlation between DRGscore and patient prognosis.

Regarding the neoantigens resulting from DNA repair deficiencies, studies have shown that an increased expression of neoantigens in DNA mismatch repair-deficient cancers can amplify immune checkpoint expression, thereby enhancing prolonged immune surveillance (Germano et al.,2017). My research findings align with these observations, revealing heightened expression levels of immune checkpoints such as CTLA-4, LAG-3, and PD-1 in the low DRGscore group, which suggests a potentially elevated sensitivity to immune checkpoint inhibitors in these patients, resonating with the discoveries in other cancer types.

5.2.3 The dual role of DNA repair mechanisms in cervical cancer

DNA repair mechanisms exert a multifaceted influence on the pathogenesis of cervical cancer, particularly in the context of human papillomavirus (HPV) integration which disrupts normal DNA repair functions. Active DNA repair pathways serve as an initial defense against DNA damage and carcinogenic progression (Chabanon et al.,2021;Nastasi et al.,2020). Yet, paradoxically, once cervical cancer is established, these same repair mechanisms contribute to resistance against standard chemoradiotherapy (Zhang et al.,2023). Conversely, high-efficiency DNA repair inhibitors, such as PARP inhibitors, demonstrate considerable therapeutic responses by targeting these pathways (Li et al.,2021; Helleday et al.,2008).

Simultaneously, defects in DNA repair escalate the mutational load, which can inadvertently enhance the efficacy of immunotherapy by increasing the formation of neoantigens that are recognized by the immune system. This dual nature of DNA repair—protective in early carcinogenesis but problematic in established cancer—highlights the complexity of targeting these pathways for therapeutic intervention and underscores the need for a nuanced understanding of their role in cancer biology (Bever and Le,2018;Teijeira et al.,2019).

5.3 T cell recognition of cervical cancer and HPV infected cells

5.3.1 Tumor-associated antigens in HPV-positive cervical cancer: Beyond E6E7 for immunotherapy

Prophylactic vaccines against the human papillomavirus (HPV) and regular screening programs are currently the primary preventative measures for cervical cancer. Despite their efficacy in prevention, these vaccines do not eradicate existing HPV infections or halt the progression of precancerous lesions. Consequently, there is a pressing need to develop effective therapeutic strategies for patients across various clinical stages. Adoptive T-cell therapy has emerged as a particularly promising treatment in this regard. HPV infection initiates an immune response aimed at eradicating the foreign virus, yet cervical cancer often arises from the evasion of T-cell-mediated immunity by HPV. Oncogenes associated with HPV, specifically E6 and E7, as well as genes upregulated in response to HPV infection, may serve as sources of tumor-associated antigens (TAAs) that provoke T-cell responses, offering a viable target for immunotherapy interventions (Eskander and Tewari,2015;Zhang et al.,2020).

TAAs represent proteins that are predominantly overexpressed in tumor cells compared to normal cells and are considered vital for therapeutic and prognostic applications. TAAs can be presented on the tumor cell surface in two primary forms: either as full-length proteins acting as ligands for immune cell receptors or as processed peptides presented by HLA

molecules, recognized by the T-cell receptors of CD8+ cytotoxic T-cells (Ritz and Seliger,2001). In the specific case of HPV-positive cervical cancer, the integration of HPV DNA leads to the overexpression of oncogenes, particularly E6 and E7, which are presumed to be sources of TAAs or peptides eliciting an immune response. Counterintuitively, Boilesen et al. observed that the overexpression of E6 and E7 occurred prior to cellular malignancy, suggesting that their reduced expression in established cervical cancer cells may contribute to immune evasion and diminish the effectiveness of E6E7-targeted therapeutic vaccines (Boilesen et al.,2021).

In the present study, no TAA or peptides originating from HPV oncogenes were detected on HPV-positive cervical cancer organoids, casting doubt on the feasibility of targeting HPV oncoproteins with therapeutic vaccines or adoptive T-cell therapies. Furthermore, the development of T-cell tolerance, the interplay of immune checkpoints, and an immunosuppressive tumor microenvironment are contributing factors to the inefficacy of HPV-targeted treatments (Arbyn et al.,2008; Arbyn et al.,2017; Bruno et al.,2019; Ghaem-Maghami et al.,2011). Therefore, a broadened search for additional TAAs from diverse origins is necessary to enhance the success of immunotherapies in combating cervical cancer.

In light of these findings, my multi-omics analysis has led me to propose that DNA repair-related genes may also give rise to TAAs and corresponding peptides that could be recognized by αβ T-cells in cervical cancer. The upregulation of DNA repair-related genes and the presence of HLA-I-restricted DNA repair-related peptides in my cervical cancer organoids support the notion that these elements could activate CD8+ T-cells to target and eliminate cancer cells.

To corroborate this theory, one strategy would be to synthesize a pool of DNA repair-related peptides and rigorously assess their immunogenicity through a combination of *in vivo* and *in vitro* assays. Concurrently, evaluating the potential for off-target effects is critical to preclude adverse reactions that may impact the cardiovascular system, nervous system, or other critical organs (Sterner and Sterner,2021).

5.3.2 Cervical carcinoma cells as a γδ T cells target

In the pursuit of novel immunotherapeutic targets, my research has expanded beyond HLA-I-restricted peptides to include overexpressed genes that may function as ligands for various immune cell populations (Müller et al.,2020). In particular, γδ T cells, known for their cytotoxic response to infection and stress-induced phosphoantigens (pAgs), have become a focal point of my study on Vγ9Vδ2 T cell-mediated cytotoxicity against cervical cancer using an organoid-T cell co-culture system developed in our laboratory.

Remarkably, I observed a pronounced cytotoxic effect by Vγ9Vδ2 T cells on HPV+ and cancerous organoids even in the absence of BrHPP, a known activating agent. This suggests an innate ability of Vγ9Vδ2 T cells to discern subtle transformations induced by HPV infection and subsequent cancer progression. This finding is particularly significant, considering the prevailing view that Vγ9Vδ2 T cells require external activation to exert anti-tumor effects and the lack of evidence supporting their intrinsic ability to distinguish between healthy and cancerous cells (Gu et al.,2018;Kabelitz et al.,2020;Ridgley et al.,2022). However, the addition of BrHPP resulted in a partially non-selective targeting by Vγ9Vδ2 T cells, exerting a degree of cytotoxicity to healthy cells, as well.

5.3.3 Dissecting the mechanism of Vγ9Vδ2 T cell response in cervical cancers

A pivotal question in my investigations pertains to the mechanism that enables Vγ9Vδ2 T cells to specifically target HPV+ and cancer cells. These T cells exhibit anti-infection and anti-tumor activities through a plethora of mechanisms (Hudecek et al.,2021;Li et al.,2020;Raverdeau et al.,2019;Vallvé-Juanico et al.,2019), including the release of cytotoxic molecules such as granzyme B and perforin, secretion of pro-inflammatory cytokines like IFNγ and TNFα, induction of Fas/FasL-mediated apoptosis, and the recognition of tumor cell ligands, all of which synergize with other immune cells to exert a robust antitumor response (Li et al.,2021;Pennington et al.,2005;Schönefeldt et al.,2021).

Key to this process are the ligands BTN2A1 and BTN3A1, which facilitate Vγ9Vδ2 T cell activation by binding to phosphoantigens enriched in infected and tumorous cells (Giannotta et al.,2023). My study corroborates BTN2A1 and BTN3A1's indispensable role in Vγ9Vδ2 T cell activation post-self-activation, aligning with findings from other research (Gu et al.,2018;Rigau et al.,2020). Significantly, CD107a elevation was noted in Vγ9Vδ2 T cells when stimulated with BrHPP, irrespective of the organoid line in co-culture. This suggests that while BTN2A1 and BTN3A1 interaction, along with degranulation, are predominantly triggered by BrHPP stimulation, leading to non-specific cytotoxicity, the differential cytotoxic effects observed against various organoid cells may rely on distinct ligand-receptor interactions (Laplagne et al.,2021).

Vγ9Vδ2 T cells harbor multiple receptors that are instrumental in recognizing and eradicating tumor and infected cells. Among these, the NKG2D receptor notably binds to ligands such as MICA, MICB, and ULBP1-4, which play a pivotal role in the activation of these T cells (Groh et al.,1998). Furthermore, hMSH2—a key player in DNA mismatch and repair pathways—emerges as a strong candidate ligand present on target cells that can be detected by Vγ9Vδ2

T receptor and NKG2D, bolstering Vγ9Vδ2 T cell-mediated cytolysis (Nedellec et al.,2010; Von Lilienfeld-Toal et al.,2006; Liu et al.,2022; Chen et al.,2008).

My transcriptomic analysis revealed a marked overexpression of genes associated with DNA damage and repair pathways, including hMSH2, in HPV+ and cancer organoids. This overexpression is hypothesized to influence Vγ9Vδ2 T cell cytotoxicity. Supporting this, our latest research demonstrated a discernible reduction in Vγ9Vδ2 T cell cytotoxicity following hMSH2 inhibition, notably in conjunction with BrHPP (Dong et al.,2023). This observation underscores the potential role of DNA repair-related antigens in Vγ9Vδ2 T cell activation, warranting further exploration.

Moreover, genes such as HSPD1, KLRG2, and BTNL9, which are implicated in cellular stress responses, may also engage with Vγ9Vδ2 T cell receptors, thereby modulating their activation (Ma et al.,2018). These findings suggest a complex network of interactions influencing Vγ9Vδ2 T cell responses, with DNA repair-related genes at the forefront of this intricate interplay.

5.4 Outlook

Cervical cancer, exhibiting regional differences of prevalence amongst women, serves as a paradigm for HPV-associated malignancies. The significant role of DNA repair mechanisms uncovered in cervical cancer research may extend to other HPV-related cancers, including those of the head and neck, oral cavity, and anus. The innovative organoid-T cell coculture system and automated live-cell imaging techniques developed in this study offer robust tools for probing the interactions between various organoids and immune cell subsets, promising to advance our understanding of cellular communication in oncology.

In this context, my investigations have provided substantial insights into the capacity of non-self-activated Vγ9Vδ2 T cells to discern between normal and cancerous cervical cells, bolstering the potential of allogeneic Vγ9Vδ2 T cell therapy as a ready-to-use therapeutic option. Additionally, the roles of BTN3A1, BTN2A1, and degranulation in directing Vγ9Vδ2 T cell cytotoxicity were reaffirmed using the cervical organoid model. For a more profound comprehension of the molecular dialogues that guide Vγ9Vδ2 T cell cytotoxicity in HPV-positive and cancerous cells, future research should delve into the expression and functionality of additional molecules present on both Vγ9Vδ2 T cells and epithelial cells.

6 REFERENCES

Adams, E. J., S. Gu and A. M. Luoma (2015). "Human gamma delta T cells: Evolution and ligand recognition." Cellular Immunology **296**(1): 31-40.

Ahmed, H. G., S. H. Bensumaidea, F. D. Alshammari, F. S. H. Alenazi, A. L. BA, M. Z. Alturkstani and I. A. Aladani (2017). "Prevalence of Human Papillomavirus subtypes 16 and 18 among Yemeni Patients with Cervical Cancer." Asian Pac J Cancer Prev **18**(6): 1543-1548.

Akinyemi I Ojesina 1, L. L., Samuel S Freeman 3, Chandra Sekhar Pedamallu 4, Ivan Imaz-Rosshandler 5, Trevor J Pugh 4, Andrew D Cherniack 3, Lauren Ambrogio 3, Kristian Cibulskis 3, Bjørn Bertelsen 6, Sandra Romero-Cordoba 5, Victor Treviño 7, Karla Vazquez-Santillan 5, Alberto Salido Guadarrama 5, Alexi A Wright 8, Mara W Rosenberg 3, Fujiko Duke 9, Bethany Kaplan 4, Rui Wang 10, Elizabeth Nickerson 3, Heather M Walline 11, Michael S Lawrence 3, Chip Stewart 3, Scott L Carter 3, Aaron McKenna 3, Iram P Rodriguez-Sanchez 12, Magali Espinosa-Castilla 5, Kathrine Woie 13, Line Bjorge 14, Elisabeth Wik 14, Mari K Halle 14, Erling A Hoivik 14, Camilla Krakstad 14, Nayeli Belem Gabiño 5, Gabriela Sofia Gómez-Macías 12, Lezmes D Valdez-Chapa 12, María Lourdes Garza-Rodríguez 12, German Maytorena 15, Jorge Vazquez 15, Carlos Rodea 15, Adrian Cravioto 15, Maria L Cortes 3, Heidi Greulich 16, Christopher P Crum 17, Donna S Neuberg 18, Alfredo Hidalgo-Miranda 5, Claudia Rangel Escareno 19, Lars A Akslen 20, Thomas E Carey 21, Olav K Vintermyr 20, Stacey B Gabriel 3, Hugo A Barrera-Saldaña 12, Jorge Melendez-Zajgla 5, Gad Getz 22, Helga B Salvesen 23, Matthew Meyerson 24 (2017). "Integrated genomic and molecular characterization of cervical cancer." Nature **543**(7645): 378-384.

Albert, E. and L. Laimins (2020). "Regulation of the Human Papillomavirus Life Cycle by DNA Damage Repair Pathways and Epigenetic Factors." Viruses **12**(7): 744.

Alhmoud, J. F., J. F. Woolley, A. E. Al Moustafa and M. I. Malki (2020). "DNA Damage/Repair Management in Cancers." Cancers (Basel) **12**(4).

Alitalo, K., E. Kuismanen, R. Myllylä, U. Kiistala, S. Asko-Seljavaara and A. Vaheri (1982). "Extracellular matrix proteins of human epidermal keratinocytes and feeder 3T3 cells." J Cell Biol **94**(3): 497-505.

Alnaggar, M., Y. Xu, J. Li, J. He, J. Chen, M. Li, Q. Wu, L. Lin, Y. Liang, X. Wang, J. Li, Y. Hu, Y. Chen, K. Xu, Y. Wu and Z. Yin (2019). "Allogenic Vγ9Vδ2 T cell as new potential immunotherapy drug for solid tumor: a case study for cholangiocarcinoma." J Immunother Cancer **7**(1): 36.

Alzamil, L., K. Nikolakopoulou and M. Y. Turco (2021). "Organoid systems to study the human female reproductive tract and pregnancy." Cell Death & Differentiation **28**(1): 35-51.

Amini, L., T. Vollmer, D. J. Wendering, A. Jurisch, S. Landwehr-Kenzel, N. M. Otto, K. Jürchott, H.-D. Volk, P. Reinke and M. Schmueck-Henneresse (2019). "Comprehensive Characterization of a Next-Generation Antiviral T-Cell Product and Feasibility for Application in Immunosuppressed Transplant Patients." Frontiers in Immunology **10**.

Anderson, N. M. and M. C. Simon (2020). "The tumor microenvironment." Curr Biol **30**(16): R921-r925.

Angelosanto, J. M., S. D. Blackburn, A. Crawford and E. J. Wherry (2012). "Progressive loss of memory T cell potential and commitment to exhaustion during chronic viral infection." J Virol **86**(15): 8161-8170.

Antill, Y. C., J. G. Dowty, A. K. Win, T. Thompson, M. D. Walsh, M. C. Cummings, S. Gallinger, N. M. Lindor, L. Le Marchand, J. L. Hopper, P. A. Newcomb, R. W. Haile, J. Church, K. M. Tucker, D. D. Buchanan, J. P. Young, I. M. Winship and M. A. Jenkins (2015). "Lynch syndrome and cervical cancer." Int J Cancer **137**(11): 2757-2761.

Antill-O'Brien, N., J. Bourke and C. D. O'Connell (2019). "Layer-By-Layer: The Case for 3D Bioprinting Neurons to Create Patient-Specific Epilepsy Models." Materials **12**(19): 3218.

Atkins, J. T., G. C. George, K. Hess, K. L. Marcelo-Lewis, Y. Yuan, G. Borthakur, S. Khozin, P. Lorusso and D. S. Hong (2020). "Pre-clinical animal models are poor predictors of human toxicities in phase 1 oncology clinical trials." British Journal of Cancer **123**(10): 1496-1501.

Ayers, M., J. Lunceford, M. Nebozhyn, E. Murphy, A. Loboda, D. R. Kaufman, A. Albright, J. D. Cheng, S. P. Kang, V. Shankaran, S. A. Piha-Paul, J. Yearley, T. Y. Seiwert, A. Ribas and T. K. McClanahan (2017). "IFN-γ–related mRNA profile predicts clinical response to PD-1 blockade." Journal of Clinical Investigation **127**(8): 2930-2940.

Baniahmad, A. (2021). "Tumor spheroids and organoids as preclinical model systems." Medizinische Genetik **33**(3): 229-234.

Basu, A. K. (2018). "DNA Damage, Mutagenesis and Cancer." Int J Mol Sci **19**(4).

Baulu, E., C. Gardet, N. Chuvin and S. Depil (2023). "TCR-engineered T cell therapy in solid tumors: State of the art and perspectives." Sci Adv **9**(7): eadf3700.

Bernard, D., J. D. Hansen, L. Du Pasquier, M. P. Lefranc, A. Benmansour and P. Boudinot (2007). "Costimulatory receptors in jawed vertebrates: conserved CD28, odd CTLA4 and multiple BTLAs." Dev Comp Immunol **31**(3): 255-271.

Bever, K. M. and D. T. Le (2018). "DNA repair defects and implications for immunotherapy." J Clin Invest **128**(10): 4236-4242.

Bhatla, N., D. Aoki, D. N. Sharma and R. Sankaranarayanan (2021). "Cancer of the cervix uteri: 2021 update." International Journal of Gynecology & Obstetrics **155**(S1): 28-44.

Boccellato, F., S. Woelffling, A. Imai-Matsushima, G. Sanchez, C. Goosmann, M. Schmid, H. Berger, P. Morey, C. Denecke, J. Ordemann and T. F. Meyer (2019). "Polarised epithelial monolayers of the gastric mucosa reveal insights into mucosal homeostasis and defence against infection." Gut **68**(3): 400-413.

Boilesen, D. R., K. N. Nielsen and P. J. Holst (2021). "Novel Antigenic Targets of HPV Therapeutic Vaccines." Vaccines (Basel) **9**(11).

Bold, A., H. Gross, E. Holzmann, S. Knop, T. Hoeres and M. Wilhelm (2023). "An optimized cultivation method for future *in vivo* application of γδ T cells." Frontiers in Immunology **14**.

Bonneville, M. and E. Scotet (2006). "Human Vgamma9Vdelta2 T cells: promising new leads for immunotherapy of infections and tumors." Curr Opin Immunol **18**(5): 539-546.

Bordigoni, A., A. Motte, H. Tissot-Dupont, P. Colson and C. Desnues (2021). "Development and validation of a multiplex qPCR assay for detection and relative quantification of HPV16 and HPV18 E6 and E7 oncogenes." Scientific Reports **11**(1).

Brown, J. A., D. M. Dorfman, F. R. Ma, E. L. Sullivan, O. Munoz, C. R. Wood, E. A. Greenfield and G. J. Freeman (2003). "Blockade of programmed death-1 ligands on dendritic cells enhances T cell activation and cytokine production." J Immunol **170**(3): 1257-1266.

Buccheri, S., G. Guggino, N. Caccamo, P. Li Donni and F. Dieli (2014). "Efficacy and safety of γδT cell-based tumor immunotherapy: a meta-analysis." J Biol Regul Homeost Agents **28**(1): 81-90.

Buchbinder, E. I. and A. Desai (2016). "CTLA-4 and PD-1 Pathways: Similarities, Differences, and Implications of Their Inhibition." Am J Clin Oncol **39**(1): 98-106.

Campos-Parra, A. D., M. Pérez-Quintanilla, A. D. Martínez-Gutierrez, D. Pérez-Montiel, J. Coronel-Martínez, O. Millan-Catalan, D. C. De León and C. Pérez-Plasencia (2022). "Molecular Differences between Squamous Cell Carcinoma and Adenocarcinoma Cervical Cancer Subtypes: Potential Prognostic Biomarkers." Curr Oncol **29**(7): 4689-4702.

Cano, C. E., C. Pasero, A. De Gassart, C. Kerneur, M. Gabriac, M. Fullana, E. Granarolo, R. Hoet, E. Scotet, C. Rafia, T. Herrmann, C. Imbert, L. Gorvel, N. Vey, A. Briantais, A. C. le Floch and D. Olive (2021). "BTN2A1, an immune checkpoint targeting Vγ9Vδ2 T cell cytotoxicity against malignant cells." Cell Rep **36**(2): 109359.

Cantini, L., L. Calzone, L. Martignetti, M. Rydenfelt, N. Blüthgen, E. Barillot and A. Zinovyev (2017). "Classification of gene signatures for their information value and functional redundancy." npj Systems Biology and Applications **4**(1): 2.

Chabanon, R. M., M. Rouanne, C. J. Lord, J. C. Soria, P. Pasero and S. Postel-Vinay (2021). "Targeting the DNA damage response in immuno-oncology: developments and opportunities." Nat Rev Cancer **21**(11): 701-717.

Chabeda, A., R. J. R. Yanez, R. Lamprecht, A. E. Meyers, E. P. Rybicki and Hitzeroth, II (2018). "Therapeutic vaccines for high-risk HPV-associated diseases." Papillomavirus Res **5**: 46-58.

Chan, K. F., J. D. G. Duarte, S. Ostrouska and A. Behren (2022). "γδ T Cells in the Tumor Microenvironment—Interactions With Other Immune Cells." Frontiers in Immunology **13**.

Chatterjee, A. (2014). "The next generation of HPV vaccines: nonavalent vaccine V503 on the horizon." Expert Rev Vaccines **13**(11): 1279-1290.

Chauhan, S. R., P. G. Singhal, U. Sharma, K. Bandil, K. Chakraborty and M. Bharadwaj (2019). "Th9 cytokines curb cervical cancer progression and immune evasion." Hum Immunol **80**(12): 1020-1025.

Chen, B., H. Liu, Z. Liu and F. Yang (2023). "Benefits and limitations of humanized mouse models for human red blood cell-related disease research." Frontiers in Hematology **1**.

Chen, H., He, X., Wang, Z., Wu, D., Zhang, H., Xu, C., He, H., Cui, L., Ba, D., & He, W. (2008). Identification of human T cell receptor gammadelta-recognized epitopes/proteins via CDR3delta peptide-based immunobiochemical strategy. The Journal of biological chemistry, 283(18), 12528–12537. https://doi.org/10.1074/jbc.M708067200

Chen, S., Z. Li, W. Huang, Y. Wang and S. Fan (2021). "Prognostic and Therapeutic Significance of BTN3A Proteins in Tumors." Journal of Cancer **12**: 4505-4512.

Chumduri, C., R. K. Gurumurthy, H. Berger, O. Dietrich, N. Kumar, S. Koster, V. Brinkmann, K. Hoffmann, M. Drabkina, P. Arampatzi, D. Son, U. Klemm, H.-J. Mollenkopf, H. Herbst, M. Mangler, J. Vogel, A.-E. Saliba and T. F. Meyer (2021). "Opposing Wnt signals regulate cervical squamocolumnar homeostasis and emergence of metaplasia." Nature Cell Biology **23**(2): 184-197.

Chumduri, C., R. K. Gurumurthy, H. Berger, O. Dietrich, N. Kumar, S. Koster, V. Brinkmann, K. Hoffmann, M. Drabkina, P. Arampatzi, D. Son, U. Klemm, H. J. Mollenkopf, H. Herbst, M. Mangler, J. Vogel, A. E. Saliba and T. F. Meyer (2021). "Opposing Wnt signals regulate cervical squamocolumnar homeostasis and emergence of metaplasia." Nat Cell Biol **23**(2): 184-197.

Chumduri, C. and M. Y. Turco (2021). "Organoids of the female reproductive tract." J Mol Med (Berl) **99**(4): 531-553.

Ciccia, A. and S. J. Elledge (2010). "The DNA damage response: making it safe to play with knives." Mol Cell **40**(2): 179-204.

Ciccia, A. and S. J. Elledge (2010). "The DNA Damage Response: Making It Safe to Play with Knives." Molecular Cell **40**(2): 179-204.

Clevers, H., K. M. Loh and R. Nusse (2014). "Stem cell signaling. An integral program for tissue renewal and regeneration: Wnt signaling and stem cell control." Science **346**(6205): 1248012.

Cordeiro, M. N., R. C. P. De Lima, F. Paolini, A. Melo, A. P. F. Campos, A. Venuti and A. C. De Freitas (2018). "Current research into novel therapeutic vaccines against cervical cancer." Expert Rev Anticancer Ther **18**(4): 365-376.

Cordova, A., F. Toia, C. La Mendola, V. Orlando, S. Meraviglia, G. Rinaldi, M. Todaro, G. Cicero, L. Zichichi, P. L. Donni, N. Caccamo, G. Stassi, F. Dieli and F. Moschella (2012). "Characterization of Human γδ T Lymphocytes Infiltrating Primary Malignant Melanomas." PLoS ONE **7**(11): e49878.

Criscitiello, C. (2012). "Tumor-Associated Antigens in Breast Cancer." Breast Care **7**(4): 262-266.

Das, S., A. Babu, T. Medha, G. Ramanathan, A. G. Mukherjee, U. R. Wanjari, R. Murali, S. Kannampuzha, A. V. Gopalakrishnan, K. Renu, D. Sinha and C. George Priya Doss (2023). "Molecular mechanisms augmenting resistance to current therapies in clinics among cervical cancer patients." Medical Oncology **40**(5): 149.

De Mattos-Arruda, L., M. Vazquez, F. Finotello, R. Lepore, E. Porta, J. Hundal, P. Amengual-Rigo, C. K. Y. Ng, A. Valencia, J. Carrillo, T. A. Chan, V. Guallar, N. McGranahan, J. Blanco and M. Griffith (2020). "Neoantigen prediction and computational perspectives towards clinical benefit: recommendations from the ESMO Precision Medicine Working Group." Ann Oncol **31**(8): 978-990.

Del Prete, A., V. Salvi, A. Soriani, M. Laffranchi, F. Sozio, D. Bosisio and S. Sozzani (2023). "Dendritic cell subsets in cancer immunity and tumor antigen sensing." Cell Mol Immunol **20**(5): 432-447.

Di Marco, M., H. Schuster, L. Backert, M. Ghosh, H.-G. Rammensee and S. Stevanović (2017). "Unveiling the Peptide Motifs of HLA-C and HLA-G from Naturally Presented Peptides and Generation of Binding Prediction Matrices." The Journal of Immunology **199**(8): 2639-2651.

Donaldson, M. M., L. J. Mackintosh, J. M. Bodily, E. S. Dornan, L. A. Laimins and I. M. Morgan (2012). "An Interaction between Human Papillomavirus 16 E2 and TopBP1 Is Required for Optimum Viral DNA Replication and Episomal Genome Establishment." Journal of Virology **86**(23): 12806-12815.

Dong, J., D. Holthaus, C. Peters, S. Koster, M. Ehsani, A. Quevedo-Olmos, H. Berger, M. Zarobkiewicz, M. Mangler, R. K. Gurumurthy, N. Hedemann, C. Chumduri, D. Kabelitz and T. F. Meyer (2023). "γδ T cell-mediated cytotoxicity against patient-derived healthy and cancer cervical organoids." Frontiers in Immunology **14**. 1281646.

Dotti, G., S. Gottschalk, B. Savoldo and M. K. Brenner (2014). "Design and development of therapies using chimeric antigen receptor-expressing T cells." Immunol Rev **257**(1): 107-126.

Draper, L. M., M. L. M. Kwong, A. Gros, S. Stevanović, E. Tran, S. Kerkar, M. Raffeld, S. A. Rosenberg and C. S. Hinrichs (2015). "Targeting of HPV-16+ Epithelial Cancer Cells by TCR Gene Engineered T Cells Directed against E6." Clinical Cancer Research **21**(19): 4431-4439.

Duan, S., W. Guo, Z. Xu, Y. He, C. Liang, Y. Mo, Y. Wang, F. Xiong, C. Guo, Y. Li, X. Li, G. Li, Z. Zeng, W. Xiong and F. Wang (2019). "Natural killer group 2D receptor and its ligands in cancer immune escape." Molecular Cancer **18**(1): 29.

Dziubańska-Kusibab, P. J., H. Berger, F. Battistini, B. A. M. Bouwman, A. Iftekhar, R. Katainen, T. Cajuso, N. Crosetto, M. Orozco, L. A. Aaltonen and T. F. Meyer (2020). "Colibactin DNA-damage signature indicates mutational impact in colorectal cancer." Nat Med **26**(7): 1063-1069.

Eckert, R. L. and E. A. Rorke (1989). "Molecular biology of keratinocyte differentiation." Environ Health Perspect **80**: 109-116.

Edwards, L. J., V. I. Zarnitsyna, J. D. Hood, B. D. Evavold and C. Zhu (2012). "Insights into T cell recognition of antigen: significance of two-dimensional kinetic parameters." Front Immunol **3**: 86.

Egawa N. (2023). "Papillomaviruses and cancer: commonalities and differences in HPV carcinogenesis at different sites of the body." International journal of clinical oncology, 28(8), 956–964.

Eskander, R. N. and K. S. Tewari (2015). "Immunotherapy: an evolving paradigm in the treatment of advanced cervical cancer." Clin Ther **37**(1): 20-38.

Fan, C., Q. Wang, G. van der Zon, J. Ren, C. Agaser, R. C. Slieker, P. V. Iyengar, H. Mei and P. Ten Dijke (2022). "OVOL1 inhibits breast cancer cell invasion by enhancing the degradation of TGF-β type I receptor." Signal Transduct Target Ther **7**(1): 126.

Fan, W., D. Wang, G. Li, J. Xu, C. Ren, Z. Sun, Z. Wang, W. Ma, Z. Zhao, Z. Bao, T. Jiang and Y. Zhang (2022). "A novel chemokine-based signature for prediction of prognosis and therapeutic response in glioma." CNS Neurosci Ther **28**(12): 2090-2103.

Fan, Z., X. Feng, W. Zhang, N. Li, X. Zhang and J. M. Lin (2020). "Visual detection of high-risk HPV16 and HPV18 based on loop-mediated isothermal amplification." Talanta **217**: 121015.

Farhood, B., M. Najafi and K. Mortezaee (2019). "CD8(+) cytotoxic T lymphocytes in cancer immunotherapy: A review." J Cell Physiol **234**(6): 8509-8521.

Feng, N.-N., X.-Y. Du, Y.-S. Zhang, Z.-K. Jiao, X.-H. Wu and B.-M. Yang (2023). "Overweight/obesity-related transcriptomic signature as a correlate of clinical outcome, immune microenvironment, and treatment response in hepatocellular carcinoma." Frontiers in Endocrinology **13**.

Fichtner, A. S., M. M. Karunakaran, S. Gu, C. T. Boughter, M. T. Borowska, L. Starick, A. Nöhren, T. W. Göbel, E. J. Adams and T. Herrmann (2020). "Alpaca (Vicugna pacos), the first nonprimate species with a phosphoantigen-reactive Vγ9Vδ2 T cell subset." Proceedings of the National Academy of Sciences **117**(12): 6697-6707.

Fisch, P., M. Malkovsky, S. Kovats, E. Sturm, E. Braakman, B. S. Klein, S. D. Voss, L. W. Morrissey, R. DeMars, W. J. Welch, R. L. H. Bolhuis and P. M. Sondel (1990). "Recognition by Human Vγ9/Vδ2 T Cells of a GroEL Homolog on Daudi Burkitt's Lymphoma Cells." Science **250**(4985): 1269-1273.

Fritsch, H., R. Auer, R. Hörmann, E. Pechriggl, S. Regauer and O. Reich (2021). "The development of the human vaginal fornix and the portio cervicis." Clinical Anatomy **34**(7): 1059-1067.

Gagnon, S. J., O. Y. Borbulevych, R. L. Davis-Harrison, R. V. Turner, M. Damirjian, A. Wojnarowicz, W. E. Biddison and B. M. Baker (2006). "T cell receptor recognition via cooperative conformational plasticity." J Mol Biol **363**(1): 228-243.

Galati, L., Chiocca, S., Duca, D., Tagliabue, M., Simoens, C., Gheit, T., Arbyn, M., & Tommasino, M. (2022). "HPV and head and neck cancers: Towards early diagnosis and prevention." Tumour virus research, 14, 200245.

Gao, Z., Y. Bai, A. Lin, A. Jiang, C. Zhou, Q. Cheng, Z. Liu, X. Chen, J. Zhang and P. Luo (2023). "Gamma delta T-cell-based immune checkpoint therapy: attractive candidate for antitumor treatment." Molecular Cancer **22**(1).

Garcia-Diaz, A., D. S. Shin, B. H. Moreno, J. Saco, H. Escuin-Ordinas, G. A. Rodriguez, J. M. Zaretsky, L. Sun, W. Hugo, X. Wang, G. Parisi, C. P. Saus, D. Y. Torrejon, T. G. Graeber, B. Comin-Anduix, S. Hu-Lieskovan, R. Damoiseaux, R. S. Lo and A. Ribas (2017). "Interferon Receptor Signaling Pathways Regulating PD-L1 and PD-L2 Expression." Cell Rep **19**(6): 1189-1201.

Gentles, A. J., A. M. Newman, C. L. Liu, S. V. Bratman, W. Feng, D. Kim, V. S. Nair, Y. Xu, A. Khuong, C. D. Hoang, M. Diehn, R. B. West, S. K. Plevritis and A. A. Alizadeh (2015). "The prognostic landscape of genes and infiltrating immune cells across human cancers." Nat Med **21**(8): 938-945.

Germano, G., S. Lamba, G. Rospo, L. Barault, A. Magrì, F. Maione, M. Russo, G. Crisafulli, A. Bartolini, G. Lerda, G. Siravegna, B. Mussolin, R. Frapolli, M. Montone, F. Morano, F. de Braud, N. Amirouchene-Angelozzi, S. Marsoni, M. D'Incalci, A. Orlandi, E. Giraudo, A. Sartore-Bianchi, S. Siena, F. Pietrantonio, F. Di Nicolantonio and A. Bardelli (2017). "Inactivation of DNA repair triggers neoantigen generation and impairs tumour growth." Nature **552**(7683): 116-120.

Giannotta, C., F. Autino and M. Massaia (2023). "Vγ9Vδ2 T-cell immunotherapy in blood cancers: ready for prime time?" Frontiers in Immunology **14**.

Gober, H.-J. R., M. Kistowska, L. Angman, P. Jenö, L. Mori and G. De Libero (2003). "Human T Cell Receptor γδ Cells Recognize Endogenous Mevalonate Metabolites in Tumor Cells." Journal of Experimental Medicine **197**(2): 163-168.

Gomes, A. Q., D. S. Martins and B. Silva-Santos (2010). "Targeting γδ T Lymphocytes for Cancer Immunotherapy: From Novel Mechanistic Insight to Clinical Application: Table 1." Cancer Research **70**(24): 10024-10027.

Groh, V., A. Steinle, S. Bauer and T. Spies (1998). "Recognition of Stress-Induced MHC Molecules by Intestinal Epithelial γδ T Cells." Science **279**(5357): 1737-1740.

Gu, S., M. T. Borowska, C. T. Boughter and E. J. Adams (2018). "Butyrophilin3A proteins and Vγ9Vδ2 T cell activation." Semin Cell Dev Biol **84**: 65-74.

Gurumurthy, R. K., S. Koster, N. Kumar, T. F. Meyer and C. Chumduri (2022). "Patient-derived and mouse endo-ectocervical organoid generation, genetic manipulation and applications to model infection." Nat Protoc **17**(7): 1658-1690.

Gusho, E. and L. Laimins (2021). "Human Papillomaviruses Target the DNA Damage Repair and Innate Immune Response Pathways to Allow for Persistent Infection." Viruses **13**(7): 1390.

Hanahan, D. and Robert (2011). "Hallmarks of Cancer: The Next Generation." Cell **144**(5): 646-674.

He, X. and C. Xu (2020). "Immune checkpoint signaling and cancer immunotherapy." Cell Research **30**(8): 660-669.

Helleday, T., E. Petermann, C. Lundin, B. Hodgson and R. A. Sharma (2008). "DNA repair pathways as targets for cancer therapy." Nature Reviews Cancer **8**(3): 193-204.

Helt, C. E., W. A. Cliby, P. C. Keng, R. A. Bambara and M. A. O'Reilly (2005). "Ataxia Telangiectasia Mutated (ATM) and ATM and Rad3-related Protein Exhibit Selective Target Specificities in Response to Different Forms of DNA Damage." Journal of Biological Chemistry **280**(2): 1186-1192.

Herfs, M., Y. Yamamoto, A. Laury, X. Wang, M. R. Nucci, M. E. McLaughlin-Drubin, K. Münger, S. Feldman, F. D. McKeon, W. Xian and C. P. Crum (2012). "A discrete population of squamocolumnar junction cells implicated in the pathogenesis of cervical cancer." Proceedings of the National Academy of Sciences **109**(26): 10516-10521.

Herrmann, T. (2023). "Caveat: Monoclonal antibodies 20.1 and 103.2 bind all human BTN3A proteins and are not suited to study BTN3A1-specific features." Proceedings of the National Academy of Sciences **120**(20).

Herrmann, T., A. S. Fichtner and M. M. Karunakaran (2020). "An Update on the Molecular Basis of Phosphoantigen Recognition by Vγ9Vδ2 T Cells." Cells **9**(6): 1433.

Hintz, M., A. Reichenberg, B. Altincicek, U. Bahr, R. M. Gschwind, A. K. Kollas, E. Beck, J. Wiesner, M. Eberl and H. Jomaa (2001). "Identification of (E)-4-hydroxy-3-methyl-but-2-enyl pyrophosphate as a major activator for human gammadelta T cells in Escherichia coli." FEBS Lett **509**(2): 317-322.

Holler, P. D. and D. M. Kranz (2003). "Quantitative analysis of the contribution of TCR/pepMHC affinity and CD8 to T cell activation." Immunity **18**(2): 255-264.

Hong, S., S. Cheng, A. Iovane and L. A. Laimins (2015). "STAT-5 Regulates Transcription of the Topoisomerase IIβ-Binding Protein 1 (TopBP1) Gene To Activate the ATR Pathway and Promote Human Papillomavirus Replication." mBio **6**(6): e02006-02015.

Hong, S. and L. A. Laimins (2013). "Regulation of the life cycle of HPVs by differentiation and the DNA damage response." Future Microbiol **8**(12): 1547-1557.

Horvath, P., N. Aulner, M. Bickle, A. M. Davies, E. D. Nery, D. Ebner, M. C. Montoya, P. Östling, V. Pietiäinen, L. S. Price, S. L. Shorte, G. Turcatti, C. Von Schantz and N. O. Carragher (2016). "Screening out irrelevant cell-based models of disease." Nature Reviews Drug Discovery **15**(11): 751-769.

Huang, Z. D., Z. Z. Liu, Y. Y. Liu, Y. C. Fu, L. L. Lin, C. Hu, H. Y. Gu and R. X. Wei (2021). "Molecular Subtypes Based on Cell Differentiation Trajectories in Head and Neck Squamous Cell Carcinoma: Differential Prognosis and Immunotherapeutic Responses." Front Immunol **12**: 791621.

Huch, M., H. Gehart, R. van Boxtel, K. Hamer, F. Blokzijl, M. M. Verstegen, E. Ellis, M. van Wenum, S. A. Fuchs, J. de Ligt, M. van de Wetering, N. Sasaki, S. J. Boers, H. Kemperman, J. de Jonge, J. N. Ijzermans, E. E. Nieuwenhuis, R. Hoekstra, S. Strom, R. R. Vries, L. J. van der Laan, E. Cuppen and H. Clevers (2015). "Long-term culture of genome-stable bipotent stem cells from adult human liver." Cell **160**(1-2): 299-312.

Hudecek, R., B. Kohlova, I. Siskova, M. Piskacek and A. Knight (2021). "Blocking of EphA2 on Endometrial Tumor Cells Reduces Susceptibility to Vδ1 Gamma-Delta T-Cell-Mediated Killing." Front Immunol **12**: 752646.

Huh, W. K., E. A. Joura, A. R. Giuliano, O. E. Iversen, R. P. de Andrade, K. A. Ault, D. Bartholomew, R. M. Cestero, E. N. Fedrizzi, A. L. Hirschberg, M. H. Mayrand, A. M. Ruiz-Sternberg, J. T. Stapleton, D. J. Wiley, A. Ferenczy, R. Kurman, B. M. Ronnett, M. H. Stoler, J. Cuzick, S. M. Garland, S. K. Kjaer, O. M. Bautista, R. Haupt, E. Moeller, M. Ritter, C. C. Roberts, C. Shields and A. Luxembourg (2017). "Final efficacy, immunogenicity, and safety analyses of a nine-valent human papillomavirus vaccine in women aged 16-26 years: a randomised, double-blind trial." Lancet **390**(10108): 2143-2159.

Jackson, S. P. and J. Bartek (2009). "The DNA-damage response in human biology and disease." Nature **461**(7267): 1071-1078.

Jain, S. and J. I. Clark (2015). "Ipilimumab for the treatment of melanoma." Melanoma Manag **2**(1): 33-39.

Janeway Jr, C. A., P. Travers, M. Walport and M. J. Shlomchik (2001). T-cell receptor gene rearrangement. Immunobiology: The Immune System in Health and Disease. 5th edition, Garland Science.

Jia, L., Y. Gao, T. Zhou, X. L. Zhao, H. Y. Hu, D. W. Chen and M. X. Qiao (2021). "Enhanced response to PD-L1 silencing by modulation of TME via balancing glucose metabolism and robust co-delivery of siRNA/Resveratrol with dual-responsive polyplexes." Biomaterials **271**: 120711.

Jiang, P., S. Gu, D. Pan, J. Fu, A. Sahu, X. Hu, Z. Li, N. Traugh, X. Bu, B. Li, J. Liu, G. J. Freeman, M. A. Brown, K. W. Wucherpfennig and X. S. Liu (2018). "Signatures of T cell dysfunction and exclusion predict cancer immunotherapy response." Nat Med **24**(10): 1550-1558.

Jiang, T., T. Shi, H. Zhang, J. Hu, Y. Song, J. Wei, S. Ren and C. Zhou (2019). "Tumor neoantigens: from basic research to clinical applications." Journal of Hematology & Oncology **12**(1).

Jiang, X., J. Xu, M. Liu, H. Xing, Z. Wang, L. Huang, A. L. Mellor, W. Wang and S. Wu (2019). "Adoptive CD8(+) T cell therapy against cancer:Challenges and opportunities." Cancer Lett **462**: 23-32.

Jin, B. Y., T. E. Campbell, L. M. Draper, S. Stevanović, B. Weissbrich, Z. Yu, N. P. Restifo, S. A. Rosenberg, C. L. Trimble and C. S. Hinrichs (2018). "Engineered T cells targeting E7 mediate regression of human papillomavirus cancers in a murine model." JCI Insight **3**(8).

Kabelitz, D., R. Serrano, L. Kouakanou, C. Peters and S. Kalyan (2020). "Cancer immunotherapy with γδ T cells: many paths ahead of us." Cellular & Molecular Immunology **17**(9): 925-939.

Kabelitz, D., R. Serrano, L. Kouakanou, C. Peters and S. Kalyan (2020). "Cancer immunotherapy with γδ T cells: many paths ahead of us." Cellular & Molecular Immunology **17**(9): 925-939.

Kaminski, P., S. Hong, T. Kono, P. Hoover and L. Laimins (2021). "Topoisomerase 2β Induces DNA Breaks To Regulate Human Papillomavirus Replication." mBio **12**(1).

Karunakaran, M. M., C. R. Willcox, M. Salim, D. Paletta, A. S. Fichtner, A. Noll, L. Starick, A. Nöhren, C. R. Begley, K. A. Berwick, R. A. G. Chaleil, V. Pitard, J. Déchanet-Merville, P. A. Bates, B. Kimmel, T. J. Knowles, V. Kunzmann, L. Walter, M. Jeeves, F. Mohammed, B. E. Willcox and T. Herrmann (2020). "Butyrophilin-2A1 Directly Binds Germline-Encoded Regions of the Vγ9Vδ2 TCR and Is Essential for Phosphoantigen Sensing." Immunity **52**(3): 487-498.e486.

Karzai, F., D. VanderWeele, R. A. Madan, H. Owens, L. M. Cordes, A. Hankin, A. Couvillon, E. Nichols, M. Bilusic, M. L. Beshiri, K. Kelly, V. Krishnasamy, S. Lee, M. J. Lee, A. Yuno, J. B. Trepel, M. J. Merino, R. Dittamore, J. Marté, R. N. Donahue, J. Schlom, K. J. Killian, P. S. Meltzer, S. M. Steinberg, J. L. Gulley, J. M. Lee and W. L. Dahut (2018). "Activity of durvalumab plus olaparib in metastatic castration-resistant prostate cancer in men with and without DNA damage repair mutations." J Immunother Cancer **6**(1): 141.

Kast, J., S. Nozohouri, D. Zhou, M. R. Yago, P. W. Chen, M. Ahamadi, S. Dutta and V. V. Upreti (2022). "Recent advances and clinical pharmacology aspects of Chimeric Antigen Receptor (CAR) T-cellular therapy development." Clinical and Translational Science **15**(9): 2057-2074.

Kaur, G. and J. M. Dufour (2012). "Cell lines: Valuable tools or useless artifacts." Spermatogenesis **2**(1): 1-5.

Kavanagh, K., K. G. Pollock, K. Cuschieri, T. Palmer, R. L. Cameron, C. Watt, R. Bhatia, C. Moore, H. Cubie, M. Cruickshank and C. Robertson (2017). "Changes in the prevalence of human papillomavirus following a national bivalent human papillomavirus vaccination programme in Scotland: a 7-year cross-sectional study." Lancet Infect Dis **17**(12): 1293-1302.

Kjaer, S. K., M. Nygård, J. Dillner, J. Brooke Marshall, D. Radley, M. Li, C. Munk, B. T. Hansen, L. G. Sigurdardottir, M. Hortlund, L. Tryggvadottir, A. Joshi, R. Das and A. J. Saah (2018). "A 12-Year Follow-up on the Long-Term Effectiveness of the Quadrivalent Human Papillomavirus Vaccine in 4 Nordic Countries." Clin Infect Dis **66**(3): 339-345.

Knaul, F. M., N. M. Rodriguez, H. Arreola-Ornelas and J. R. Olson (2019). "Cervical cancer: lessons learned from neglected tropical diseases." The Lancet Global Health **7**(3): e299-e300.

Kong, J. C. H., G. R. Guerra, R. M. Millen, S. Roth, H. Xu, P. J. Neeson, P. K. Darcy, M. H. Kershaw, S. Sampurno, J. Malaterre, D. S. H. Liu, T. D. Pham, V. Narasimhan, M. Wang, Y. K. Huang, K. Visvanathan, J. McCormick, A. C. Lynch, S. Warrier, M. Michael, J. Desai, W. Murray, C. Mitchell, S. Ngan, W. A. Phillips, A. G. Heriot and R. G. Ramsay (2018). "Tumor-Infiltrating Lymphocyte Function Predicts Response to Neoadjuvant Chemoradiotherapy in Locally Advanced Rectal Cancer." JCO Precis Oncol **2**: 1-15.

Kong, Y., W. Cao, X. Xi, C. Ma, L. Cui and W. He (2009). "The NKG2D ligand ULBP4 binds to TCRgamma9/delta2 and induces cytotoxicity to tumor cells through both TCRgammadelta and NKG2D." Blood **114**(2): 310-317.

Kono, T., Hoover, P., Poropatich, K., Paunesku, T., Mittal, B. B., Samant, S., & Laimins, L. A. (2020). Activation of DNA damage repair factors in HPV positive oropharyngeal cancers. Virology, 547, 27–34.

Koster, S., R. K. Gurumurthy, N. Kumar, P. G. Prakash, J. Dhanraj, S. Bayer, H. Berger, S. M. Kurian, M. Drabkina, H.-J. Mollenkopf, C. Goosmann, V. Brinkmann, Z. Nagel, M. Mangler, T. F. Meyer and C. Chumduri (2022). "Modelling Chlamydia and HPV co-infection in patient-derived ectocervix organoids reveals distinct cellular reprogramming." Nature Communications **13**(1): 1030.

Koster, S., R. K. Gurumurthy, N. Kumar, P. G. Prakash, J. Dhanraj, S. Bayer, H. Berger, S. M. Kurian, M. Drabkina, H.-J. Mollenkopf, C. Goosmann, V. Brinkmann, Z. Nagel, M. Mangler, T. F. Meyer and C. Chumduri (2022). "Modelling Chlamydia and HPV co-infection in patient-derived ectocervix organoids reveals distinct cellular reprogramming." Nature Communications **13**(1).

Kousar, K., T. Ahmad, F. Naseer, S. Kakar and S. Anjum (2022). "Review Article: Immune Landscape and Immunotherapy Options in Cervical Carcinoma." Cancers **14**(18): 4458.

Kretzschmar, K. (2021). "Cancer research using organoid technology." Journal of Molecular Medicine **99**(4): 501-515.

Kühl, A. A., N. N. Pawlowski, K. Grollich, M. Blessenohl, J. Westermann, M. Zeitz, C. Loddenkemper and J. C. Hoffmann (2009). "Human peripheral γδ T cells possess regulatory potential." Immunology **128**(4): 580-588.

Kumar, A., R. Watkins and A. E. Vilgelm (2021). "Cell Therapy With TILs: Training and Taming T Cells to Fight Cancer." Front Immunol **12**: 690499.

Kunzmann, V., M. Smetak, B. Kimmel, K. Weigang-Koehler, M. Goebeler, J. Birkmann, J. Becker, I. G. Schmidt-Wolf, H. Einsele and M. Wilhelm (2012). "Tumor-promoting versus tumor-antagonizing roles of γδ T cells in cancer immunotherapy: results from a prospective phase I/II trial." J Immunother **35**(2): 205-213.

Labani-Motlagh, A., M. Ashja-Mahdavi and A. Loskog (2020). "The Tumor Microenvironment: A Milieu Hindering and Obstructing Antitumor Immune Responses." Frontiers in Immunology **11**.

Lafont, V., F. Sanchez, E. Laprevotte, H. A. Michaud, L. Gros, J. F. Eliaou and N. Bonnefoy (2014). "Plasticity of γδ T Cells: Impact on the Anti-Tumor Response." Front Immunol **5**: 622.

Lama-Sherpa, T. D. and L. A. Shevde (2020). "An Emerging Regulatory Role for the Tumor Microenvironment in the DNA Damage Response to Double-Strand Breaks." Mol Cancer Res **18**(2): 185-193.

Lança, T., D. V. Correia, C. F. Moita, H. Raquel, A. Neves-Costa, C. Ferreira, J. S. Ramalho, J. T. Barata, L. F. Moita, A. Q. Gomes and B. Silva-Santos (2010). "The MHC class Ib protein ULBP1 is a nonredundant determinant of leukemia/lymphoma susceptibility to gammadelta T-cell cytotoxicity." Blood **115**(12): 2407-2411.

Latchman, Y., C. R. Wood, T. Chernova, D. Chaudhary, M. Borde, I. Chernova, Y. Iwai, A. J. Long, J. A. Brown, R. Nunes, E. A. Greenfield, K. Bourque, V. A. Boussiotis, L. L. Carter, B. M. Carreno, N. Malenkovich, H. Nishimura, T. Okazaki, T. Honjo, A. H. Sharpe and G. J. Freeman (2001). "PD-L2 is a second ligand for PD-1 and inhibits T cell activation." Nature Immunology **2**(3): 261-268.

Layman, H., K. W. Rickert, S. Wilson, A. A. Aksyuk, J. M. Dunty, D. Natrakul, N. Swaminathan and C. J. Delnagro (2020). "Development and validation of a multiplex immunoassay for the simultaneous quantification of type-specific IgG antibodies to E6/E7 oncoproteins of HPV16 and HPV18." PLOS ONE **15**(3): e0229672.

Lee, H. J., Y. A. Kim, C. K. Sim, S. H. Heo, I. H. Song, H. S. Park, S. Y. Park, W. S. Bang, I. A. Park, M. Lee, J. H. Lee, Y. S. Cho, S. Chang, J. Jung, J. Kim, S. B. Lee, S. Y. Kim, M. S. Lee and G. Gong (2017). "Expansion of tumor-infiltrating lymphocytes and their potential for application as adoptive cell transfer therapy in human breast cancer." Oncotarget **8**(69): 113345-113359.

Leko, V. and S. A. Rosenberg (2020). "Identifying and Targeting Human Tumor Antigens for T Cell-Based Immunotherapy of Solid Tumors." Cancer Cell **38**(4): 454-472.

Li, G., F. Wu, F. Zeng, Y. Zhai, Y. Feng, Y. Chang, D. Wang, T. Jiang and W. Zhang (2021). "A novel DNA repair-related nomogram predicts survival in low-grade gliomas." CNS Neurosci Ther **27**(2): 186-195.

Li, Y., G. Li, J. Zhang, X. Wu and X. Chen (2020). "The Dual Roles of Human γδ T Cells: Anti-Tumor or Tumor-Promoting." Front Immunol **11**: 619954.

Li, Y., G. Li, J. Zhang, X. Wu and X. Chen (2021). "The Dual Roles of Human γδ T Cells: Anti-Tumor or Tumor-Promoting." Frontiers in Immunology **11**.

Ligaba, S. B., A. Khurana, G. Graham, E. Krawczyk, S. Jablonski, E. F. Petricoin, R. I. Glazer and G. Upadhyay (2015). "Multifactorial analysis of conditional reprogramming of human keratinocytes." PLoS One **10**(2): e0116755.

Lin, M., X. Zhang, S. Liang, H. Luo, M. Alnaggar, A. Liu, Z. Yin, J. Chen, L. Niu and Y. Jiang (2020). "Irreversible electroporation plus allogenic Vγ9Vδ2 T cells enhances antitumor effect for locally advanced pancreatic cancer patients." Signal Transduction and Targeted Therapy **5**(1).

Liu C, Xu Y, Chen H, Zhang J, He W. Tumor-associated protein ligands recognized by human γδ T cell receptor and their implications in cancer therapy. Explor Immunol. 2022;2:64–78. https://doi.org/10.37349/ei.2022.00037

Liu, J., M. Zhu, X. Xia, Y. Huang, Q. Zhang and X. Wang (2016). "Jumonji domain-containing protein 1A promotes cell growth and progression via transactivation of c-Myc expression and predicts a poor prognosis in cervical cancer." Oncotarget **7**(51): 85151-85162.

Liu, W., L. Ju, S. Cheng, G. Wang, K. Qian, X. Liu, Y. Xiao and X. Wang (2020). "Conditional reprogramming: Modeling urological cancer and translation to clinics." Clinical and Translational Medicine **10**(2).

Liu, X., J. Fang, S. Huang, X. Wu, X. Xie, J. Wang, F. Liu, M. Zhang, Z. Peng and N. Hu (2021). "Tumor-on-a-chip: from bioinspired design to biomedical application." Microsystems & Nanoengineering **7**(1): 50.

Llames, S., E. García-Pérez, Á. Meana, F. Larcher and M. del Río (2015). "Feeder Layer Cell Actions and Applications." Tissue Eng Part B Rev **21**(4): 345-353.

Lõhmussaar, K., M. Boretto and H. Clevers (2020). "Human-Derived Model Systems in Gynecological Cancer Research." Trends in Cancer **6**(12): 1031-1043.

Lõhmussaar, K., R. Oka, J. Espejo Valle-Inclan, M. H. H. Smits, H. Wardak, J. Korving, H. Begthel, N. Proost, M. Van De Ven, O. W. Kranenburg, T. G. N. Jonges, R. P. Zweemer, S. Veersema, R. Van Boxtel and H. Clevers (2021). "Patient-derived organoids model cervical tissue dynamics and viral oncogenesis in cervical cancer." Cell Stem Cell **28**(8): 1380-1396.e1386.

Luca, B. A., C. B. Steen, M. Matusiak, A. Azizi, S. Varma, C. Zhu, J. Przybyl, A. Espín-Pérez, M. Diehn, A. A. Alizadeh, M. van de Rijn, A. J. Gentles and A. M. Newman (2021). "Atlas of clinically distinct cell states and ecosystems across human solid tumors." Cell **184**(21): 5482-5496.e5428.

Ma, J., J. Setton, N. Y. Lee, N. Riaz and S. N. Powell (2018). "The therapeutic significance of mutational signatures from DNA repair deficiency in cancer." Nat Commun **9**(1): 3292.

Macleod, A. S. and W. L. Havran (2011). "Functions of skin-resident γδ T cells." Cellular and Molecular Life Sciences **68**(14): 2399-2408.

Mahdavi, M. and V. Moreau (2016). "In silico designing breast cancer peptide vaccine for binding to MHC class I and II: A molecular docking study." Comput Biol Chem **65**: 110-116.

Mansoori, B., A. Mohammadi, S. Davudian, S. Shirjang and B. Baradaran (2017). "The Different Mechanisms of Cancer Drug Resistance: A Brief Review." Advanced Pharmaceutical Bulletin **7**(3): 339-348.

Marabelle, A., M. Fakih, J. Lopez, M. Shah, R. Shapira-Frommer, K. Nakagawa, H. C. Chung, H. L. Kindler, J. A. Lopez-Martin, W. H. Miller, Jr., A. Italiano, S. Kao, S. A. Piha-Paul, J. P. Delord, R. R. McWilliams, D. A. Fabrizio, D. Aurora-Garg, L. Xu, F. Jin, K. Norwood and Y. J. Bang (2020). "Association of tumour mutational burden with outcomes in patients with advanced solid tumours treated with pembrolizumab: prospective biomarker analysis of the multicohort, open-label, phase 2 KEYNOTE-158 study." Lancet Oncol **21**(10): 1353-1365.

Mboko, W. P., P. Chhabra, M. D. Valcarce, V. Costantini and J. Vinjé (2022). "Advances in understanding of the innate immune response to human norovirus infection using organoid models." J Gen Virol **103**(1).

Mehta, K. and L. Laimins (2018). "Human Papillomaviruses Preferentially Recruit DNA Repair Factors to Viral Genomes for Rapid Repair and Amplification." mBio **9**(1): e00064-00018.

Mookerjee-Basu, J., P. Vantourout, L. O. Martinez, B. Perret, X. Collet, C. Périgaud, S. Peyrottes and E. Champagne (2010). "F1-adenosine triphosphatase displays properties characteristic of an antigen presentation molecule for Vgamma9Vdelta2 T cells." J Immunol **184**(12): 6920-6928.

Müller, L., A. Tunger, I. Plesca, R. Wehner, A. Temme, D. Westphal, F. Meier, M. Bachmann and M. Schmitz (2020). "Bidirectional Crosstalk Between Cancer Stem Cells and Immune Cell Subsets." Front Immunol **11**: 140.

Nabhan, M., D. Egan, M. Kreileder, V. Zhernovkov, E. Timosenko, T. Slidel, S. Dovedi, K. Glennon, D. Brennan and W. Kolch (2023). "Deciphering the tumour immune microenvironment cell by cell." Immunooncol Technol **18**: 100383.

Nakamura, T. and T. Sato (2018). "Advancing Intestinal Organoid Technology Toward Regenerative Medicine." Cell Mol Gastroenterol Hepatol **5**(1): 51-60.

Nastasi, C., L. Mannarino and M. D'Incalci (2020). "DNA Damage Response and Immune Defense." International Journal of Molecular Sciences **21**(20): 7504.

Nedellec, S., M. Bonneville and E. Scotet (2010). "Human Vgamma9Vdelta2 T cells: from signals to functions." Semin Immunol **22**(4): 199-206.

Nelde, A., D. J. Kowalewski and S. Stevanović (2019). "Purification and Identification of Naturally Presented MHC Class I and II Ligands." Methods Mol Biol **1988**: 123-136.

Nicol, A. J., H. Tokuyama, S. R. Mattarollo, T. Hagi, K. Suzuki, K. Yokokawa and M. Nieda (2011). "Clinical evaluation of autologous gamma delta T cell-based immunotherapy for metastatic solid tumours." Br J Cancer **105**(6): 778-786.

Nishimura, H., M. Nose, H. Hiai, N. Minato and T. Honjo (1999). "Development of Lupus-like Autoimmune Diseases by Disruption of the PD-1 Gene Encoding an ITIM Motif-Carrying Immunoreceptor." Immunity **11**(2): 141-151.

Noordhoek, J., V. Gulmans, K. van der Ent and J. M. Beekman (2016). "Intestinal organoids and personalized medicine in cystic fibrosis: a successful patient-oriented research collaboration." Curr Opin Pulm Med **22**(6): 610-616.

Nurieva, R., S. Thomas, T. Nguyen, N. Martin-Orozco, Y. Wang, M.-K. Kaja, X.-Z. Yu and C. Dong (2006). "T-cell tolerance or function is determined by combinatorial costimulatory signals." The EMBO Journal **25**(11): 2623-2633.

Nussbaumer, O. and M. Koslowski (2019). "The emerging role of γδ T cells in cancer immunotherapy." Immunooncol Technol **1**: 3-10.

Ojesina, A. I., L. Lichtenstein, S. S. Freeman, C. S. Pedamallu, I. Imaz-Rosshandler, T. J. Pugh, A. D. Cherniack, L. Ambrogio, K. Cibulskis, B. Bertelsen, S. Romero-Cordoba, V. Treviño, K. Vazquez-Santillan, A. S. Guadarrama, A. A. Wright, M. W. Rosenberg, F. Duke, B. Kaplan, R. Wang, E. Nickerson, H. M. Walline, M. S. Lawrence, C. Stewart, S. L. Carter, A. McKenna, I. P. Rodriguez-Sanchez, M. Espinosa-Castilla, K. Woie, L. Bjorge, E. Wik, M. K. Halle, E. A. Hoivik, C. Krakstad, N. B. Gabiño, G. S. Gómez-Macías, L. D. Valdez-Chapa, M. L. Garza-Rodríguez, G. Maytorena, J. Vazquez, C. Rodea, A. Cravioto, M. L. Cortes, H. Greulich, C. P. Crum, D. S. Neuberg, A. Hidalgo-Miranda, C. R. Escareno, L. A. Akslen, T. E. Carey, O. K. Vintermyr, S. B. Gabriel, H. A. Barrera-Saldaña, J. Melendez-Zajgla, G. Getz, H. B. Salvesen and M. Meyerson (2014). "Landscape of genomic alterations in cervical carcinomas." Nature **506**(7488): 371-375.

Okada, M., K. Shimizu and S.-I. Fujii (2022). "Identification of Neoantigens in Cancer Cells as Targets for Immunotherapy." International Journal of Molecular Sciences **23**(5): 2594.

Okunade, K. S. (2020). "Human papillomavirus and cervical cancer." J Obstet Gynaecol **40**(5): 602-608.

Otter, S. J., J. Chatterjee, A. J. Stewart and A. Michael (2019). "The Role of Biomarkers for the Prediction of Response to Checkpoint Immunotherapy and the Rationale for the Use of Checkpoint Immunotherapy in Cervical Cancer." Clinical Oncology **31**(12): 834-843.

Ozcelikkale, A., K. Shin, V. Noe-Kim, B. D. Elzey, Z. Dong, J.-T. Zhang, K. Kim, I. C. Kwon, K. Park and B. Han (2017). "Differential response to doxorubicin in breast cancer subtypes simulated by a microfluidic tumor model." Journal of Controlled Release **266**: 129-139.

Papadaki, G. F., O. Ani, T. J. Florio, M. C. Young, J. N. Danon, Y. Sun, D. Dersh and N. G. Sgourakis (2023). "Decoupling peptide binding from T cell receptor recognition with engineered chimeric MHC-I molecules." Frontiers in Immunology **14**.

Pearl, L. H., A. C. Schierz, S. E. Ward, B. Al-Lazikani and F. M. G. Pearl (2015). "Therapeutic opportunities within the DNA damage response." Nature Reviews Cancer **15**(3): 166-180.

Peigné, C. M., A. Léger, M. C. Gesnel, F. Konczak, D. Olive, M. Bonneville, R. Breathnach and E. Scotet (2017). "The Juxtamembrane Domain of Butyrophilin BTN3A1 Controls Phosphoantigen-Mediated Activation of Human Vγ9Vδ2 T Cells." J Immunol **198**(11): 4228-4234.

Pennington, D. J., D. Vermijlen, E. L. Wise, S. L. Clarke, R. E. Tigelaar and A. C. Hayday (2005). "The integration of conventional and unconventional T cells that characterizes cell-mediated responses." Adv Immunol **87**: 27-59.

Peters, C., L. Kouakanou, H.-H. Oberg, D. Wesch and D. Kabelitz (2020). Chapter Eleven - *In vitro* expansion of Vγ9Vδ2 T cells for immunotherapy. Methods in Enzymology. L. Galluzzi and N.-P. Rudqvist, Academic Press. **631:** 223-237.

Phan, G. Q., J. C. Yang, R. M. Sherry, P. Hwu, S. L. Topalian, D. J. Schwartzentruber, N. P. Restifo, L. R. Haworth, C. A. Seipp, L. J. Freezer, K. E. Morton, S. A. Mavroukakis, P. H. Duray, S. M. Steinberg, J. P. Allison, T. A. Davis and S. A. Rosenberg (2003). "Cancer regression and autoimmunity induced by cytotoxic T lymphocyte-associated antigen 4 blockade in patients with metastatic melanoma." Proceedings of the National Academy of Sciences **100**(14): 8372-8377.

Pierce, B. G. and Z. Weng (2013). "A flexible docking approach for prediction of T cell receptor-peptide-MHC complexes." Protein Sci **22**(1): 35-46.

Pollen, A. A., U. Kilik, C. B. Lowe and J. G. Camp (2023). "Human-specific genetics: new tools to explore the molecular and cellular basis of human evolution." Nature Reviews Genetics.

Prati, B., B. Marangoni and E. Boccardo (2018). "Human papillomavirus and genome instability: from productive infection to cancer." Clinics (Sao Paulo) **73**(suppl 1): e539s.

Prati, B., B. Marangoni and E. Boccardo (2018). "Human papillomavirus and genome instability: from productive infection to cancer." Clinics **73**: e539s.

Qin, Y., S. Ekmekcioglu, M. A. Forget, L. Szekvolgyi, P. Hwu, E. A. Grimm, A. A. Jazaeri and J. Roszik (2017). "Cervical Cancer Neoantigen Landscape and Immune Activity is Associated with Human Papillomavirus Master Regulators." Front Immunol **8**: 689.

Qing, T., T. Jun, K. E. Lindblad, A. Lujambio, M. Marczyk, L. Pusztai and K. L. Huang (2021). "Diverse immune response of DNA damage repair-deficient tumors." Cell Rep Med **2**(5): 100276.

Qureshi, O. S., Y. Zheng, K. Nakamura, K. Attridge, C. Manzotti, E. M. Schmidt, J. Baker, L. E. Jeffery, S. Kaur, Z. Briggs, T. Z. Hou, C. E. Futter, G. Anderson, L. S. K. Walker and D. M. Sansom (2011). "Trans-Endocytosis of CD80 and CD86: A Molecular Basis for the Cell-Extrinsic Function of CTLA-4." Science **332**(6029): 600-603.

Ramakrishnan, S., S. Partricia and G. Mathan (2015). "Overview of high-risk HPV's 16 and 18 infected cervical cancer: pathogenesis to prevention." Biomed Pharmacother **70**: 103-110.

Raverdeau, M., S. P. Cunningham, C. Harmon and L. Lynch (2019). "γδ T cells in cancer: a small population of lymphocytes with big implications." Clinical & Translational Immunology **8**(10).

Riazi Rad, F., S. Ajdary, R. Omranipour, M. H. Alimohammadian and Z. M. Hassan (2015). "Comparative analysis of CD4+ and CD8+ T cells in tumor tissues, lymph nodes and the peripheral blood from patients with breast cancer." Iran Biomed J **19**(1): 35-44.

Ridgley, L. A., J. Caron, A. Dalgleish and M. Bodman-Smith (2022). "Releasing the restraints of Vγ9Vδ2 T-cells in cancer immunotherapy." Front Immunol **13**: 1065495.

Rigau, M., S. Ostrouska, T. S. Fulford, D. N. Johnson, K. Woods, Z. Ruan, H. E. G. McWilliam, C. Hudson, C. Tutuka, A. K. Wheatley, S. J. Kent, J. A. Villadangos, B. Pal, C. Kurts, J. Simmonds, M. Pelzing, A. D. Nash, A. Hammet, A. M. Verhagen, G. Vairo, E. Maraskovsky, C. Panousis, N. A. Gherardin, J. Cebon, D. I. Godfrey, A. Behren and A. P. Uldrich (2020). "Butyrophilin 2A1 is essential for phosphoantigen reactivity by γδ T cells." Science **367**(6478): eaay5516.

Rock, K. L., E. Reits and J. Neefjes (2016). "Present Yourself! By MHC Class I and MHC Class II Molecules." Trends in Immunology **37**(11): 724-737.

Rodriguez, G. M., E. Yakubovich and B. C. Vanderhyden (2023). "Unveiling the Immunogenicity of Ovarian Tumors as the Crucial Catalyst for Therapeutic Success." Cancers **15**(23): 5694.

Sacchi, A., N. Tumino, A. Sabatini, E. Cimini, R. Casetti, V. Bordoni, G. Grassi and C. Agrati (2018). "Myeloid-Derived Suppressor Cells Specifically Suppress IFN-γ Production and Antitumor Cytotoxic Activity of Vδ2 T Cells." Frontiers in Immunology **9**.

Sahin, U., P. Oehm, E. Derhovanessian, R. A. Jabulowsky, M. Vormehr, M. Gold, D. Maurus, D. Schwarck-Kokarakis, A. N. Kuhn, T. Omokoko, L. M. Kranz, M. Diken, S. Kreiter, H. Haas, S. Attig, R. Rae, K. Cuk, A. Kemmer-Brück, A. Breitkreuz, C. Tolliver, J. Caspar, J. Quinkhardt, L. Hebich, M. Stein, A. Hohberger, I. Vogler, I. Liebig, S. Renken, J. Sikorski, M. Leierer, V. Müller, H. Mitzel-Rink, M. Miederer, C. Huber, S. Grabbe, J. Utikal, A. Pinter, R. Kaufmann, J. C. Hassel, C. Loquai and Ö. Türeci (2020). "An RNA vaccine drives immunity in checkpoint-inhibitor-treated melanoma." Nature **585**(7823): 107-112.

Sakakibara, N., D. Chen and A. A. McBride (2013). "Papillomaviruses Use Recombination-Dependent Replication to Vegetatively Amplify Their Genomes in Differentiated Cells." PLoS Pathogens **9**(7): e1003321.

Samstein, R. M. and N. Riaz (2018). "The DNA damage response in immunotherapy and radiation." Adv Radiat Oncol **3**(4): 527-533.

Sandstrom, A., C.-M. Peigné, A. Léger, James, F. Konczak, M.-C. Gesnel, R. Breathnach, M. Bonneville, E. Scotet and Erin (2014). "The Intracellular B30.2 Domain of Butyrophilin 3A1 Binds Phosphoantigens to Mediate Activation of Human Vγ9Vδ2 T Cells." Immunity **40**(4): 490-500.

Sandstrom, A., C. M. Peigné, A. Léger, J. E. Crooks, F. Konczak, M. C. Gesnel, R. Breathnach, M. Bonneville, E. Scotet and E. J. Adams (2014). "The intracellular B30.2 domain of butyrophilin 3A1 binds phosphoantigens to mediate activation of human Vγ9Vδ2 T cells." Immunity **40**(4): 490-500.

Saorin, G., I. Caligiuri and F. Rizzolio (2022). "Microfluidic organoids-on-a-chip: The future of human models." Semin Cell Dev Biol.

Schönefeldt, S., T. Wais, M. Herling, S. Mustjoki, V. Bekiaris, R. Moriggl and H. A. Neubauer (2021). "The Diverse Roles of γδ T Cells in Cancer: From Rapid Immunity to Aggressive Lymphoma." Cancers **13**(24): 6212.

Sebestyen, Z., I. Prinz, J. Déchanet-Merville, B. Silva-Santos and J. Kuball (2020). "Translating gammadelta (γδ) T cells and their receptors into cancer cell therapies." Nat Rev Drug Discov **19**(3): 169-184.

Serrano, B., S. de Sanjosé, S. Tous, B. Quiros, N. Muñoz, X. Bosch and L. Alemany (2015). "Human papillomavirus genotype attribution for HPVs 6, 11, 16, 18, 31, 33, 45, 52 and 58 in female anogenital lesions." European Journal of Cancer **51**(13): 1732-1741.

Sha, D., Z. Jin, J. Budczies, K. Kluck, A. Stenzinger and F. A. Sinicrope (2020). "Tumor Mutational Burden as a Predictive Biomarker in Solid Tumors." Cancer Discovery **10**(12): 1808-1825.

Shen, T.-T., C.-Y. Long and M.-P. Wu (2023). "Favorable cervical cancer mortality-to-incidence ratios of countries with good human development index rankings and high health expenditures." BMC Women's Health **23**(1): 284.

Shepherd, J. (2000). "Cervical cancer and sexual lifestyle: a systematic review of health education interventions targeted at women." Health Education Research **15**(6): 681-694.

Sherwood, A. M., C. Desmarais, R. J. Livingston, J. Andriesen, M. Haussler, C. S. Carlson and H. Robins (2011). "Deep sequencing of the human TCRγ and TCRβ repertoires suggests that TCRβ rearranges after αβ and γδ T cell commitment." Sci Transl Med **3**(90): 90ra61.

Shi, X., C. W. Li, L. C. Tan, S. S. Wen, T. Liao, Y. Zhang, T. Z. Chen, B. Ma, P. C. Yu, Z. W. Lu, N. Qu, Y. Wang, R. L. Shi, Y. L. Wang, Q. H. Ji and W. J. Wei (2021). "Immune Co-inhibitory Receptors PD-1, CTLA-4, TIM-3, LAG-3, and TIGIT in Medullary Thyroid Cancers: A Large Cohort Study." J Clin Endocrinol Metab **106**(1): 120-132.

Sobin, L. H., M. K. Gospodarowicz and C. Wittekind (2011). TNM classification of malignant tumours, John Wiley & Sons.

Spriggs, C. and L. Laimins (2017). "Human Papillomavirus and the DNA Damage Response: Exploiting Host Repair Pathways for Viral Replication." Viruses **9**(8): 232.

Standring, S., H. Ellis, J. Healy, D. Johnson, A. Williams, P. Collins and C. Wigley (2005). "Gray's anatomy: the anatomical basis of clinical practice." American journal of neuroradiology **26**(10): 2703.

Stone, J. D., A. S. Chervin and D. M. Kranz (2009). "T-cell receptor binding affinities and kinetics: impact on T-cell activity and specificity." Immunology **126**(2): 165-176.

Szeto, C., C. A. Lobos, A. T. Nguyen and S. Gras (2020). "TCR Recognition of Peptide-MHC-I: Rule Makers and Breakers." Int J Mol Sci **22**(1).

Tan, S., D. Li and X. Zhu (2020). "Cancer immunotherapy: Pros, cons and beyond." Biomedicine & Pharmacotherapy 124: 109821.

Tabatabaeian, H., Bai, Y., Huang, R. et al (2024). "Navigating therapeutic strategies: HPV classification in head and neck cancer." Br J Cancer.

Teijeira, A., S. Garasa, I. Etxeberria, M. Gato-Cañas, I. Melero and G. M. Delgoffe (2019). "Metabolic Consequences of T-cell Costimulation in Anticancer Immunity." Cancer Immunol Res **7**(10): 1564-1569.

Tian, S., R. Maile, E. J. Collins and J. A. Frelinger (2007). "CD8+ T cell activation is governed by TCR-peptide/MHC affinity, not dissociation rate." J Immunol **179**(5): 2952-2960.

Tibshirani, R. (1997). "The lasso method for variable selection in the Cox model." Stat Med **16**(4): 385-395.

Tokarew, N., J. Ogonek, S. Endres, M. Von Bergwelt-Baildon and S. Kobold (2019). "Teaching an old dog new tricks: next-generation CAR T cells." British Journal of Cancer **120**(1): 26-37.

Toulon, A., L. Breton, K. R. Taylor, M. Tenenhaus, D. Bhavsar, C. Lanigan, R. Rudolph, J. Jameson and W. L. Havran (2009). "A role for human skin–resident T cells in wound healing." Journal of Experimental Medicine **206**(4): 743-750.

Toutirais, O., F. Cabillic, G. Le Friec, S. Salot, P. Loyer, M. Le Gallo, M. Desille, C. T. De La Pintière, P. Daniel, F. Bouet and V. Catros (2009). "DNAX accessory molecule-1 (CD226) promotes human hepatocellular carcinoma cell lysis by Vγ9Vδ2 T cells." European Journal of Immunology **39**(5): 1361-1368.

Trimble, C. L., M. P. Morrow, K. A. Kraynyak, X. Shen, M. Dallas, J. Yan, L. Edwards, R. L. Parker, L. Denny, M. Giffear, A. S. Brown, K. Marcozzi-Pierce, D. Shah, A. M. Slager, A. J. Sylvester, A. Khan, K. E. Broderick, R. J. Juba, T. A. Herring, J. Boyer, J. Lee, N. Y. Sardesai, D. B. Weiner and M. L. Bagarazzi (2015). "Safety, efficacy, and immunogenicity of VGX-3100, a therapeutic synthetic DNA vaccine targeting human papillomavirus 16 and 18 E6 and E7 proteins for cervical intraepithelial neoplasia 2/3: a randomised, double-blind, placebo-controlled phase 2b trial." The Lancet **386**(10008): 2078-2088.

Tsang, S. H., J. N. Sampson, J. Schussler, C. Porras, S. Wagner, J. Boland, B. Cortes, D. R. Lowy, J. T. Schiller, M. Schiffman, T. J. Kemp, A. C. Rodriguez, W. Quint, M. H. Gail, L. A. Pinto, P. Gonzalez, A. Hildesheim, A. R. Kreimer and R. Herrero (2020). "Durability of Cross-Protection by Different Schedules of the Bivalent HPV Vaccine: The CVT Trial." J Natl Cancer Inst **112**(10): 1030-1037.

Tumeh, P. C., C. L. Harview, J. H. Yearley, I. P. Shintaku, E. J. M. Taylor, L. Robert, B. Chmielowski, M. Spasic, G. Henry, V. Ciobanu, A. N. West, M. Carmona, C. Kivork, E. Seja, G. Cherry, A. J. Gutierrez, T. R. Grogan, C. Mateus, G. Tomasic, J. A. Glaspy, R. O. Emerson, H. Robins, R. H. Pierce, D. A. Elashoff, C. Robert and A. Ribas (2014). "PD-1 blockade induces responses by inhibiting adaptive immune resistance." Nature **515**(7528): 568-571.

Uldrich, A. P., M. Rigau and D. I. Godfrey (2020). "Immune recognition of phosphoantigen-butyrophilin molecular complexes by γδ T cells." Immunological Reviews **298**(1): 74-83.

Upadhaya, S., J. X. Yu, M. Shah, D. Correa, T. Partridge and J. Campbell (2021). "The clinical pipeline for cancer cell therapies." Nat. Rev. Drug Discov **20**: 503-504.

Vallvé-Juanico, J., S. Houshdaran and L. C. Giudice (2019). "The endometrial immune environment of women with endometriosis." Hum Reprod Update **25**(5): 564-591.

van Luijk, I. F., S. M. Smith, M. C. Marte Ojeda, A. L. Oei, G. G. Kenter and E. S. Jordanova (2022). "A Review of the Effects of Cervical Cancer Standard Treatment on Immune Parameters in Peripheral Blood, Tumor Draining Lymph Nodes, and Local Tumor Microenvironment." J Clin Med **11**(9).

Veglia, F., E. Sanseviero and D. I. Gabrilovich (2021). "Myeloid-derived suppressor cells in the era of increasing myeloid cell diversity." Nature Reviews Immunology **21**(8): 485-498.

Venkatas, J. and M. Singh (2020). "Cervical cancer: a meta-analysis, therapy and future of nanomedicine." Ecancermedicalscience **14**: 1111.

Volkova, N. V., B. Meier, V. González-Huici, S. Bertolini, S. Gonzalez, H. Vöhringer, F. Abascal, I. Martincorena, P. J. Campbell, A. Gartner and M. Gerstung (2020). "Mutational signatures are jointly shaped by DNA damage and repair." Nature Communications **11**(1): 2169.

Von Lilienfeld-Toal, M., J. Nattermann, G. Feldmann, E. Sievers, S. Frank, J. Strehl and I. G. H. Schmidt-Wolf (2006). "Activated γδ T cells express the natural cytotoxicity receptor natural killer p44 and show cytotoxic activity against myeloma cells." Clinical and Experimental Immunology **144**(3): 528-533.

Vonsky, M. S., A. L. Runov, I. V. Gordeychuk and M. G. Isaguliants (2019). "Therapeutic Vaccines Against Human Papilloma Viruses: Achievements and Prospects." Biochemistry (Moscow) **84**(7): 800-816.

Vunjak-Novakovic, G., K. Ronaldson-Bouchard and M. Radisic (2021). "Organs-on-a-chip models for biological research." Cell **184**(18): 4597-4611.

Wacker, M., J. Bauer, L. Wessling, M. Dubbelaar, A. Nelde, H.-G. Rammensee and J. S. Walz (2023). "Immunoprecipitation methods impact the peptide repertoire in immunopeptidomics." Frontiers in Immunology **14**.

Wang, C., C. Xiong, Y.-c. Hsu, X. Wang and L. Chen (2020). "Human leukocyte antigen (HLA) and cancer immunotherapy: HLA-dependent and -independent adoptive immunotherapies." Annals of Botany **5**: 14-14.

Wei, X., F. Chen, K. Xin, Q. Wang, L. Yu, B. Liu and Q. Liu (2019). "Cancer-Testis Antigen Peptide Vaccine for Cancer Immunotherapy: Progress and Prospects." Transl Oncol **12**(5): 733-738.

Willcox, C. R., P. Vantourout, M. Salim, I. Zlatareva, D. Melandri, L. Zanardo, R. George, S. Kjaer, M. Jeeves, F. Mohammed, A. C. Hayday and B. E. Willcox (2019). "Butyrophilin-like 3 Directly Binds a Human Vγ4+ T Cell Receptor Using a Modality Distinct from Clonally-Restricted Antigen." Immunity **51**(5): 813-825.e814.

Williams, V. M., M. Filippova, U. Soto and P. J. Duerksen-Hughes (2011). "HPV-DNA integration and carcinogenesis: putative roles for inflammation and oxidative stress." Future Virology **6**(1): 45-57.

Wirth, T. C. and F. Kühnel (2017). "Neoantigen Targeting-Dawn of a New Era in Cancer Immunotherapy?" Front Immunol **8**: 1848.

Wojtukiewicz, M. Z., M. M. Rek, K. Karpowicz, M. Górska, B. Polityńska, A. M. Wojtukiewicz, M. Moniuszko, P. Radziwon, S. C. Tucker and K. V. Honn (2021). "Inhibitors of immune checkpoints-PD-1, PD-L1, CTLA-4-new opportunities for cancer patients and a new challenge for internists and general practitioners." Cancer Metastasis Rev **40**(3): 949-982.

Wolf, J. and Y. Xu (2023). "Immune checkpoint inhibitor therapy in advanced cervical cancer: Deepened response with prolonged treatment and repeat response to re-initiation of therapy." Gynecologic Oncology Reports **48**: 101244.

Wong, K. K., W. A. Li, D. J. Mooney and G. Dranoff (2016). "Advances in Therapeutic Cancer Vaccines." Adv Immunol **130**: 191-249.

Xie, N., G. Shen, W. Gao, Z. Huang, C. Huang and L. Fu (2023). "Neoantigens: promising targets for cancer therapy." Signal Transduction and Targeted Therapy **8**(1).

Xinaris, C., V. Brizi and G. Remuzzi (2015). "Organoid Models and Applications in Biomedical Research." Nephron **130**(3): 191-199.

Xu, Y., S. Nowsheen and M. Deng (2023). "DNA Repair Deficiency Regulates Immunity Response in Cancers: Molecular Mechanism and Approaches for Combining Immunotherapy." Cancers (Basel) **15**(5).

Xu, Y., X. Wang, Y. Huang, D. Ye and P. Chi (2022). "A LASSO-based survival prediction model for patients with synchronous colorectal carcinomas based on SEER." Translational Cancer Research **11**(8): 2795-2809.

Xu, Y., Z. Xia, X. Sun, B. Wei, Y. Fu, D. Shi and Y. Zhu (2023). "Identification of a glutamine metabolism reprogramming signature for predicting prognosis, immunotherapy efficacy, and drug candidates in bladder cancer." Frontiers in Immunology **14**.

Xu, Y., Z. Xiang, M. Alnaggar, L. Kouakanou, J. Li, J. He, J. Yang, Y. Hu, Y. Chen, L. Lin, J. Hao, J. Li, J. Chen, M. Li, Q. Wu, C. Peters, Q. Zhou, J. Li, Y. Liang, X. Wang, B. Han, M. Ma, D. Kabelitz, K. Xu, W. Tu, Y. Wu and Z. Yin (2021). "Allogeneic Vγ9Vδ2 T-cell immunotherapy exhibits promising clinical safety and prolongs the survival of patients with late-stage lung or liver cancer." Cell Mol Immunol **18**(2): 427-439.

Yamaguchi, R. and G. Perkins (2018). "Animal models for studying tumor microenvironment (TME) and resistance to lymphocytic infiltration." Cancer Biol Ther **19**(9): 745-754.

Yang, J., A. Zhang, H. Luo and C. Ma (2022). "Construction and validation of a novel gene signature for predicting the prognosis of osteosarcoma." Scientific Reports **12**(1): 1279.

Yang, Y., L. Li, L. Yuan, X. Zhou, J. Duan, H. Xiao, N. Cai, S. Han, X. Ma, W. Liu, C.-C. Chen, L. Wang, X. Li, J. Chen, N. Kang, J. Chen, Z. Shen, S. R. Malwal, W. Liu, Y. Shi, E. Oldfield, R.-T. Guo and Y. Zhang (2019). "A Structural Change in Butyrophilin upon Phosphoantigen Binding Underlies Phosphoantigen-Mediated Vγ9Vδ2 T Cell Activation." Immunity **50**(4): 1043-1053.e1045.

Yu, S., G. Wang, Y. Shi, H. Xu, Y. Zheng and Y. Chen (2020). "MCMs in Cancer: Prognostic Potential and Mechanisms." Anal Cell Pathol (Amst) **2020**: 3750294.

Yuan, J., X. Li and S. Yu (2022). "Cancer organoid co-culture model system: Novel approach to guide precision medicine." Front Immunol **13**: 1061388.

Yuki, K., N. Cheng, M. Nakano and C. J. Kuo (2020). "Organoid Models of Tumor Immunology." Trends in Immunology **41**(8): 652-664.

Zemanek, T., Z. Nova and A. Nicodemou (2023). "Tumor-Infiltrating Lymphocytes and Adoptive Cell Therapy: State of the Art in Colorectal, Breast and Lung Cancer." Physiol Res **72**(S3): S209-s224.

Zhang, H., X. Wang, Y. Ma, Q. Zhang, R. Liu, H. Luo and Z. Wang (2023). "Review of possible mechanisms of radiotherapy resistance in cervical cancer." Front Oncol **13**: 1164985.

Zhang, L., Z. Mao, Y. Lai, T. Wan, K. Zhang and B. Zhou (2020). "A review of the research progress in T-lymphocyte immunity and cervical cancer." Translational Cancer Research **9**(3): 2026-2036.

Zhao, Z., X. Chen, A. M. Dowbaj, A. Sljukic, K. Bratlie, L. Lin, E. L. S. Fong, G. M. Balachander, Z. Chen, A. Soragni, M. Huch, Y. A. Zeng, Q. Wang and H. Yu (2022). "Organoids." Nature Reviews Methods Primers **2**(1).

Zhao, Z., X. Chen, A. M. Dowbaj, A. Sljukic, K. Bratlie, L. Lin, E. L. S. Fong, G. M. Balachander, Z. Chen, A. Soragni, M. Huch, Y. A. Zeng, Q. Wang and H. Yu (2022). "Organoids." Nature Reviews Methods Primers **2**(1): 94.

Zhou, B.-B. S. and S. J. Elledge (2000). "The DNA damage response: putting checkpoints in perspective." Nature **408**(6811): 433-439.

Zhou, J., J. Zhang, Z. Zhang and L. Shen (2023). "Reply to Herrmann: The BTN3A isoform BTN3A1 is responsible for phosphoantigen-induced Vγ9Vδ2 T cell activation." Proceedings of the National Academy of Sciences **120**(20).

Zhu, H., H. Luo, W. Zhang, Z. Shen, X. Hu and X. Zhu (2016). "Molecular mechanisms of cisplatin resistance in cervical cancer." Drug Des Devel Ther **10**: 1885-1895.

Zhu, L., J. Liu, J. Chen and Q. Zhou (2021). "The developing landscape of combinatorial therapies of immune checkpoint blockade with DNA damage repair inhibitors for the treatment of breast and ovarian cancers." Journal of Hematology & Oncology **14**(1).

9 ABBREVIATIONS

Quantities and units were abbreviated according to the International System of Units.

2D	two-dimensional
3D	three-dimensional
AF488	Alexa Fluor488
APC	Allophycocyanin
APCs	Antigen-presenting cell
ATCC	the American Type Culture Collection
ATM	ataxia-telangiectasia mutated
ATP	adenosine triphosphate
ATR	ataxia telangiectasia and Rad3-related protein
B7	B7 family protein
Bcl-xL	B-cell lymphoma-extra large
BCMA	B-cell maturation antigen
BP	biological process
BRCA1	Breast Cancer gene 1
BRCA2	Breast Cancer gene 2
BrHPP	bromohydrin pyrophosphate
BSA	bovine serum albumin
BTLA	B and T lymphocyte attenuator
BTN	butyrophilin
BTN2A1	BTN subfamily 2 member A1

BTN3A1	BTN subfamily 3 member A1
BTN3A2	BTN subfamily 3 member A2
BTN3A3	BTN subfamily 3 member A3
BTNL9	BTN-Like Protein 9
CAMP	human cathelicidin antimicrobial peptide
CAR	chimeric antigen receptor
CCRT	Concurrent chemoradiotherapy
CD	Cluster of Differentiation
CESC	Cervical Squamous Cell Carcinoma and Endocervical Adenocarcinoma
CFSE	Carboxyfluorescein succinimidyl ester
CHAPS	3-[(3-cholamidopropyl) dimethylammonio]-1-propanesulfonate
CHK1	Checkpoint kinase 1
CIN	cervical intraepithelial neoplasia
CO2	carbon dioxide
COX	cyclooxygenase 2
CRISPR	clustered regularly interspaced short palindromic repeats
CT	cancer/testis
CTLA-4	Cytotoxic T-lymphocyte-associated protein 4
D	Asparticacid
DAVID	Database for Annotation, Visualization, and Integrated Discovery
DEG	different expressed genes

DMD	dystrophin gene
DMEM	Dulbecco’s Modified Eagle Medium
DNA	deoxyribonucleic acid
DNAM-1	DNAX accessory molecule 1
dNTP	deoxy-ribonucleoside triphosphate
DPBS	dulbecco’s phosphate-buffered saline
DRG	DNA repair-related genes
dsDNA	double stranded deoxyribonucleic acid
E1	oncogenic protein early gene 1
E2	oncogenic protein early gene 2
E4	oncogenic protein early gene 3
E5	oncogenic protein early gene 4
E6	oncogenic protein early gene 5
E7	oncogenic protein early gene 6
EDTA	ethylenediaminetetraacetic acid
EGF	epidermal growth factor
EGFR	epidermal growth factor receptor
EP300	E1A Binding Protein P300
ER	endoplasmic reticulum
EXO1	exonuclease 1
E:T ratio	effector/target ratio
F	Phenylalanine

F1-ATPase	ATP syntase
FACS	fluorescence-activated cell sorting
FAS	The Fas antigen
FBS	Fetal bovine serum
FCS	fetal calf serum
FGF10	fibroblast growth factor 10
FIGO	the International Federation of Gynecology and Obstetrics
FITC	fluorescein isothiocyanate
FLG	filaggrin
FSK	forskolin
GAPDH	Glyceraldehyde-3-phosphate dehydrogenase
GD2	disialoganglioside
GEO	Gene Expression Omnibus
GO	Gene Ontology
GSEA	gene set enrichment analysis
GVHD	graft-versus-host disease
GzmB	Granzyme B
HBSS	hank’s balanced salt solution
HEMA	2-hydroxyethyl methacrylate
HER2	Human Epidermal Growth Factor Receptor 2
HLA	human leukocyte antigen
HMBPP	I-4-hydroxy-3-methyl-but-2-enyl pyrophosphate

HPV16/18	human papillomaviruses type 16 or 18
HPV+	human papillomaviruses E6 E7 positive
HR-HPV	high-risk human papillomaviruses
HSPD1	heat shock protein family D (Hsp60) member 1
I	Isoleucine
IC50	binding affinity score
IEDB	the Immune Epitope Database
IF	Immunofluorescence
IFB	Immunofluorescence buffer
IFNγ	interferon gamma
IL	Interleukin
IPP	isopentenyl pyrophosphate
iPSC	induced pluripotent stem cells
IRE	irreversible electroporation
K	Lysine
KCl	Potassium Chloride
KEGG	Kyoto Encyclopedia of Genes and Genomes
KH_2PO_4	Potassium dihydrogen phosphate
Ki67	antigen Kiel 67
KLRG2	Killer Cell Lectin Like Receptor G2
KMT2C	Lysine (K)-specific methyltransferase 2C
KMT2D	Lysine (K)-specific methyltransferase 2D

KRT14	cytokeratin 14
KRT17	cytokeratin 17
KRT18	cytokeratin 18
KRT5	cytokeratin 5
KRT7	cytokeratin 7
KRT8	cytokeratin 8
L	Leucine
L1	oncogenic protein late gene 1
L2	oncogenic protein late gene 2
LAG-3	Lymphocyte-activation gene 3
LAMP	Lysosomal-associated membrane protein 1
LASSO	The least absolute shrinkage and selection operator
MAGE	melanoma antigen
MCM	The minichromosome maintenance protein complex
MDSC	myeloid-derived suppressor cells
$MgCl_2$	Magnesium dichloride
MGMT	Methylguanine methyltransferase
MHC	Major Histocompatibility Complex
MICA	MHC class I polypeptide–related sequence A
MICB	MHC class I polypeptide–related sequence B
MS	mass spectrometry
MSH2	MutS homolog 2

MSLN	Mesothelin
MUC16	Mucin-16
MUC4	Mucin-4
Na_2HPO_4	Sodium phosphate dibasic
NAC	N-Acetyl-L-Cystein
NaCl	sodium chloride
NIC	nicotinamid
NK	natural killer cells
NKG2D	The natural killer 2D receptor
NKR	natural killer receptor
NY-ESO-1	New York esophageal squamous cell carcinoma 1
OGG1	8-Oxoguanine glycosylase
ORF	open reading frames
OS	overall survival
OVOL1	OVO Like Transcriptional Repressor 1
p53	protein 53
pAgs	phosphoantigens
PARP	Poly (ADP-ribose) polymerase
PBMC	peripheral blood mononuclear cells
PBS	phosphate buffered saline
PBST	phosphate-buffered saline with Tween 20
PCR	polymerase chain reaction

PD-1	Programmed cell death protein 1
PD-L1	programmed death-ligand 1
PD-L2	programmed death-ligand 2
PE	phycoerythrin
PFA	Paraformaldehyde
PI	propidium iodide
PIK3CA	Phosphatidylinositol 4,5-bisphosphate 3-kinase catalytic subunit alpha isoform
Prf	Platelet-rich fibrin
qRT-PCR	quantitative reverse transcription polymerase chain reaction
R	Arginine
RAD50	RAD50 homolog
RAD51	RAD51 recombinase
RNA	ribonucleic acid
ROC curve	receiver operating characteristic curve
ROCK	Rho kinase
RT	reverse transcription
SCC	squamous cell carcinomas
SNP	single nucleotide polymorphism
SNV	single nucleotide variants
STAT5	Signal Transducer and Activator of Transcription 5 A and B
SUCLA2	Succinate-CoA Ligase ADP-Forming Subunit Beta

SV	structural variants
SYNE1	Spectrin Repeat Containing Nuclear Envelope Protein 1
T	Threonine
TAA	tumor-associated antigen
TAE	Tris-acetate EDTA buffer
TAM	tumor-associated macrophages
TAP	Transporter associated with antigen processing
TBS	Tris buffered saline
TCGA	The Cancer Genome Atlas Program
TCR	T-cell receptor
TFA	trifluoro acetic acid
TGF	transforming growth factor
TGFB1	transforming growth factor beta 1
Th17	T Helper 17 Cell
Th2	T Helper 2 Cell
TIDE	Tumor Immune Dysfunction and Exclusion
TIGIT	T cell immunoreceptor with Ig and ITIM domains
TIL	Tumor-infiltrating lymphocytes
TIM-3	T cell immunoglobulin and mucin domain-3
TIS	Tumor Inflammation Signature
TLR	toll-like receptor
TMB	tumor mutational burden

TME	tumor microenvironment
TNF	tumor necrosis factor
TOP2β	Topoisomerase 2β
TopBP1	DNA Topoisomerase II Binding Protein 1
Tregs	regulatory T cells
TSA	tumor-specific antigen
TTN	Titin
TZ	transformation zone
ULBP1	UL16 binding protein 1
ULBP4	UL16 binding protein 4
UV	Ultraviolet
V	Valine
VISTA	V-domain Ig suppressor of T cell activation
XPA	xeroderma pigmentosum group A
Y	Tyrosine
ZOL	zoledronic acid
γH2AX	Phosphorylated histone H2AX